



HAL
open science

Compared and functional morphology of the hoatzin (*Opisthocomus hoazin*)

Fanny Pagès

► **To cite this version:**

Fanny Pagès. Compared and functional morphology of the hoatzin (*Opisthocomus hoazin*). Tissues and Organs [q-bio.TO]. Museum national d'histoire naturelle - MNHN PARIS, 2019. English. NNT : 2019MNHN0013 . tel-02929631

HAL Id: tel-02929631

<https://theses.hal.science/tel-02929631>

Submitted on 3 Sep 2020

HAL is a multi-disciplinary open access archive for the deposit and dissemination of scientific research documents, whether they are published or not. The documents may come from teaching and research institutions in France or abroad, or from public or private research centers.

L'archive ouverte pluridisciplinaire **HAL**, est destinée au dépôt et à la diffusion de documents scientifiques de niveau recherche, publiés ou non, émanant des établissements d'enseignement et de recherche français ou étrangers, des laboratoires publics ou privés.

MUSÉUM NATIONAL D'HISTOIRE NATURELLE



École Doctorale 227

Sciences de la Nature et de l'Homme : évolution et écologie

Année 2019

N° attribué par la bibliothèque

|||||

THÈSE

pour obtenir le grade de

DOCTEUR DU MUSÉUM NATIONAL D'HISTOIRE NATURELLE

Spécialité : Anatomie fonctionnelle

présentée et soutenue publiquement par

Fanny PAGÈS

le 13 décembre 2019

Anatomie comparée et fonctionnelle de l'hoazin (*Opisthocomus hoazin*)

Sous la direction de : **Pr Anick ABOURACHID, Directrice**
Dr Anne-Claire FABRE, Encadrante

Devant le jury :

Dr Anthony HERREL, Directeur de recherche, Muséum National d'Histoire Naturelle, Paris, France, Président

Pr Jesús MARUGÁN-LOBÓN, Associate Professor, Université de Madrid, Madrid, Spain, Rapporteur

Dr Philipp HEEB, Directeur de recherche, Université de Toulouse, Toulouse, France, Rapporteur

Pr Dominique ADRIAENS, Professeur, Université de Ghent, Ghent, Belgium, Examineur

Dr Ryan FELICE, Lecturer, University College London, London, United Kingdom, Examineur

“Success is stumbling from failure to failure with no loss of enthusiasm.”

Winston Churchill

A mes parents

Remerciements

Table of contents

General introduction	6
Context.....	7
Hoatzin	8
Ecology	9
Digestive system.....	11
Anatomy.....	13
Fossil record.....	16
Phylogeny.....	17
Goals	20
Interest of geometric morphometric methods.....	21
Chapter 1 - The skeletal anatomy of the hoatzin (<i>Opisthocomus hoazin</i>): functional consequences of an extreme life-style?	23
Abstract.....	26
Introduction	27
Material and methods	29
Results	30
Skull.....	30
Vertebral column	38
Ribs.....	42
Pectoral girdle	43
Wing bones.....	46
Pelvic girdle.....	49
Hind limb.....	51
Discussion	55

Chapter 2 - Does bone preparation impact its shape: consequences for comparative analyses of bone shape? 60

Abstract..... 63

Introduction 64

Materials and methods 66

 Material..... 66

 Methods 68

Results 74

 Intraspecific level..... 74

 Interspecific level analyses to assess the impact of bone deformation in a broader context..... 82

Discussion 84

 What is the impact of deformation due to preparation on the bone shape at the intraspecific level? 84

 What is the impact of deformation due to preparation on shape analysis at the interspecific level? 88

Conclusions..... 88

Chapter 3 - Does flight type constrain the shape of the scapular girdle in birds? Inferences on the flying ability of the hoatzin (*Opisthocomus hoazin*)..... 90

Abstract..... 93

Introduction 94

Material and methods 96

 Data collection..... 96

 Shape quantification using geometric morphometrics..... 97

 Statistical analysis 100

Results 102

 Principal Component analyses 102

Shape differences depending on flight type using (M)ANOVAs and phylogenetic (M)ANOVAs	107
K nearest neighbour classification and cross-validation test.....	108
Discussion	109
Chapter 4 - Preliminary description of the hoatzin development: ossification sequence, focus on scapular girdle and cranial musculature	115
Introduction	119
Material and methods	120
Specimens	120
CT-scanning.....	120
Results	121
Complete skeleton – μ CT scans	121
Comparative ossification sequence	129
Scapular girdle development	130
Cranial musculature.....	134
Discussion	138
General discussion	140
References	151
Annexes.....	166

Résumé

L'hoazin (*Opisthocomus hoazin*, Muller, 1776) est l'unique espèce vivante représentante des Opisthocomiformes. Depuis la description originale de Statius Muller en 1776, l'hoazin a fait l'objet de nombreux débats. Il fait incontestablement partie des espèces d'oiseaux les plus étranges et énigmatiques en termes d'apparence, de traits d'histoire de vie, de spécialisations morphologiques et de physiologie. L'hoazin est décrit comme un oiseau à reproduction coopérative et ses juvéniles ont des capacités exceptionnelles de nage et d'escalade grâce à des griffes entièrement fonctionnelles sur leurs ailes. C'est en outre le seul oiseau folivore à fermentation pré-gastrique, comme chez certains mammifères, avec un jabot hypertrophié en guise de chambre de fermentation. Ce régime alimentaire particulier a un impact important sur la forme de ses os, comme par exemple une carène réduite et un sternum entièrement fusionné à la fourchette et aux coracoïdes afin de laisser de l'espace au jabot. Plusieurs auteurs ont corrélé ces modifications morphologiques à des implications fonctionnelles telles que la réduction de la capacité de vol. Malgré le grand intérêt que suscite cet oiseau, depuis les premières descriptions partielles du début du 20^{ème} siècle, le squelette entier de l'hoazin n'a pas encore été décrit. Son anatomie ne reste par conséquent que partiellement connue. L'utilisation de récentes techniques 3D nous a permis d'avoir accès à des parties de son anatomie qui peuvent être difficile à décrire en dissection classique. Ainsi, une monographie complète de son squelette a été réalisée. Après la description de l'ensemble du squelette et des inférences fonctionnelles liées, la mise en évidence de caractères uniquement présents chez l'hoazin a été rendue possible grâce aux comparaisons avec la littérature déjà publiée sur les oiseaux. Il semble que la ceinture scapulaire de l'hoazin présente de nombreuses particularités morphologiques et nécessite par conséquent des analyses comparatives plus poussées.

En utilisant des techniques 3D, des méthodes morphométrie géométrique et des spécimens de collection, nous avons étudié quantitativement l'évolution des changements de la morphologie de la ceinture scapulaire des oiseaux. Néanmoins, avant de travailler sur un grand ensemble de données comparatives des os scapulaires, l'impact possible des effets de préparation sur la forme des os de la collection ostéologique doit être quantifié. En effet, plusieurs auteurs ont décrit les effets des

processus de préparation sur les formes des os. Ainsi, la présente étude nous a permis d'évaluer l'impact du processus de préparation ostéologique sur la forme de chaque os de la ceinture scapulaire en utilisant des ensembles des jeux de données intra et interspécifiques d'oiseaux. Les effets de la préparation peuvent être correctement estimés en utilisant l'apparence de l'os. Cet indicateur a été utilisé pour collecter des spécimens supplémentaires en vue d'analyses comparatives supplémentaires sur la ceinture scapulaire des oiseaux.

La littérature sur l'hoazin fait référence à un oiseau au vol non agile en raison de la modification de la forme de son sternum, laissant peu d'espace pour les insertions musculaires servant au vol. Mais cette hypothèse de lien direct entre la forme modifiée du sternum et la capacité réduite de vol n'a jamais été testée. Grâce à un ensemble de données comparatives composé de cinquante-neuf espèces pour lesquelles le comportement locomoteur est bien documenté, des différences de forme pour chaque os de la ceinture scapulaire en fonction du type de vol ont été testées. Le sternum, les coracoïdes, les scapulas et surtout les humérus semblent avoir des formes très différentes selon le type de vol. Ces résultats ont été utilisés pour déduire le type de vol en relation directe avec les formes des os scapulaires de l'hoazin. Les tests d'assignation effectués sur les formes d'os scapulaire de l'hoazin montrent que presque tous ses os sont classés parmi les espèces d'oiseaux planeurs, à l'exception de la scapula. Il semble que la forme unique du sternum de l'hoazin ne soit pas la seule responsable de ses faibles capacités de vol rapportées dans la littérature. De plus, ces études comparatives ont été complétées par une description anatomique et comparative d'une série de développement de spécimens d'hoazin. Cette analyse développementale nous a permis d'identifier que la forme du sternum est déterminée dès le début du développement de cet oiseau. En revanche, la fusion complète du complexe du sternum s'observe uniquement chez les juvéniles tardifs. L'utilisation d'un ensemble de données comparatives et de méthodes de morphométrie géométrique 3D nous a permis de générer de nouvelles informations quantitatives sur les spécificités morphologiques de l'hoazin. Le type de vol de l'hoazin a fait l'objet de nombreuses discussions dans la littérature, mais ce travail de thèse apporte une réponse préliminaire au rôle de la forme du sternum et de sa carène dans la réduction de ses capacités de vol.

Abstract

The hoatzin (*Opisthocomus hoazin*, Muller, 1776) is the unique extant species of the Opisthocomiformes. Since the original description by Statius Muller in 1776, the hoatzin has been the subject of a lot of debate. It is unquestionably among the most bizarre and enigmatic bird species in terms of its appearance, life history, morphological specializations and physiology. The hoatzin is described as a co-operatively breeding bird, with juveniles having exceptional swimming and climbing abilities thanks to fully functional claws on the wing. It is moreover the only folivorous bird with a pre-gastric fermentation, as found in mammals, with a hypertrophied crop. This dietary specialization has an important impact on its bone shape, such as a reduced carina and a sternum fused to the furcula and to the coracoids. Several authors linked these morphological changes to functional implications such as reduced flight abilities. Despite of its unusual nature and the great interest in this bird, since the first partial descriptions in the early 20th, the whole skeleton of the hoatzin has not been described to date. Its anatomy remains consequently only partially known. Taking advantage of the recent 3D techniques allowing us to get access to part of the anatomy that can be difficult to describe based on classic dissections, a complete monography on the skeletal anatomy was realized. After the description of the whole skeleton and functional inferences, highlighting the unique characters of the hoatzin compared to other birds became possible by means of previously published comparative data on skeletal anatomy in birds. It appears that the scapular girdle of the hoatzin has a lot of morphological particularities and thus needs further comparative analyses.

Using 3D techniques, geometric morphometric methods and collection specimens, we quantitatively investigated evolutionary changes in the morphology of the scapular girdle of birds. Nevertheless, before working on a large comparative dataset of the scapular bones, the possible impact of preparation effects on the shape of bones from osteological collection should be quantified. Indeed, several authors have described the effect of preparation processes on bones. This study allowed us to assess the impact of bones preparation process on the shape of each bone of the scapula girdle using both intra- and inter-specific datasets of birds. Our results have shown that preparation effects can be well estimated using the appearance of the bone and this

proxy was used to collect data for further comparative analyses on the scapular girdle of birds.

Literature of the hoatzin refers to it as a poor flier with non-agile flight because of its sternum shape modification providing only a small area for insertion of the flight muscles. But this hypothesis of a direct link between modified sternum shape and flight capacity has never been tested. Using a comparative dataset composed of fifty-eight species for which the locomotor behavior is well known, shape differences for each bone of the scapular girdle depending on flight type were tested. Sternum, coracoids, scapulae and mainly the humeri have significantly different shapes depending on flight type. These results were used to infer the flight type of the hoatzin based on the shape of its scapular bones. Assignment tests performed on scapular bone shapes of the hoatzin showed that nearly all its bones are classified among gliding species, except for the scapula. It appears that the unique sternum shape of the hoatzin is not the sole reason for its poor flying abilities. Moreover, these comparative studies were supplemented with an anatomical and comparative description of a developmental series of hoatzin specimens. This developmental analysis allowed us to determine that sternum shape is determined in the early development whereas the complete fusion of the sternum complex happens in later in juveniles. The use of a comparative dataset and 3D geometric morphometric methods allowed us to generate quantitative data on the morphological specificities of the hoatzin. The flight type of the hoatzin has been much debated in the literature but this work provides a preliminary answer to the role of its sternum shape and reduced carina in its flight abilities.

General introduction

General introduction

Context

Studies of anatomy have a long history. The ancient Greeks were also interested in the structure and behavior of animals, and Aristotle is generally considered as the first well-known comparative anatomist (Russell, 1982). Belon, a French naturalist from the 16th century, is considered by many as the forefather of modern comparative anatomy. Edward Tyson pushed research in comparative anatomy one step further and began systematic comparative studies of the anatomy of different animals, humans included. Later comparative anatomy flourished and became the foundation of the work of many great anatomists like Cuvier, Owen, Huxley or Romer. Over the past decade there has been a true revival of comparative anatomy (Ashley-Ross and Gillis, 2002), partly due to the availability of novel methods and techniques including micro computed tomography (μ CT) scanning, contrast-enhanced μ CT data, or even synchrotron μ CT data (Bribiesca-Contreras and Sellers, 2017; Descamps et al., 2014; Genbrugge et al., 2011; Pradel et al., 2013; Voeten et al., 2018). Moreover, advances in embryology and the establishment of gene ontologies have prompted the need for better anatomical descriptions in model organisms (Constantinescu, 2018; Cox and Jeffery, 2008; DeLaurier et al., 2008; Druzinsky et al., 2016; Porro and Richards, 2017). A comprehensive knowledge of anatomy is a necessary prerequisite for understanding of muscle function and biomechanics and has led to a plethora of descriptive as well as quantitative anatomical studies in recent years (Blanke et al., 2017; Watson et al., 2018, 2014). Finally, a deep understanding of anatomy is important for creating solid data matrices allowing phylogenetic reconstructions based on anatomical traits (Davesne et al., 2014; Livezey and Zusi, 2006).

Birds have the highest number of species among vertebrate tetrapods (Lecointre, Le Guyader, and Visset, 2016). The important radiation of birds in terms of species and morphological diversity (disparity) is often linked to their adaptation to a great diversity of living environments (MacArthur and MacArthur, 1961). Birds can be found everywhere in the world, from the poles to the equator, and have colonized several habitats (from aerial to aquatic) (Hawkins et al., 2007, 2006). Birds share a common

flying ancestry. In the transition from the few dinosaur species which survived the KT mass extinction to extant birds a large number of evolutionary modifications and adaptations took place. In addition to their ability to fly, birds evolved to become specialized to their environment. Whereas some acquired unusual beak shapes such as hummingbirds, others including penguins and auks transformed their wings and body shape as an adaptation to swimming, and some almost completely lost their fore limb such as kiwis, ostriches, or rails (Abourachid, Castro, and Provini, 2019; Mariani and Martin, 2003). Some of these ecological adaptations are convergent between groups implying that these morphological adaptations are more linked to their ecological niche than their shared history. For example, swimming birds developed the same kind of morphological adaptations even if they do not share the same evolutionary history (Clifton, Carr, and Biewener, 2018). Beak shapes are also more linked to ecological factors like diet than to phylogenetic heritage (Bright et al., 2016; Mallarino et al., 2012). However, some birds appear to have unique ecological specializations. The hoatzin, for example, is the only extant bird that is completely folivorous, and that shows a foregut fermentation similar to that observed in ruminant mammals.

Hoatzin

The hoatzin (*Opisthocomus hoazin*, Muller, 1776) is a folivorous bird that is pheasant-sized, long tailed, colorful and with a crested head (Domínguez-Bello et al., 1994; Müllner, 2004). It has an un-feathered blue face with red eyes. The long tail is brown. The upper parts are dark and streaked with white, as are the proximal part on the wings. The distal parts of the wings are red (Figure 1). The under parts of the body are ash beige. The hoatzin lives along river banks, swamps and mangroves in Amazonia, South America (Domínguez-Bello et al., 1994). The hoatzin is also known as the skunk bird because of its foul odor and is reputed to have a bad taste and is consequently not hunted by humans. Thus, the hoatzin is considered as not endangered by the IUCN. The hoatzin is described as a co-operatively breeding bird, with juveniles having exceptional swimming and climbing abilities thanks to fully functional claws on the wing. It is moreover the only folivorous bird with pre-gastric fermentation (Abourachid et al., 2019; Domínguez-Bello et al., 1994; Grajal et al., 1989; Grimmer, 1962).

Since the original description by Statius Muller in 1776, the hoatzin has been the subject of a lot of debate. It is unquestionably among the most bizarre and enigmatic bird species in terms of its appearance, life history, morphological specializations and physiology (J. M. Hughes and Baker, 1999). Due to its unusual morphological characteristics this species has been placed in its own family: the Opisthocomidae (Swainson, 1837). But its phylogenetical history remains debated. Despite of its unusual nature and the great interest in this bird, its morphology has not been studied since the first descriptions in the early 20th century (Mitchell, 1896; Parker, 1891; Shufeldt, 1918). Its anatomy remains consequently only partially known.



Figure 1: Adult hoatzin specimens. Shoots from field work of the Hoatzin Project. Photographer: Anick Abourachid

Ecology

The adult hoatzin average body mass is around 700g for around 70cm of total height (Grajal, 1995; Müllner, 2004). In hoatzins, plumage features do not indicate breeding or social status and in addition both sexes look alike (Müllner, 2004). Hoatzins are obligatory folivorous and prefer fresh leaves and buds. However, unlike other birds, it uses microbial foregut fermentation to convert plant cellulose into simple sugars (Domínguez-Bello et al., 1994). This particular diet implies the presence of a specialized crop which has consequences for the rest of the skeleton (J. M. Hughes and Baker, 1999). The most obvious potential predators are diurnal birds and - at a much lower detection rate - snakes (Müllner, 2004).

The hoatzin is known as a co-operatively breeding bird and is territorial (Müllner, 2004). It belongs to the few bird species (3.2%) that are classified as co-operative breeders (Arnold and Owens, 1998; Müllner, 2004). Hoatzins breed in a manner similar to that of the cooperatively breeding cuckoos (in *Crotophaginae*) (J. M. Hughes and Baker, 1999). These breeding units defended all-purpose territories of approximately 5000–8000m², the size of which depended on the area of open water surface (Müllner, 2004). These co-breeding habits can vary according the location of the territory, the presence of predators and food availability. The breeding activity of the hoatzins is closely linked to the onset of the rainy season in Equator (Müllner, 2004), which is consistent with observations from Peru (Torres, 1987), Venezuela (Strahl, 1988), and British Guyana (Grimmer, 1962). The emergence of new leaves just after the rains coincides with the beginning of the feeding period of the young (Müllner, 2004).

According to Müllner (2004), hoatzins live in territorial social units that are usually composed of a single breeding pair and zero to six non-breeders. These additional adults are typically offspring from previous years helping with incubation, the feeding of nestlings and fledglings, as well as with territorial defense (Müllner, 2004; Strahl, 1988; VanderWerf and Strahl, 1990). Sons mainly act as helpers-at-the-nest whereas daughters appear to be the dispersing sex (Strahl, 1988). According to Strahl (2008), hoatzins do not start breeding before their third year of life. Egg laying occurred from February to June and from September to November (Müllner, 2004). The number of eggs in a single hoatzin nest ranged from one to seven with a mean of around two (Domínguez-Bello et al., 1994; Müllner, 2004; Torres, 1987). Hoatzins have a 32-days incubation period (Domínguez-Bello et al., 1994; Müllner, 2004). Both sexes incubate and feed the young (Strahl, 1988).

Because alloparental unit members contribute to the breeding effort directly through incubation and chick feeding, and indirectly through territory defense and predator detection it is reasonable to attribute the increased chance of success of raising offspring to these helpers (Arnold and Owens, 1998; VanderWerf and Strahl, 1990). Another survival strategy in juvenile hoatzin is the very specialized escape behavior: from their first days of life young hoatzins are able to leave the nest and to jump into the water when threatened. They can jump into water, swim vigorously, and use its fore and hind limb claws to climb back into the vegetation. To do so they use an unusual

quadrupedal coordination (Abourachid et al., 2019; J. M. Hughes and Baker, 1999; Karp and Root, 2009). The high water level, a consequence of the wet season, is important to be able to use this escape tactic. Young hoatzins also use the wing claws while climbing in the nesting tree before fledging (Müllner, 2004). If not disturbed, hoatzin chicks normally stay in their nest for between two and three weeks before starting to climb in the nest tree. The nest is left at 45-55 days, but young birds stay in their natal group and beg for food for a further few months. Chicks are fed with plant material which has been pre-digested and regurgitated by adults for two months. Müllner (2004) describes that she never observed hoatzins actively defending their broods when attacked by a predator or a humans. Instead the attending individual flees from the nest to a nearby tree, protesting with its typical hissy vocalization and is subsequently joined by the entire group (Müllner, 2004).

Digestive system

The hoatzin is the only completely folivorous bird. Because vertebrates do not produce the enzymes necessary to digest cellulose, many herbivores have enlarged chambers in their gut, where anaerobic microbes secrete enzymes that digest cellulose. The hoatzin diet is composed by up to 87% of leaves (Grajal et al., 1989; Jones, Amado, and Dominguez-Bello, 2000). The main trees eaten are *Coccoloba sp.*, *Machaerium sp.*, *Combretum sp.*, *Pithecellobium sp.*, and *Couropita sp.* (Domínguez-Bello et al., 1994). This unusual diet implies physiological and anatomical adaptations for the digestion of cellulose (Figure 2). Herbivorous birds typically show hindgut caecal bacterial fermentation. The hoatzin is the only bird known to possess a fully-functional foregut fermentation system where the adapted foregut serves as the major site of microbial fermentation (Dominguez-Bello et al., 1993; Grajal et al., 1989). The morphology of the hoatzin's gut is more similar to that of small mammals with foregut fermentation than to any known herbivorous bird (Hofmann, 1989). The voluminous crop and posterior esophagus have become functional fermentation chambers and have a storage function (Dominguez-Bello et al., 1993; Grajal, 1995). The large crop and lower esophagus represent 77% of the total gut capacity (Grajal, 1995). The relative gut capacity is equivalent to 9% of the adult body mass. The hypertrophied crop as a storage can

represent up to 7.5% of the hoatzin mass, and the gut and its plant content may account for 20% of the hoatzin's body mass (Grajal, 1995; Müllner, 2004). The crop is composed of two interconnected chambers and the lower esophagus is a multichambered organ. The two-crop chambers are connected through a constricted zone with circular muscles that resemble the pillars found in stomach of ruminants (Grajal, 1995). Both are unusually muscular with constrictions between chambers. The interior lining of the crop and esophagus has longitudinal ridges covered by cornified epithelium (Grajal, 1995). A combination of abrasion and microbial action effectively reduces particle size along the

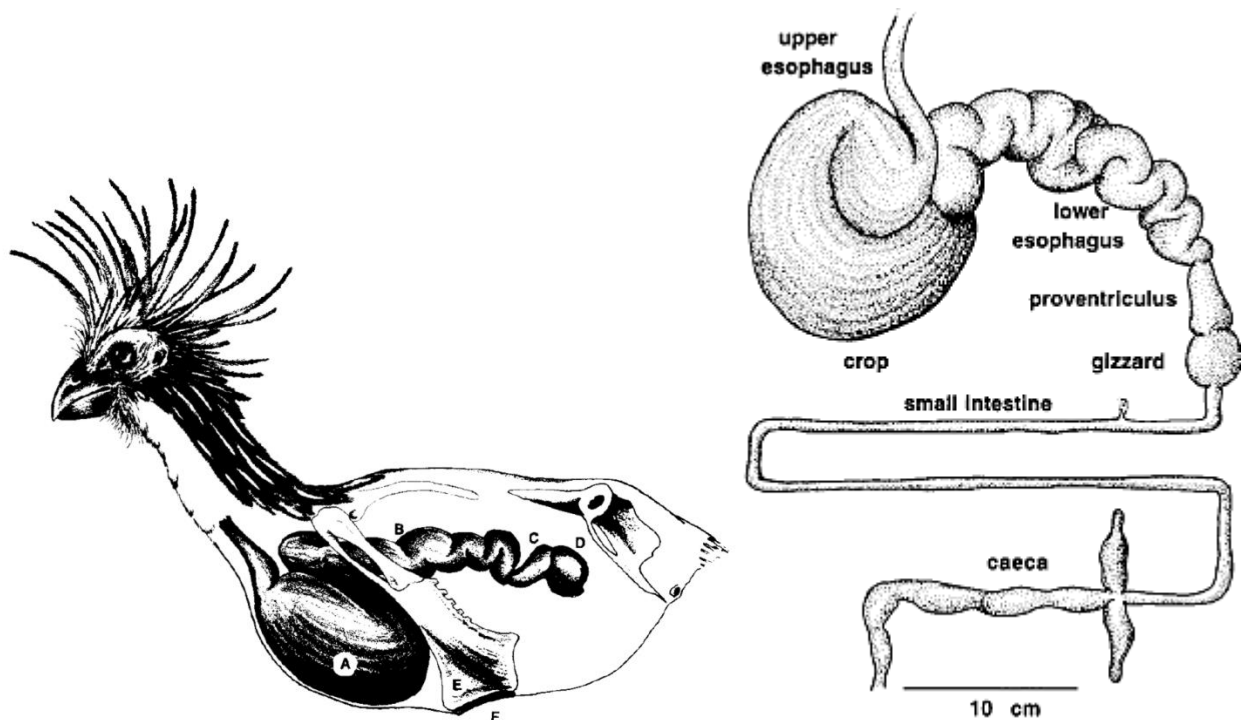


Figure 2: Schematic representations of the digestive system of the adult hoatzin, from Grajal, 1995. Left: Schematic representation of anterior gut of adult Hoatzin seen from left, showing (A) crop, (B) posterior esophagus, (C) proventriculus, and (D) gizzard. Anterior sternum is much reduced to make room for large fermentation chambers, resulting in drastic reduction in area available for flight-muscle attachment to (E) sternal carina; (F) "resting" pad at end of sternum used while perching with full crop. Right: Complete form of hoatzin digestive tract.

gut (Grajal, 1995).

Obligate folivory is unusual in birds because leaves are voluminous, have low nutritional value, and may contain noxious chemicals. These properties are in direct conflict with the flying ability and energy demands typical of most birds (Bosque, Pacheco, and Siegel, 1999; Grajal, 1995; Korzoun, Erard, and Gasc, 2003; Müllner, 2004). It has been suggested that the hoatzin is selective in their leafy diet (Jones, Amado, and

Dominguez-Bello, 2000). They choose plants where the N-content is high while the tannin content is comparatively low (Müllner, 2004). These trees belong to plant families known to have a variety of toxic agents, however (Jones, Amado, and Dominguez-Bello, 2000). Among these toxic compounds are phenols and tannins (Dominguez-Bello et al., 1994). Indeed, Domínguez-Bello et al. (1994) and Grajal (1995) suggested that a prolonged digestion is necessary to detoxify the secondary compound of leaves in the gut by microbial action. Consequently, long retention times in the fermentation chamber have strong implications on the activity pattern: hoatzins exhibit a sedentary life-style and are sitting in their tree most of the day (Müllner, 2004).

Anatomy

In the previous section we highlighted that the hoatzin has several morphological particularities such as the presence of functional claws on the wing in juveniles and a hypertrophied crop. Even if these characteristics are mentioned in the literature, they have never been completely described. Parker (1891) compared the development of the hoatzin skeleton (skull, vertebra column, scapular girdle, pelvic girdle and hind limb) with other known birds, noticing some resemblances mainly with fossil species and basal extinct species (Figure 3). His goal was to be able to put the hoatzin into an existing phylogeny.

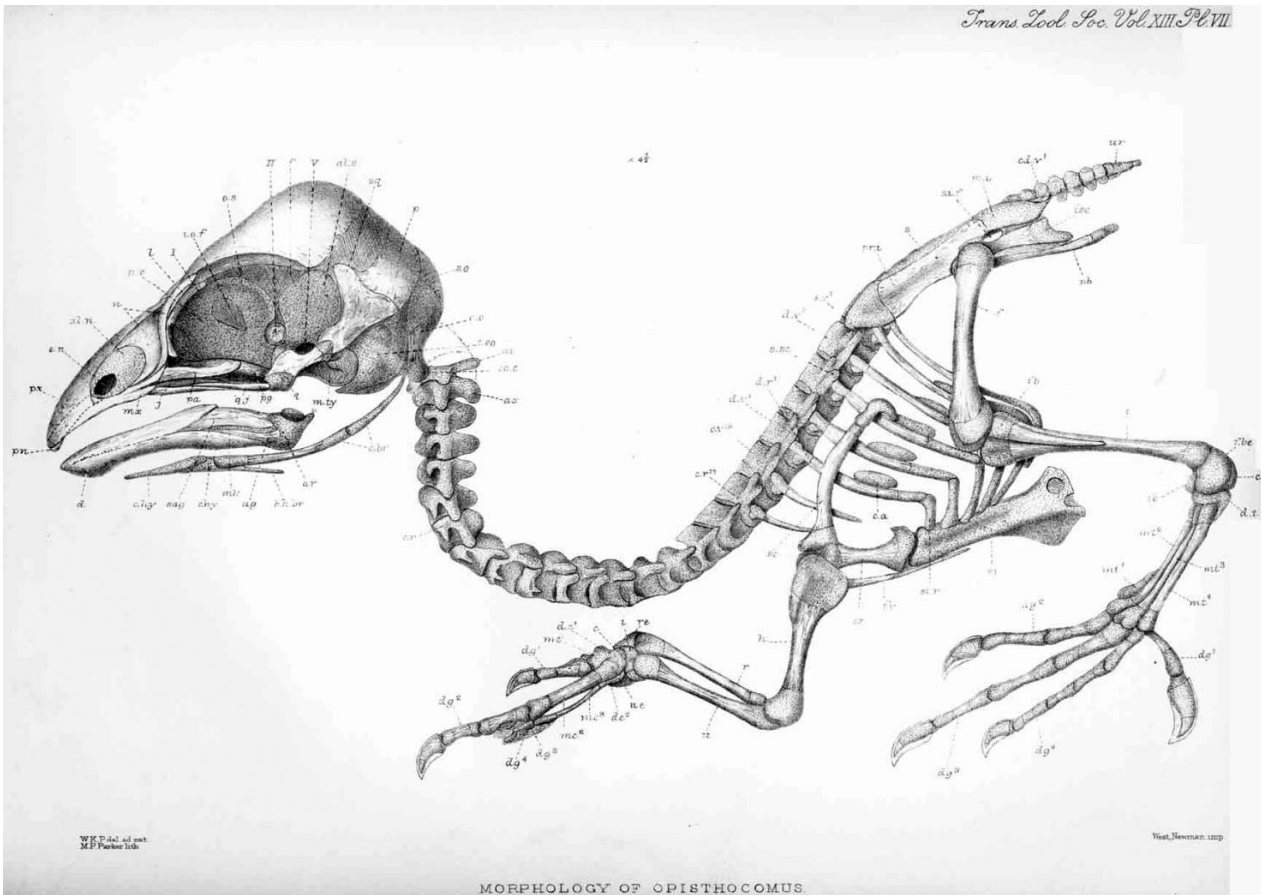


Figure 3: *Opisthocomus hoazin*: juvenile skeleton, lateral view after Parker (1891)

The claws on the wing are typically lost during growth but may be retained by some adults (Olson, 1992) (Strahl, 1988). The presence of a wing claw has been documented in several species of birds: nestling ducks, geese, kites, terns, avocets, pratincoles, godwits and coots have claws on digits one and two of the wing (Fisher, 1940). But the unique particularity of the hoatzin juvenile is that its two wing claws are fully functional and used to climb (Figure 4) (Abourachid et al., 2019).

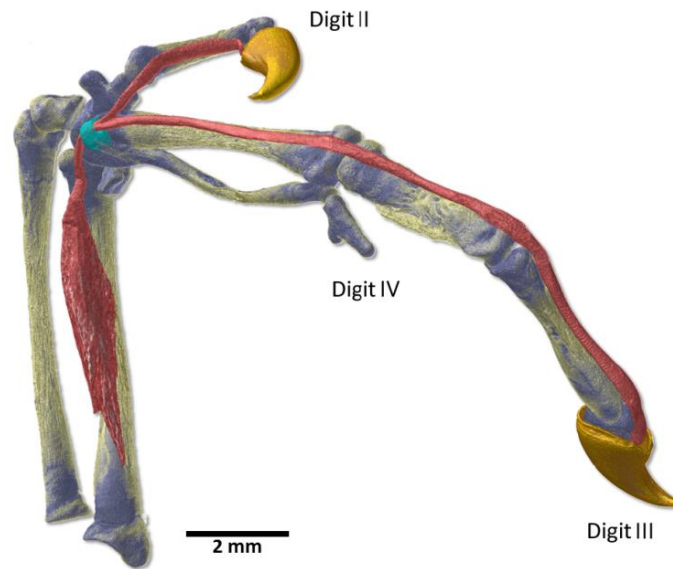


Figure 4: Musculoskeletal anatomy of a hoatzin shortly before hatching. Detailed reconstruction of the contrast-enhanced μ CT data of the wing (ventral view), with the position of the additional tendon of the flexor digitorum profundus attaching to the alula digit illustrated. Blue, cartilage; yellow, bone; red, muscle; cyan, connective tissue sling of the muscle tendon; orange, keratin. From Abourachid et al., 2019.

The exceptional size of the hypertrophied crop has consequences on the trunk morphology. The crop is placed in front of the sternum and pectoral muscles, just under the skin and surrounded by a muscular wall (Grajal, 1995). The shape of the sternum in the Hoatzin is highly modified to accommodate the large crop (Figure 2). The sternum has a markedly flattened posterior margin which the hoatzin has been suggested to use to rest on branches during the long digestion period (J. M. Hughes and Baker, 1999; Strahl, 1988). The keel of the sternum is described as very reduced, with very insertion area for the flight muscles. This modification on the sternum is suggested to induce a poor ability to fly (Gadow, 1892; Parker, 1868). Moreover, the sternum is completely fused to both coracoids and the furcula. These bones form a fused unit in the hoatzin trunk (Parker, 1868). The presence of functional claws on the wing in Hoatzin chicks, the reduced sternal carina, and the poor flying abilities reported in the literature of the Hoatzin have been regarded as 'primitive characteristics' and as such the Hoatzin has even been suggested to form a "missing link" between the first fossil birds such as Archaeopteryx and modern birds (Grajal, 1995; Parker, 1891).

Fossil record

Fossil record is well described taking into account the unresolved phylogeny of the group. The discovery of *Onychopteryx* is important in that the fossil demonstrates that opisthocomid-like birds had become differentiated by the early Eocene and that they were part of the South American avifauna by this time (Cracraft, 1971a).

The first reported fossil referable to Opisthocomiformes is *Hoazinoides magdalenae* from the Middle Miocene (Villavieja Formation, 11.8–13.5 mya) of Colombia. This documents the occurrence of hoatzins west of the Andes (Miller, 1953). This species was described from a cranium fragment and seems to be slightly larger than the extant hoatzin (Mayr, Alvarenga, and Mourer-Chauviré, 2011). The earliest fossil the Opisthocomiformes, *Hoazinavis lacustris*, was dated to the Oligo-Miocene (22–24 mya) and was found in Brazil. The bones, a humerus, scapula and coracoid, closely resemble those of the extant hoatzin and were confidently identified as an opisthocomiform bird (Mayr, Alvarenga, and Mourer-Chauviré, 2011). *Hoazinavis* differs from *Opisthocomus* in that the coracoid and furcula are not fused. *Namibiavis* (16mya Middle Miocene, south Namibia), has been discovered and associated to the Opisthocomiformes thanks to its hind limb characteristics (Mayr, 2014; Mourer-Chauviré, 2003). *Namibiavis* was of particular biogeographic significance because it is the only stem group representative of these birds that is known from Africa (Mayr, Alvarenga, and Mourer-Chauviré, 2011). The identification of hoatzin ancestors in the Miocene of Africa shows that part of the evolution of this group has taken place outside the Neotropics (Mayr and De Pietri, 2014). In the absence of North American opisthocomiform fossils, however, a transatlantic dispersal remains the most plausible hypothesis to explain colonization of the New World by hoatzins (Figure 5). Oceanic rafting is the most plausible explanation for transatlantic dispersal (Mayr and De Pietri, 2014).

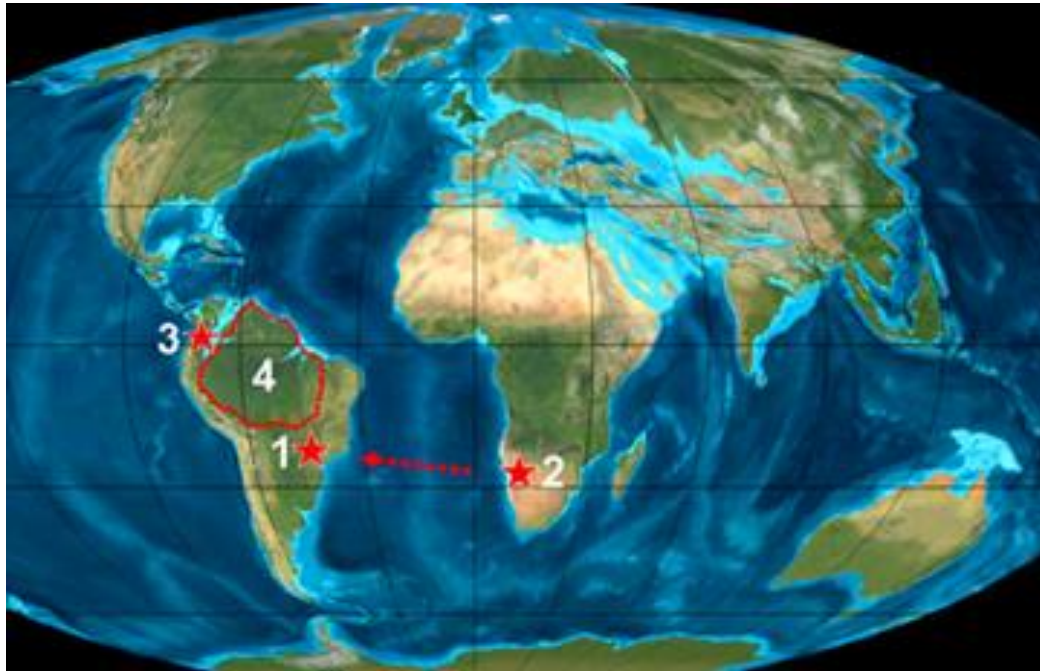


Figure 5: Palaeomap of the continents in the early Oligocene (35 mya). Asterisks indicate localities of *Hoazinavis lacustris* et (1), *Namibiavis senutae* (2), and *Hoazinoides magdalenae* (3). The distribution area of the extant *Opisthocomus hoazin* (4) is indicated by the lines. The arrow denotes the presumed direction of hoatzin dispersal. From Mayr et al., 2011.

Phylogeny

The phylogenetic placement of the hoatzin has been debated for many years. Because of its unusual morphological characteristics this species has been placed in its own family: the Opisthocomidae (Swainson, 1837). A direct descendant relationship with *Archaeopteryx* has been suggested (Parker, 1891) but rejected afterwards. The first morphological based studies hypothesized a relationship with the clade Galliformes (Korzoun, Erard, and Gasc, 2003). Subsequently the hoatzin has been associated with Cuculiformes and Musophagiformes, or has been suggested to have a sister group relationship with the clades Cariamidae and Musophagiformes (Livezey and Zusi, 2007; Mayr and Clarke, 2003; Queiroz and Good, 1988). The use of molecular data shed new light on its relationships. The first molecular analyses placed Opisthocomiformes in the Metaves group and resulted in a polytomy together with Musophagiformes, Phaethontidae, and a clade including Gruiformes, Charadriiformes, Mesitornithidae, Phoenicopteriformes and Podicipediformes (Fain and Houde, 2004). Further analysis by Hackett et al. (2008) supported a sister group relationship between Opisthocomiformes and a clade including the “waterbird assemblage”, Gruiformes, Cuculiformes, Musophagiformes and Otididae, but this grouping received no significant bootstrap

support. Although molecular data likewise do not strongly reject closer affinities to Cuculiformes and Musophagiformes (Mayr, 2011). The latest studies suggest that the Opisthocomidae is one of the oldest bird lineages (64 million years) consisting of only a single extant species and that they could possibly be sister group to all other landbirds (Figure 1-6) (Jarvis et al., 2015; Prum et al., 2015). This lineage has been supported by the fossil record, showing that opisthocomid-like birds had differentiated during the early Eocene in South America and the Oligo-Miocene of Brazil (Cracraft, 1971a; Jarvis et al., 2014; Mayr, Alvarenga, and Mourer-Chauviré, 2011).

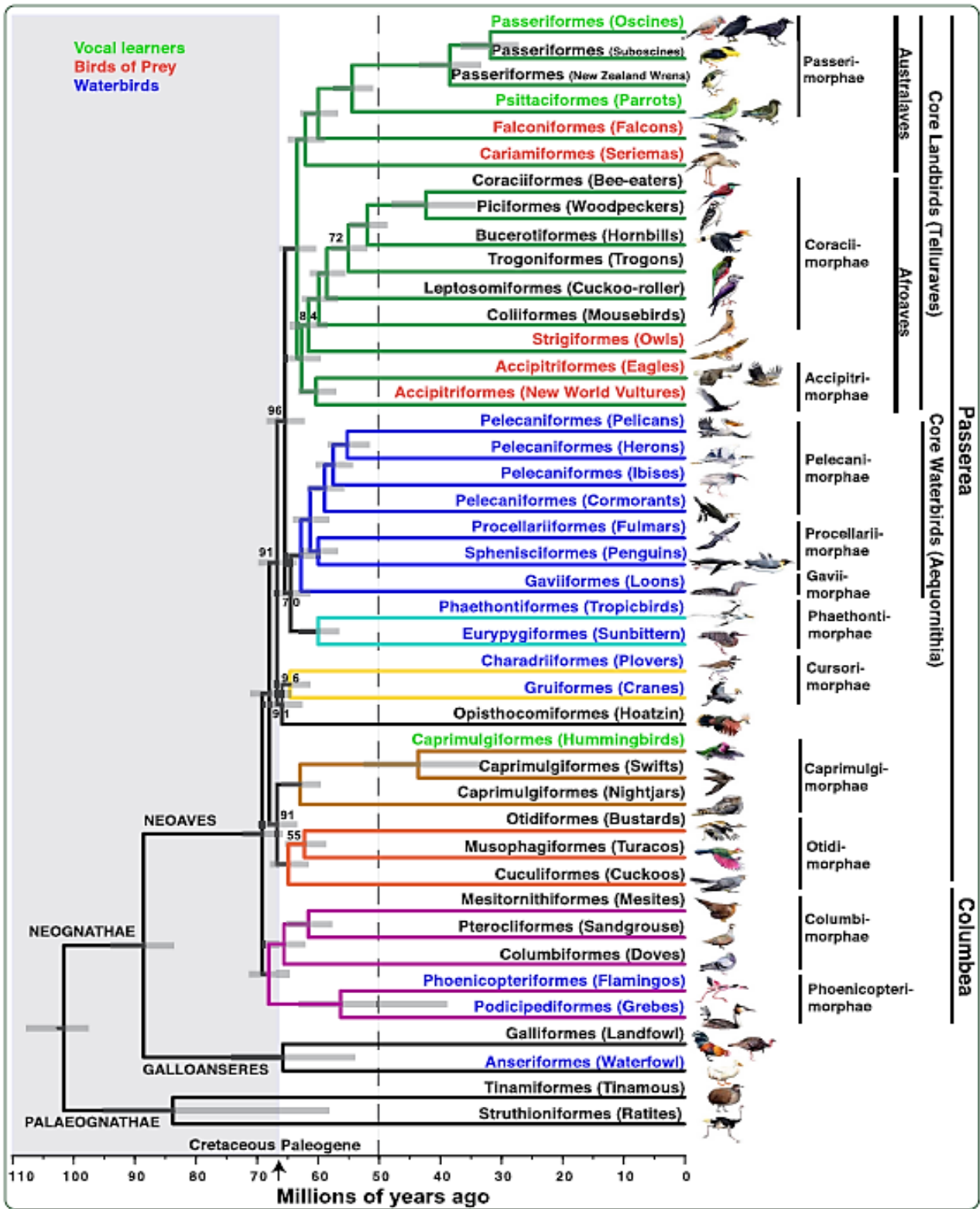


Figure 6: Bird phylogeny from Jarvis et al., 2014.

Goals

The aims of the present thesis are to describe the anatomy of the hoatzin in detail and to quantify the consequences of the impact of its unusual dietary specialization and the morphological consequences thereof on the shape and function of the rest of the skeleton. Finally, we explore the development of the different skeletal and some muscular elements to explore whether these unusual features develop.

In the first chapter, we describe the whole skeleton of the adult hoatzin in detail based on microcomputed tomography scans and 3D visualizations. Moreover, we highlight traits specific to the hoatzin in comparison to a data matrix established for 188 species of birds (Livezey and Zusi, 2006). We provide plausible functional explanations for the derived features of the hoatzin using the existing literature on bone morphology, muscle insertions, and muscle functions in birds.

This description showed that the scapular girdle of the hoatzin is the most unusual part of its skeleton. Indeed, most of the anatomical particularities of the hoatzin are observed on there. Thus, in the following chapters we focused on a comparative analysis of the scapular girdle of birds. To quantitatively study evolutionary changes in the morphology of the scapular girdle of birds, 3D geometric morphometric methods were used. As shape changes with functional significance may occur at articular surfaces as well as along the diaphysis, it was necessary to quantify the whole bone shape using surface landmarks.

Because the bone morphology could be impacted by preservation artifacts, we first decide to test the impact of the preparation on bone shape using osteological collections focusing both on intra and interspecific variability.

Next, we quantified the bones of the scapular girdle of 59 species from the MNHN collections to identify and quantify the effect of ecological traits on bone shape in birds. We gathered ecological information on each species of our study including flight types from the literature to test whether these ecological features impact bone shape. We then use these data to determine the most likely flight type of the hoatzin to test the assumptions from the literature about its modified keel and how it impacts its flight capacity.

Finally, we provide preliminary data on the development of the hoatzin, by describing the ossification sequence of the whole skeleton in comparison to other bird

species. We then focused on the development of the scapular girdle in embryos and juveniles based on contrast-enhanced micro computed tomography (μ CT) scans. We finally describe the development of the cranial muscles in the hoatzin.

Interest of geometric morphometric methods

Geometric morphometric methods aim to comprehensively capture phenotypic diversity (disparity), allowing a more accurate and precise representation of organismal morphology. Quantifying morphology has been a cornerstone of biology for centuries, and even more since the recent advances in specimen digitization. Specifically, computed tomography and surface scanning have allowed the efficient creation of digital specimen reconstructions (Bardua et al., 2019).

The geometric morphometric method has added to the sophistication of quantitative biological shape analysis, while at the same time making it easier to collect and analyze data to answer questions about shape of the phenotype (Lawing and Polly, 2010). Shape is the geometric information of an object after removing location, orientation and scale (Kendall, 1977) such as studies that address differences within and between species, developmental stability, the role of development in shaping evolution, and problems arising in addressing these issues in the fossil record (Lawing and Polly, 2010). The material studied in this thesis is entirely composed of 3D scans of whole and separated bones. The questions were about the bone shapes in relation to preparation or ecological traits. Thus, the geometric morphometric was the most suitable method.

**Chapter 1 - The skeletal anatomy
of the hoatzin (*Opisthocomus
hoazin*): functional consequences
of an extreme life-style?**

The whole skeleton of the hoatzin has not been described yet. Whereas some skeletal elements such as the limbs or the skull have been largely described in the literature (Korzoun, Erard, and Gasc, 2003; Parker, 1891) other ones remains undescribed. Previous anatomical studies have mainly focused on the diet implications on the skull morphology or the developmental growth of the functional wing claws (Stegmann, 1978). Furthermore, all these previous descriptions were using traditional dissection methods of collection specimens. In our study, we decided to take advantage of the recent 3D techniques allowing us to get access to part of the anatomy that can be difficult to access in order to describe more accurately the anatomy of the hoatzin.

Thus, a better understanding of the anatomical characters that made the hoatzin so unique among birds seems crucial to start this thesis. Here, the principal aim of our study is to provide a whole description of the skeleton anatomy of the hoatzin, in order to be able to determine which part of its anatomy seems to differ from other birds. Using Livezey and Zusi (2006) comparative work, we were able to highlight unique characters among birds present in the hoatzin. We also provided plausible functional explanations for the derived features of the hoatzin using the existing literature on bone morphology, muscle insertions, and muscle functions in birds.

The skeletal anatomy of the hoatzin (*Opisthocomus hoazin*): functional consequences of an extreme life-style?

Fanny Pagès, Anthony Herrel, Dominique Adriaens, Barbara De Kegel, Maria Alexandra Garcia Amado, Anick Abourachid

Submitted to Anatomical Record

Abstract

We here describe the skeletal anatomy of the hoatzin (*Opisthocomus hoazin*), the only extant species of the Opisthocomidae. The hoatzin presents peculiar life history traits, unique among extant birds. It is a strictly vegetarian species with a diet mainly based on young leaves. The esophageal crop is modified into a hypertrophied rumen-like structure and is positioned in front of the sternum. This feature has been suggested to impact the shape of the sternum. Moreover, young hoatzins have a feature unique among birds, i.e. two fully functional claws on their wings that they use to climb. Despite these unique features, the skeleton of the hoatzin has not been described since the first studies in the early 20th century. Moreover, our understanding of the anatomy and biology of the hoatzin remains largely incomplete. The aim of the present anatomical study is to illustrate and describe the entire skeleton based on μ CT data and 3D visualizations. We describe the morphology of each bone of the hoatzin and compare it to the descriptive character matrix of Livezey and Zusi (2007). Finally, we discuss features unique to the hoatzin from a functional point of view.

Keywords: 3D scans; skeleton, function, skull, limbs, vertebrae.

Introduction

Since the original description by Statius Muller in 1776, the hoatzin (*Opisthocomus hoazin*) has been the subject of considerable debate. It is unquestionably among the most bizarre and enigmatic birds in terms of its appearance, life history, morphological specializations and physiology (J. M. Hughes and Baker, 1999). Because of its unusual morphological characteristics, this species is placed in its own family: the Opisthocomidae (Swainson, 1837). Based on its external morphology and its internal morphology, the hoatzin was formerly associated to the Galliformes (Korzoun, Erard, and Gasc, 2003). This relationship has been refuted based on skeletal traits and since then the hoatzin has been assigned to several different groups including the Coliidae and Musophagidae (J. M. Hughes and Baker, 1999), Cariamidae and Cuculiformes (Mayr and Clarke, 2003), Columbidae (Brown et al., 2008; Sorenson et al., 2003), and then successively to Pteroclididae, Rallidae, Otididae, or Tinamidae (Livezey and Zusi, 2007, 2006). The use of molecular data shed new light on its relationships and suggested that Opisthocomidae is one of the oldest bird lineages (64 million years) consisting of only a single extant species (Jarvis et al., 2015; Mayr, 2011; Prum et al., 2015). This lineage has been supported by the fossil records, showing that opisthocomid-like birds had differentiated during the early Eocene in South America and the Oligo-Miocene of Brazil (Cracraft, 1971a; Mayr, Alvarenga, and Mourer-Chauviré, 2011).

In addition to the hoatzin's uncertain place in the phylogeny, it also shows original life history traits, unique among extant birds. One of them is the presence of claws on the wing claws in juvenile and embryonic hoatzins (Grajal, 1995; Parker, 1891; Strahl, 1988). Young hoatzins have two fully functional claws on their wings that they use to climb. They can jump from their nest into water if perturbed and are capable of climbing back to the nest through branches using their clawed wings (Müllner, 2004; Strahl, 1988). Recent data further demonstrate that the chicks move their wings with alternating movements when climbing, a locomotor mode not observed in other birds (Abourachid et al., 2019). Furthermore, the hoatzin is strictly vegetarian, with a diet mainly based on young leaves. It is the only folivorous bird with pre-stomachal fermentation in an enlarged rumen-like crop, analogous to what is observed in ruminant mammals (Fain and Houde, 2004; Grajal, 1995; Grajal et al., 1989). The size of the crop has been suggested to impact the shape of the sternum and the size of the pectoral

muscles as the carina is reduced, leaving little space for the insertion of these muscles (Figure 7; Korzoun et al., 2003). The furcula and coracoids are further completely fused with the sternum (Huxley, 1868; Perin, 1875).

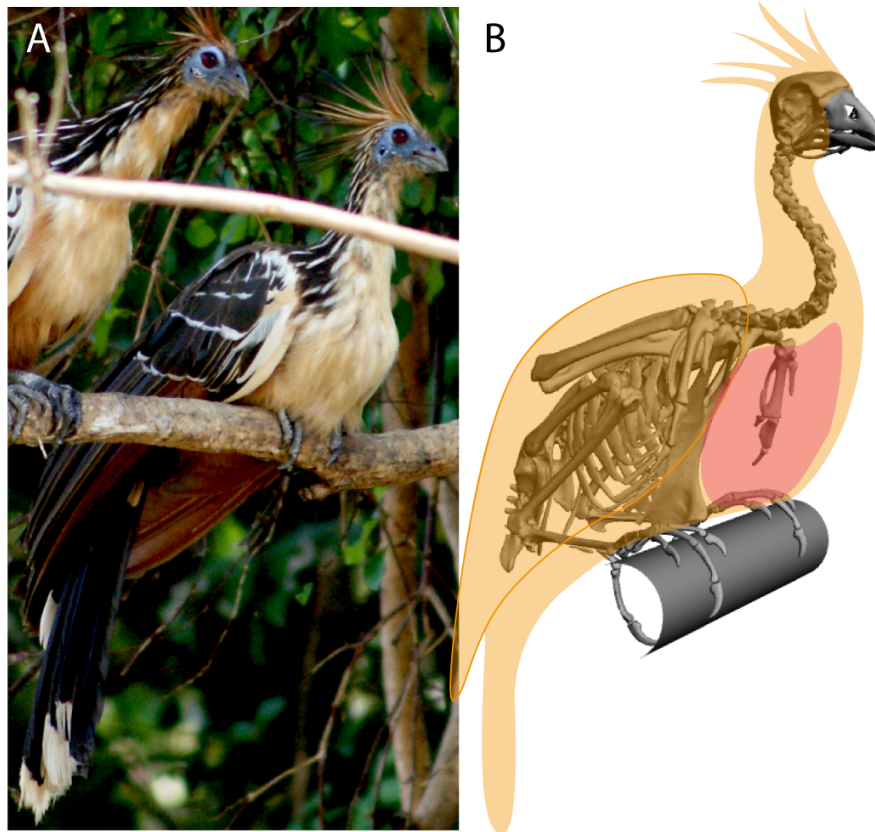


Figure 7: A: Field photograph of hoatzins, Venezuela, August 2015. B: Reconstructed skeleton of a bird in resting position based on the μ CT scan of an adult hoatzin specimen. The position of the crop is indicated in red after Godoy-Vitorino *et al.* (2008); the body and wing shape are indicated in orange.

Despite its unusual nature, the skeletal anatomy of the hoatzin is only partly known. Descriptions remain partial and focused on different parts of the skeleton (Beddard, 1889; Gadow, 1892; Garrod, 1879; Huxley, 1868; Mitchell, 1896; Parker, 1891; Perin, 1875; Shufeldt, 1918). The aim of the present study is to describe the skeletal anatomy of the adult hoatzin and to identify features of its morphology that appear unique and are likely linked to functional adaptations.

Material and methods

Our descriptions are based on μ CT scans of two adult hoatzin specimens collected in Venezuela in 2014. These specimens are further compared to two collection specimens (MNHN-ZO-AC-2012-378 and MNHN-ZO-AC-1997-802). Specimens collected in the field (material transfer agreement number: SJ MNHN 518-14) were preserved in a 10% formaldehyde solution for 48 hours, rinsed and transferred to a 70% aqueous ethanol solution. These specimens were scanned at Ghent University (www.ugct.ugent.be) using a PerkinElmer detector at 120 kV voltage and amperage 60 W with a 1mm aluminum filter. For each specimen, a series of 698 projections of 728 pixels and 1820 slices was recorded covering 360 degrees. The raw data were processed and reconstructed using the in-house developed CT software Octopus (Vlassenbroeck et al., 2007). This yielded virtual slices with a voxel size of 170 μ m. Each bone was segmented and separated in Avizo v.8.1 (FEI Visualization Sciences Group). We reconstructed the likely position of the skeleton of an adult at rest using Autodesk Maya software (v.2018), based on pictures taken in the field (Figure 1). The skeletal descriptions are based on the 3D slices and segmentations. However, in the 3D reconstructions and Figures some features are not visible because of the limited resolution of the scans, but were visible on collection specimens.

The anatomical nomenclature follows the *Nomina Anatomica Avium* (Baumel et al., 1993), Livezey and Zusi (2007), and Harvey et al (1969) when structures are not identified in the *Nomina Anatomica Avium*. We identified features specific to the hoatzin using the character matrix provided by Livezey & Zusi (2007). They used literature sources and their own observations to carry out a phylogenetic analysis based on the anatomical characteristics of bird skeletons. The authors defined the states of 2451 bone characters in 188 avian species, including the hoatzin, using unique codes. From this matrix, we determined the most common states among the 188 species, and the ones specific to the hoatzin. Thus, we were able to compare the anatomy of the hoatzin to the other bird species. Coded features identified as unique to the hoatzin are indicated in bold in the descriptions of the skeletal anatomy.

separately. Although bones are fused, delimitations between bones can still be observed on the CT slices.

Parietal

This paired bone is the most caudal one of the dorsal bones of the cranium. It is bounded anteriorly by the frontal, laterally by the temporal bone, and caudally by the dorsal border of the occipital complex. The parietal is quadrilateral in shape.

Frontal

The paired frontal bone is positioned at the anterior end of the braincase and limited by the parietal posteriorly. Its anterior limit with the upper jaw (lacrima and nasal) is straight. The posterior portion of the frontal forms the roof of the orbital fossa.

Mesethmoid

The mesethmoid lies medially under the anterior part of the frontal, to which it is fused. It is limited anteriorly by the upper jaw. The large lateral area of the mesethmoid is bounded by (but not fused to) the lacrima. In the hoatzin, this bone extends caudally to form much of the osseous part of the interorbital septum

Squamosal

The paired squamosal is a laterally positioned bone, surrounded by the occipital caudally, the parietal dorsally, the quadrate lateroventrally, the sphenoid complex ventrally and the frontal anteriorly. The squamosal forms the lateral wall of the posterior cranium and contains the inner ear. It has two processes: a zygomatic process and an anterior postorbital process, lying dorsal to the latter. The long and thick postorbital process forms the caudoventral border of the orbit.

The occipital complex

The occipital complex is the most caudal group of bones of the cranium and is composed of the supraoccipital, exoccipital and basioccipital bones. It is bounded dorsally and anteriorly by the caudal border of the parietals, laterally by the caudal border of the squamosum, and ventrally by the caudal border of the sphenoid complex. The occipital complex surrounds a caudodorsally oriented foramen magnum, bounded cranially by the supraoccipital bone, laterally by the exoccipital bones and ventrally by the basioccipital bone. Ventral to the foramen magnum, a single occipital condyle

articulates with the atlas. During extreme ventral flexion of the skull, a subcondylar fossa, ventral to the base of the occipital condyle, receives the body of the atlas. Two pairs of occipital foramina are situated lateral to the occipital condyle: the opening for the carotid and more laterally the vagus nerve foramen.

The sphenoid complex

The sphenoid complex is composed of the basisphenoid, parasphenoid and orbitosphenoid bones. The basisphenoid bone is located under the skull, bounded by the squamosals and the basioccipital bone. The caudal portion of the basisphenoid is extended by the basitemporal plate, whereas the rostral part of the basisphenoid extends dorsomedially to join the vomer. The parasphenoid element lies anterior to the basisphenoid and forms the posterior border of the orbits. The orbitosphenoid forms most of the dorsal part of the caudal wall of the orbit, and extends from the interorbital septum laterally to the postorbital process.

Upper jaw

The upper jaw is composed of the lacrimal (bounding the orbits) fused to the nasal (postero-dorsal), premaxilla (antero-medial), maxilla (antero-lateral), jugal (latero-ventral), palatine (postero-medial) and vomer (antero-medial). The nasal, premaxillary and maxillary bones form the border of the nasal cavity in the caudal half of the upper beak (upper jaws without quadratojugal and jugal bones). The upper beak forms the bony support for the rhamphotheca. The nostrils are oval with a dorsally oriented elongation. The upper beak (from the nasofrontal suture to the tip of the premaxilla bone) represents 48% of the total length of the skull. The upper edge of the beak is arched and each side is swollen on its posterior part with a medial compression on the anterior part of both sides. The craniofacial flexion zone is transversally oriented to the braincase and bulges at its contact with the upper jaw bone.

Lacrimal

The lacrimal is well developed, bearing two dorsolateral projections. The supraorbital process forms the rostral wall of the orbit, separating it from the nasal cavity. The second process is forked: the main fork sometimes is dorsally oriented and the minor fork braces the jugal bar. The anterior part of the lacrimal is solidly fused to the nasal,

rostral to the craniofacial flexor zone (**C0566**). The thick lateral part of the lacrimal is S-shaped.

Nasal

The nasal is bounded caudally by the frontal, laterally by the supraorbital process of the lacrimal, and medially by the nasal process of the premaxilla. Ventrally it is fused with the maxilla, premaxilla, and palatine. It is composed of three processes; a dorsocaudal frontal process, a lateral premaxillary process and an anterior maxillary process. The three processes form the caudolateral and medial borders of the external nostrils. The nasal is convex laterally and concave toward the midline. Its caudal border is separated from the front of the braincase by the nasofrontal suture (**C0566**). The nasal septum lies at the medial aspect of the nasal aperture. Its caudal border meets the ventral process of the mesethmoid and is bounded by the mesethmoid caudally, the vomer ventrally, the oblique process of the vomer cranially, and dorsally by the caudal fourth of the nasal process of the premaxilla.

Premaxilla

The premaxilla forms the upper part of the upper beak and the anterior border of the nasal aperture. It bears three pairs of caudally projected processes. The frontal process extends to the frontal, overlays the mesethmoid and is bounded laterally by the nasal. The maxillary process of the premaxillary joins the premaxillary process of the nasal medially and the anterior extensions of the palatine and maxilla at its caudal limit. The thin palatine process extends caudally and joins the palatine process of the maxillary.

Maxilla

The maxilla is curved, concave and pointed at its rostral extremity. The lateral parts bulge outwards. The maxilla extends caudally from the maxillary process of the nasal and connects to the jugal through the jugal process of the maxillary. The maxilla is bounded rostrally by the maxillary process of the premaxilla, visible as a lateral compression on the side of the skull. Caudally, the maxilla forms the premaxilla process. The palatine process projects caudally and runs parallel but medial to the maxillary process. The maxillopalatine process contributes to the formation of the nasal cavity.

Quadratojugal

The quadratojugal is long and thin. At its caudal limit it articulates with the ventral process of the quadrate. It extends anteriorly to about the middle of the ventral orbital region where it fuses with the caudal projection of the jugal.

Jugal

The jugal lies dorsally over the cranial projection of the quadratojugal and the caudal projection of the maxilla. The jugal is thick and oblique and is connected to the maxilla.

Palatine

The palatine is triangular and fused to the long and thin palatine process of the maxilla. Towards the back, the right and left palatines are separated. The pars lateralis is convex dorsally and concave ventrally. The palatine articulates with the medial articular surface of the pterygoid with very thin bony processes (which is not visible on the μ CT scan because of the resolution but clearly identifiable on collection specimen). The palatine is part of the caudal part of the interorbital septum.

Vomer

The vomer is slender and very long. The rostral part bulges outwards and is bifid. It is caudally linked to the rostral part of the basisphenoid. This bone does not have a direct link with the palatines.

Quadrate

The quadrate is Y-shaped with three processes. Its otic process projects dorsocaudally to articulate with the squamosal bone, the orbital process projects anteromedially in a line parallel with that of the pterygoid with which it articulates, and its mandibular process articulates with the quadratojugal and the lower jaw. The mandibular process is composed by four condyles transversally oriented: the largest is the lateral condyle which has a large contact area with the quadratojugal bone and smaller contact with the lateral process of the articular bone of the lower jaw; the medial condyle presents a large articulation with the articular bone of the lower jaw; the smallest is the caudal condyle which is not in contact with any bone but is in front of the retroarticular process of the lower jaw. The pterygoid condyle articulates with the quadrate process of the pterygoid bone. The otic process has two small condyles, the

prootic one and the squamosal one. Both condyles are participating to the articulation of the quadrate with the braincase. The orbital process is not in contact with any bone.

Pterygoid

The pterygoid lies medial to the quadrate and lies caudoventrally under the orbit. It articulates laterally with the pterygoid condyle of the mandibular process of the quadrate and the caudal limit of the palatine (through a very thin bony process, not visible on the Figure and the μ CT scans, but clearly visible on collection specimens). This bone is positioned obliquely relative to the skull.

Lower jaw

All the elements of the lower jaw are fully fused in the adult hoatzin. Each ramus of the mandible is considered to consist of six bones. The lower jaw is composed of the dental, splenial, supra angular, angular, prearticular and articular bones. The posterior part of the lower jaw articulates with the braincase by means of the quadrate bone (Figure 9).

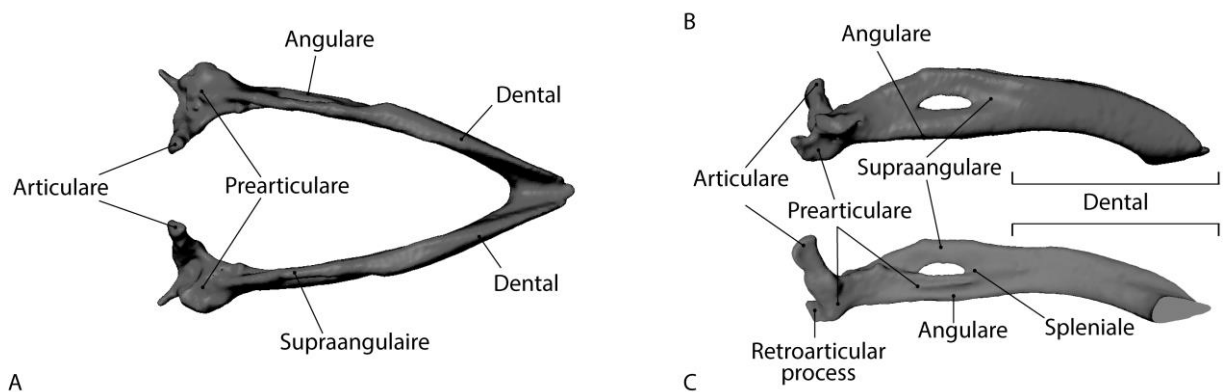


Figure 9 : (A) dorsal view of the entire lower jaw; (B) lateral view; (C) medial view of right hemi-mandible of the adult hoatzin.

Dental

The dental bone is the rostral part of the lower jaw and has a triangular shape. This is the principal element of each mandibular ramus; it lies in contact with the supraangular and splenial bones.

Splénial

This bone lies medial to the supraangular and is bounded rostrally by the dental, dorsally by the prearticular and ventrally by the angular bone.

Supraangular

This bone is bounded by the dental and the prearticular, and positioned above the angular. It borders the cranial part of the caudal mandibular fenestra and bears a coronoid process that is medially oriented.

Angular

This bone is bounded by the dentary and the prearticular. It is caudally oriented and lies beneath the prearticular and supraangular.

Prearticular

This bone is bounded ventrally by the splénial, the angular, anteriorly by the supraangular and dorsocranially by the articular. It is the caudal part of the bones surrounding the caudal mandibular fenestra.

Articular

This bone is the most caudal part of the lower jaw and is bounded rostrally by the prearticular. It presents three processes: a lateral process which articulates with the lateral condyle of the quadrate, an elongated medial one which is oriented towards the caudal part of the squamosal bone and which include a medial cotyle forming the articulation with the medial condyle of the mandibular process of the quadrate. It contains no sesamoid bones, and finally the retroarticular process which is caudally the most developed.

Hyoid apparatus

The hyoid apparatus lies between the mandibles and is partially embedded in the tongue (Figure 10). It is composed of seven units that are variably ossified from bony to mineralized cartilage (all clearly identifiable on μ CT scans, Figure 10C): the paraglossum (paired, bony); the basihyal (single, bony); the urohyal (single, cartilaginous); the ceratobranchials (paired, partly ossified); and the epibranchials (paired, cartilaginous).

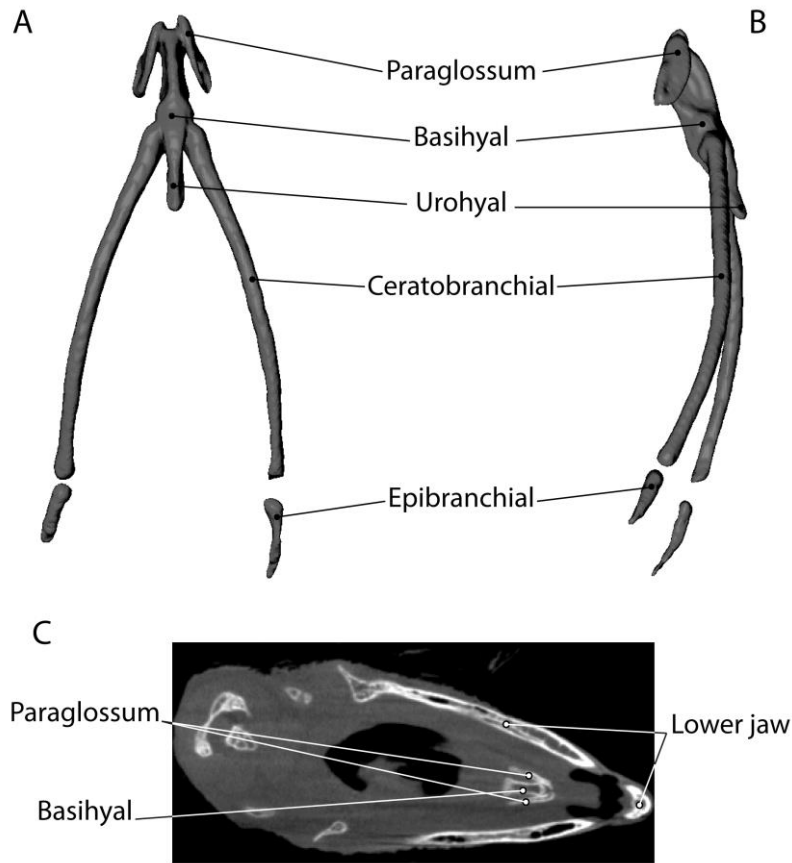


Figure 10 : Hyoid apparatus in dorsal view (A) and right lateral view (B) of an adult hoatzin. μ CT scan image of the hyoid apparatus (C) and hoatzin skull in transverse view.

Paraglossum

The paraglossum is convex caudally and concave cranially. It is separated in two parts that form two articulations with the medial basihyal (they seem partially fused to the basihyal, but this might be an artifact of the μ CT scan resolution; this could not be verified on the collection specimens where the hyoid apparatus is absent). The two parts are V shaped and the tip is rostral but not fused.

Basihyal

It is convex on its ventral surface and has a ridge on the dorsal surface medially. It is caudally fused to the urohyal. It has three articulating surfaces: a cranial one for the articulation with the two paraglossal bones; and two caudolaterally for the articulation with the ceratobranchials.

Urohyal

The median urohyal lies on the ventral surface of the larynx. It is styliiform in shape, large and directed caudally. It is fused to the basihyal rostrally.

Ceratobranchial

The ceratobranchial lies between the basihyal and the epibranchial. It is very long and styliiform.

Epibranchial

The epibranchial is very short, curved, and directed dorsally. The joints between the epibranchials and the ceratobranchials are the least mineralized but visible on the 3D data.

Vertebral column

There are fourteen cervical vertebrae in the hoatzin including the atlas and axis (Figure 11 A-E). The articular facets of the vertebral corpus are heterocoelous, with saddle-like articulating surfaces, convex cranially and concave caudally. On each vertebra, laterally projecting zygapophyses form an anti-twist interlocking system. The cranial zygapophyses extend cranially to the corpus, with upward-facing articular facets. The caudal zygapophyses extend caudally with downward-facing articular facets. The caudal zygapophyseal articular facets are more or less oblique, fitting the inverse facet of the next cranial zygapophysis. In addition to the zygapophyses, processes like the spinal processes, increase the insertion surface for the muscles. Arches, including the carotid arch, protect blood vessels. Depending on their place in the column, the vertebrae have different shapes, with more or less developed processes.

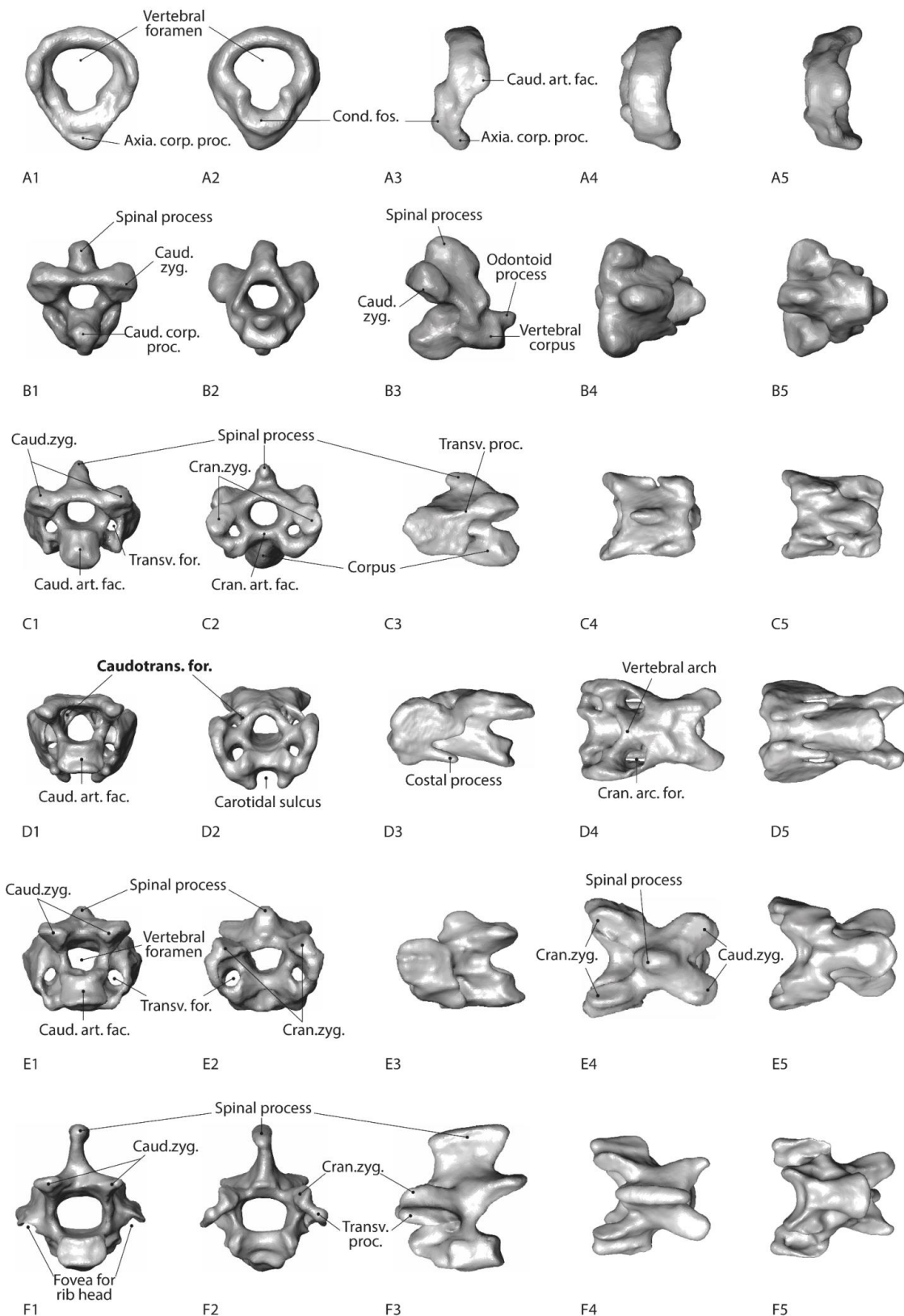


Figure 11 : Overview of the different cervical vertebrae: atlas (A), axis (B), fourth vertebra (C), ninth vertebra (D), thirteenth vertebra (E), sixteenth vertebra (D) in caudal view (1), cranial view (2), left lateral view (3), dorsal view (4) and ventral view (5). Bold characteristics are specific to the hoatzin and differ from those of most of other bird species; based on Livezey and Zusi (2007). Abbreviations: Axia.corp.proc.: axial corpus process; Caud.art.fac.: caudal articular facet; Caud.zyg.: Caudal zygapophyse; Caudotrans.for.: caudotransversal foramen; Cran.art.fac.: cranial articular facet; Cran.arc.for.: cranial arcocostal foramen; Cran.zyg.: Cranial zygapophyse; Cond.fos.: Condylloid fossa; Transv.for.: Transverse foramen; Transv.proc.: transverse process.

Atlas

The first vertebra is the smallest with roughly a ring-like shape. It articulates with the occipital condyle ventrocranially and with the second vertebra, the axis, via a convex articular facet under the condyloid fossa caudally.

Axis

The axis articulates with the atlas via the odontoid process, which sits at the top of the atlas articular facet. The odontoid process inserts in the condyloid fossa of the atlas. In contrast to previous descriptions (Livezey and Zusi 2006, Figure 11 F), no interzygapophyseal arch was present in any of our specimens (**C0795**).

Cervical vertebrae

The 3rd, 4th and 5th vertebrae are similar but their length increases from 3rd to 5th. The shape of the 3rd to 5th vertebrae is roughly rectangular in dorsal view. The spinal process is positioned in the middle of the vertebrae. They have rather short cranial and caudal zygapophyses. The oblique transverse crest, which extends caudally to the cranial zygapophysis, joins the caudal zygapophysis dorsocaudally. Transverse foramina lie behind the transverse processes (**C0829**). The 6th vertebra has a dorsal spine as in the preceding vertebrae, but a carotid sulcus as in the next ones. The 7th, 8th, 9th, 10th and 11th vertebrae do not have dorsal spines. The vertebral corpus is more cranial than the vertebral arch and the cranial zygapophyses extend cranially. The articular facets lie medially. The cranial arcocostal foramina are large. They receive the preceding caudal zygapophyses during dorsal flexion. The caudal zygapophyses extend caudally to the central articular facet. Their articular facets are ventral and rather thin and round. Ventrally, two costal processes extend caudally, lateral to the carotid sulcus. The 12th to 15th vertebrae do not have arcocostal foramina. The carotid sulcus is smaller on the 12th vertebrae and is lacking on the next ones, whereas the neural spine size is small on the 12th vertebrae and then increase on the next ones. The 15th vertebra does not have a transverse foramen.

Thoracic vertebrae

The 16th vertebra, the first thoracic vertebra, bears a short rib (Figure 11 F). The cranial zygapophyses are shorter, and positioned at the same level as the articular facet of the vertebral corpus. The transverse processes are larger. A fovea for the costal head lies laterocranially on the vertebral corpus. The 17th to 20th vertebrae are fused in the notarium (Figure 11 A). The vertebral ribs articulate on the transverse processes and the vertebral corpus. A pneumatic foramen is positioned ventrally on the corpus of the last fused vertebrae (**C0850**). The 20th vertebra has the same structure as the previous ones but is not fused in our specimens. The 23th and 24th bear ribs which are fused with the synsacrum, under the ilium.

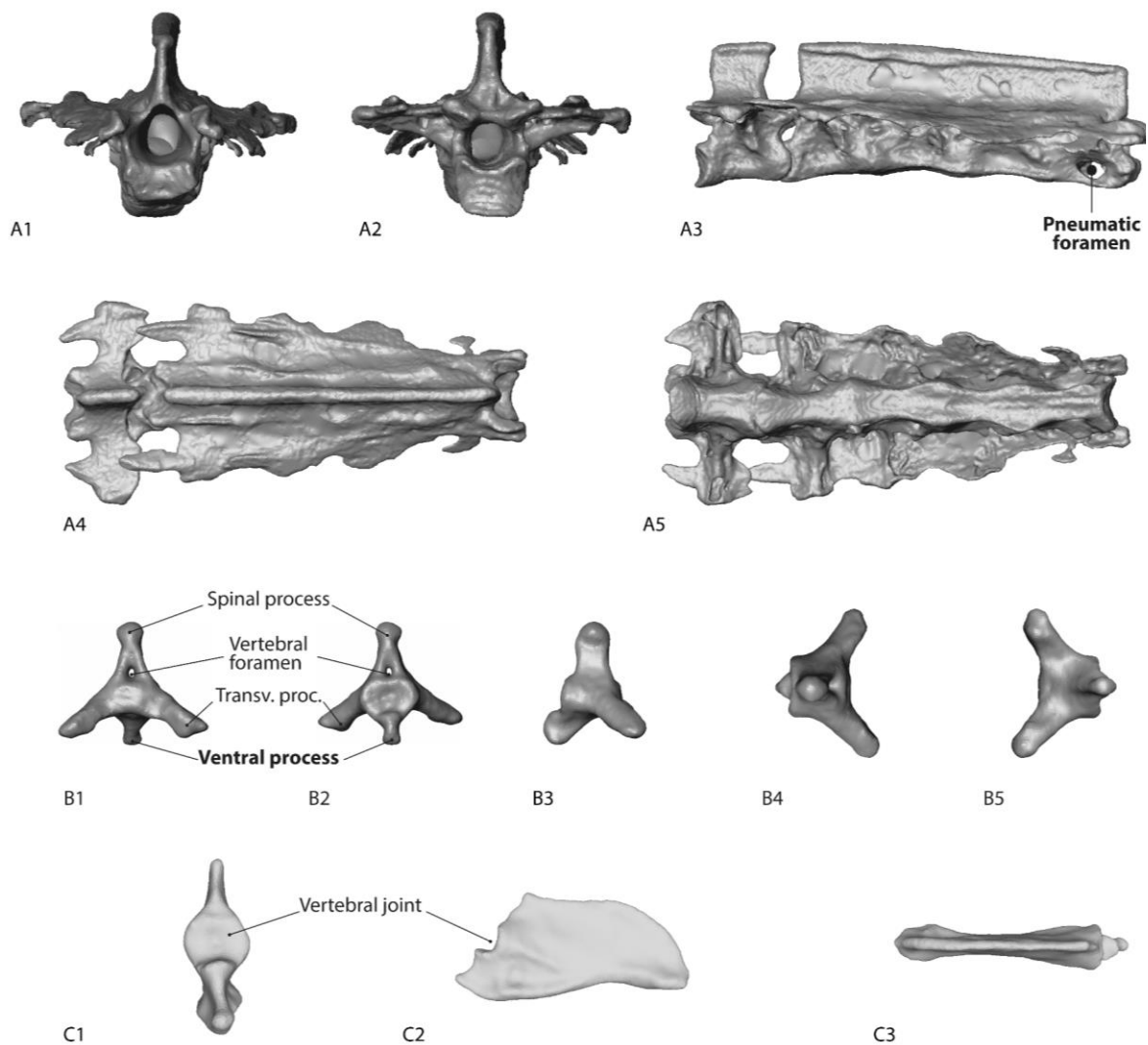


Figure 12: Dorsal vertebrae (A) and caudal vertebra (B) in caudal view (1), cranial view (2), left lateral view (3), dorsal view (4) and ventral view (5). Pygostyle (C) in cranial view (1), left lateral view (2) and dorsal view (3). Bold characteristics are features of the hoatzin which differ from those in most of the other bird species; based on Livezey and Zusi (2007).

Dorsal and caudal vertebrae

The next vertebrae are fused with the synsacrum, covered by the ilium cranially, until the acetabulum. In the caudal part, the lateral processes only are fused laterally to the ilium (**C0959**). Three free caudal vertebrae have a small neural canal, with a neural spine and a pair of transverse processes on the vertebral corpus (Figure 12 B). The 4th caudal vertebra has no neural canal. Finally, the pygostyle ends the vertebral column (Figure 12 C).

Ribs

The hoatzin has eight pairs of bicephalic ribs articulated to the thoracic vertebrae, one head articulating with the transverse process and one with the vertebral corpus (Figure 13). The first two ribs are short, styliform and incomplete, lacking the part articulated with the sternum. The 3rd is incomplete but enlarged. The next five ribs are in contact with the vertebra and the sternum (complete ribs) and are composed of two parts: the vertebral part, in contact with the vertebral joint and the sternal part which joins with the sternum. The ribs articulate laterally with the sternum. The vertebral part is flattened and very wide, including the modified uncinat process (**C1063; C1064**). The sternal part is shorter than the vertebral part. The 8th sternal rib is thinner than the previous ones and more rounded in cross section.

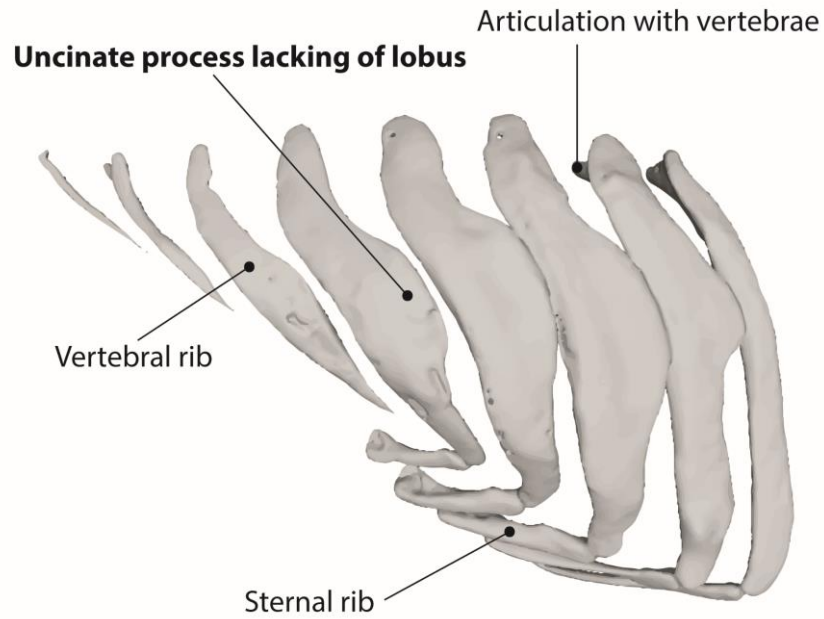


Figure 13 : Left lateral view of the rib cage composed of the vertebral ribs and the sternal ribs. Bold features are specific to the hoatzin and differ from those observed in most of other bird species; based on Livezey and Zusi (2007).

Pectoral girdle

The scapula remains free of the sternum complex (Figure 14 A).

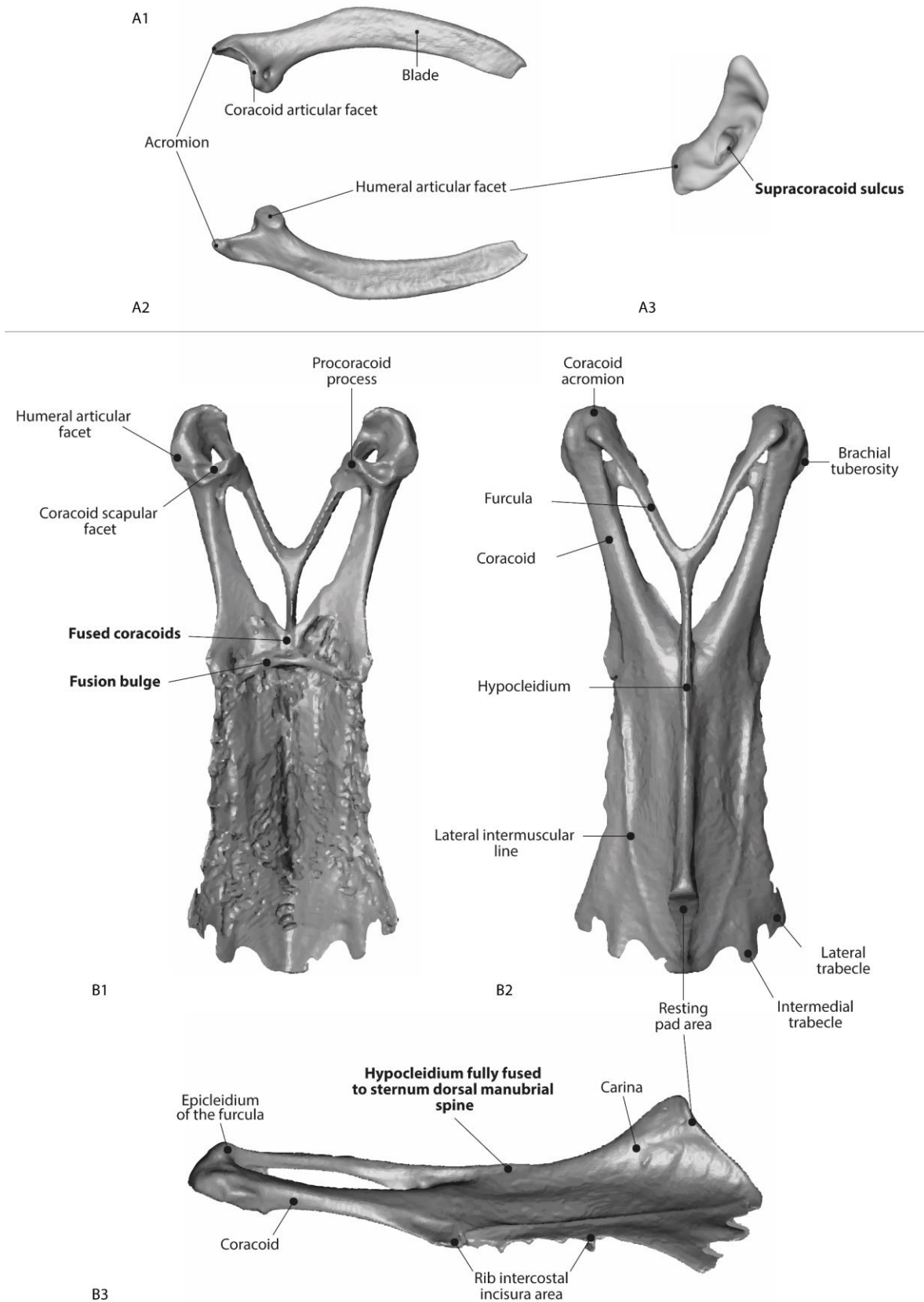


Figure 14 : Overview of the scapular girdle of the adult hoatzin. Left scapula (A) in lateral view (1), medial view (2) and cranial view (3). Sternum, coracoids and furcula which are fully fused (B) in dorsal view (1), ventral view (2) and lateral view (3). Bold features are specific to the hoatzin and differ from those observed in most of other bird species; based on Livezey and Zusi (2007).

The furcula, the coracoids and the sternum are completely fused in the adult hoatzin (Figure 14 B; note that fusion between the furcula and coracoids was not described by Mayr and Clarke, 2003). The sutures are still visible on μ CT scans and collection specimens allowing us to describe the approximate shape of each bone separately.

Scapula

The ventral face of the scapula lies over the ribs along the rib cage (Figure 14 A). It is a long, dorsally convex, arrow-like blade. The head of the scapula articulates with the coracoids via the acromion which is well developed and projects cranially (C1252). It articulates with the furcula ventromedially and with the humerus laterally. The humeral articular facets of the scapula and the coracoid form an articular socket for the head of the humerus. On the head of the scapula on the frontal side, the supracoracoid sulcus is marked by a deep foramen.

Furcula

The furcula is Y-shaped with a long and styliform caudal process: the hypocleidium which extends beyond the synostosis of the right and left clavicles until the beginning of the sternal carina, where they are fused (C1318). The extremities of the craniodorsal projections of the furcula, the epicleidia, are completely fused with the acromia of the coracoids.

Coracoid

The coracoid extends medioventrally from the shoulder apex where it is fused to the furcula and the cranial facet of the sternum. Caudally, it is fused with the sternum forming a bulge (C1329). Both coracoid bones are in contact caudomedially (C1331). The coracoid shaft is tubular. The brachial tuberosity is laterally oriented. On the head of the coracoid, the horizontal humeral articular facet is caudodorsally positioned. The acromium is medial and cranial to the humeral facet, near its point of fusion with the clavicle. The procoracoid process is medially and ventrally oriented and long enough to fuse with the furcula. This part is flattened, enlarged and curved.

Sternum

The sternum is the most ventral of the thoracic bones. The coracoid and furcula are fused with the sternum cranially and the sternal ribs articulate laterally. The manubrial

foramen is absent in the hoatzin. The craniolateral process is absent too (**C1140**). The lateral trabeculae and the intermediate trabeculae are reduced to two small processes with the same length and are caudally positioned. The sternal intercostal incisura is large, around half the length of the sternum. The dorsal manubrial spine is very reduced and fused with the hypocleideum. The lateral intermuscular line is well developed and prominent. The carina is developed caudally from the half of the sternum to the caudal extremity (**C1195; C1199**). At the caudal extremity the carina is enlarged and concave, it forms the “resting” pad. The carina is thin but robust. The pneumatic fossae appear to be covering the entire dorsal side of the sternum.

Wing bones

Humerus

The humeral head articulates with the humeral facet on the coracoid and scapula (Figure 15 A). The humerus articulates distally with the ulna and the radius. The proximal extremity has a deltopectoral crest dorsally and a convex bicipital crest laterally. A very reduced transversal ligament sulcus lies between the head and bicipital surface which is positioned between the bicipital furrow (facies bicipitalis) and the bicipital crest. The bicipital crest is ventrally positioned and has a sharpened edge. From a medial view, the proximal expansion of the humerus proximally shows towards the articular surface of the head, an incisura capitis that is well-marked and a pneumotricipitalis fossa adjacent to the bicipital crest. In the ventral view, there are two well-developed tuberosities: the angular dorsal tuberosity and the ventral tuberosity. The shaft of the humerus is tubular, dorsoventrally curvilinear and craniocaudally sigmoidal (**C1436**). The distal end has a round brachial fossa on the laterodistal surface of the shaft. Ventrally lies the dorsal epicondyle and a proximally positioned superficial pronator muscle attachment. Adjacent lies the ventral condyle and the dorsal condyle, separated by a large brachial fossa. Each condyle has a roughened epicondyle called ventral and dorsal epicondyles. The distal extremity is convex medially. In a medial view, the olecranon fossa is a slight depression lying dorsally and adjacent to the entepicondyle. The dorsal condyle is pronounced and the medial epicondyle is flattened.

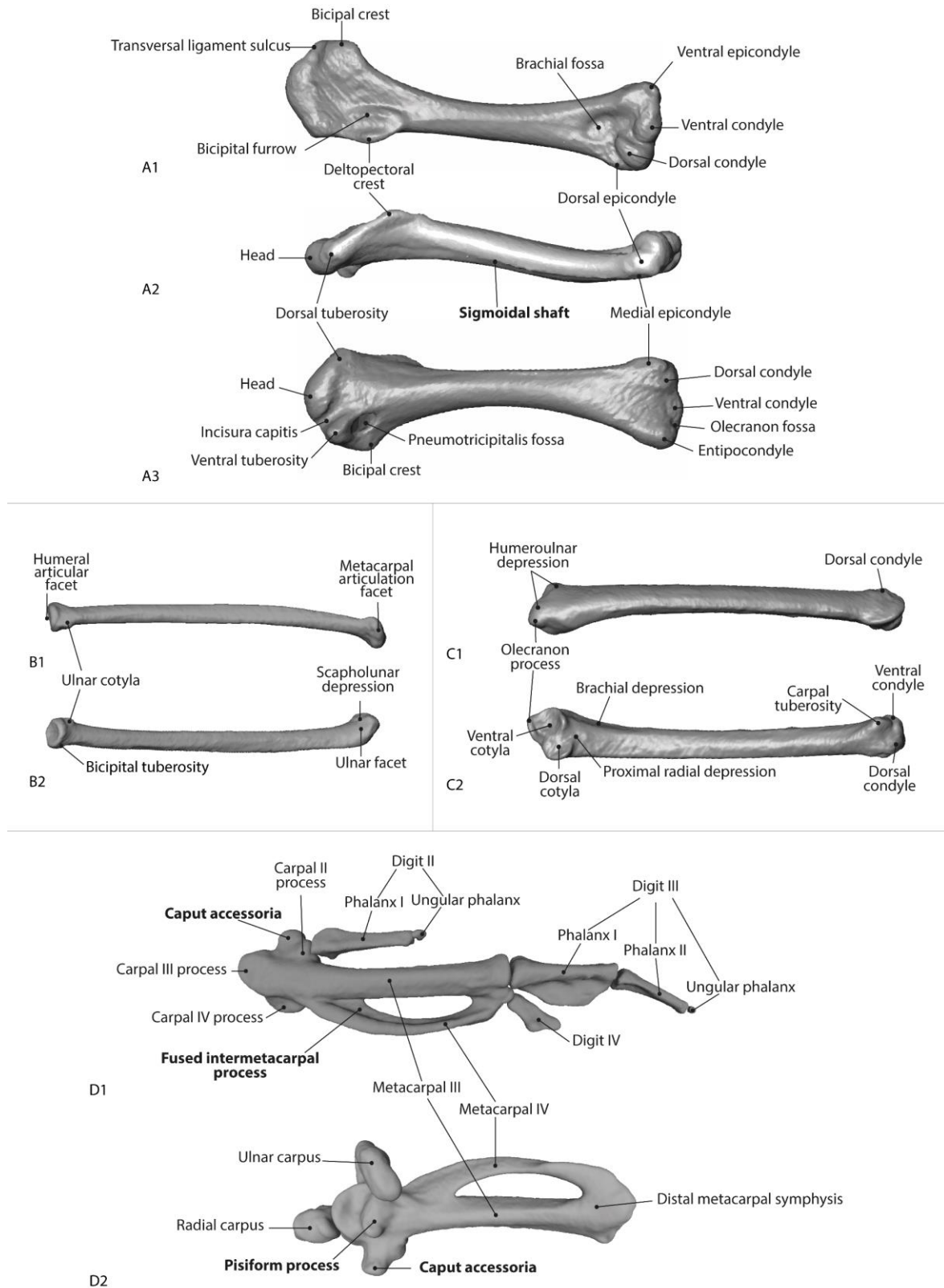


Figure 15 : Overview of the wing bones. Right humerus (A) in lateral view (1), dorsal view (2) and medial view (3). Radius (B) in dorsal view (1) and ventral view (2). Ulna (C) in dorsal view (1) and ventral view (2). Right hand bones (D) are represented in biological position in dorsal view (1) and ventral view (2). Bold features are specific to the hoatzin and differ from those observed in most of other bird species; based on Livezey and Zusi (2007).

Radius

The radius articulates proximally with the dorsal condyle of the humerus and distally with the radial carpus (Figure 15 B). The radius is concave on its ulnar face and convex dorsally. It is a long and cylindrical bone with a round, proximally articulating head. The distal articulating head is flattened and curved. Adjacent to this head, a well-developed bicipital tuberosity is visible in ventral view. The distal head is composed of a scapholunar depression where the radius articulates with the ulna.

Ulna

The ulna articulates proximally with the ventral condyle and to some extent with the dorsal condyle of the humerus and with the head of the radius (Figure 15 C). Distally the ulna articulates with the radius, the carpal bones and the metacarpus. At the proximal articulation the olecranon process is situated. Just distal to this process lies the ventral cotyla which is the large concave humeral articular surface. The dorsal cotyla is a large area distal and lateral to the ventral cotyla. A brachial depression lies below the ventral cotyla. This part of the bone is medially curved. At the distal extremity of the ulna, the ventral and dorsal ulnar condyles form a trochlear surface. Just ventral to the ventral condyle is a well-developed and compressed carpal tuberosity.

Carpus

The carpal bones are not fused with the metacarpus, the radial carpus articulates with the ulna and radius and with the metacarpus (Figure 15 D1). The radial carpus is very angular. The ulnar carpus is concave, elongated, curved dorsally and positioned perpendicular to the ulna (C1569; C1572).

Metacarpus

The metacarpus articulates with the ulnar carpus, radial carpus and ulna proximally and with digits II (alulae), III (major) and IV (minor) distally (Figure 15 D; digit number consensus based on De Bakker et al., 2013). The intermetacarpal process is completely fused along the metacarpal IV in the adult hoatzin, forming a flattened part of this bone: a large sulcus for muscle insertion (C1658). Metacarpal III is long and cylindrical and is thicker than the more flattened metacarpal IV. These two bones are separated by an inter-metacarpal space but meet proximally at the proximal metacarpal synostosis and distally at the distal metacarpal synostosis. At the distal extremity of metacarpal II is a

facet for the articulation with digit II. Articular facets for digits III and IV are present at the distal extremities of metacarpals III and IV. The pisiform process is prominent and projecting from the bone (**C1637**). The trochlear carpal is poorly developed and almost not visible as is the trochlear carpal III. The carpal II presents a caput accessoria (supernumerary belly: **C1651**).

Sesamoids

No sesamoid bones are visible, neither on the μ CT scan nor on the collection specimens of adult hoatzin.

Digit II, III and IV

Digit II is composed of one phalanx that articulates at its proximal end with metacarpal II (Figure 15 D). The phalanx is three-sided and spindle-shaped at its distal extremity. The particularity of the hoatzin is the presence of functional claws on the wing in juveniles and it has been reported that these claws are completely absent in the adult. However, on the μ CT scan we observed a small U-shaped bone at the distal extremity of the phalanx, which appears to be the regressed wing claw on digit II. Digit III is composed of two phalanges (**C1678**). The first is short and tubular and has a flat wing-like process that extends caudally. The second phalanx is similar in shape to the phalanx of digit II and has the same U-shaped claw bone at its distal extremity. Digit IV is composed of one short and sturdy phalanx that articulates with metacarpal IV.

Pelvic girdle

The pelvic bone, is formed by the fused ilium, ischium and pubis, and supported by the synsacrum, with transverse processes completely fused with ilium cranially and abutting against the ilium caudally (Figure 16). The 7th and 8th ribs are covered by the preacetabular part of the ilium. The ilium, ischium and pubis form the walls of the acetabulum, the articulation with the femoral head.

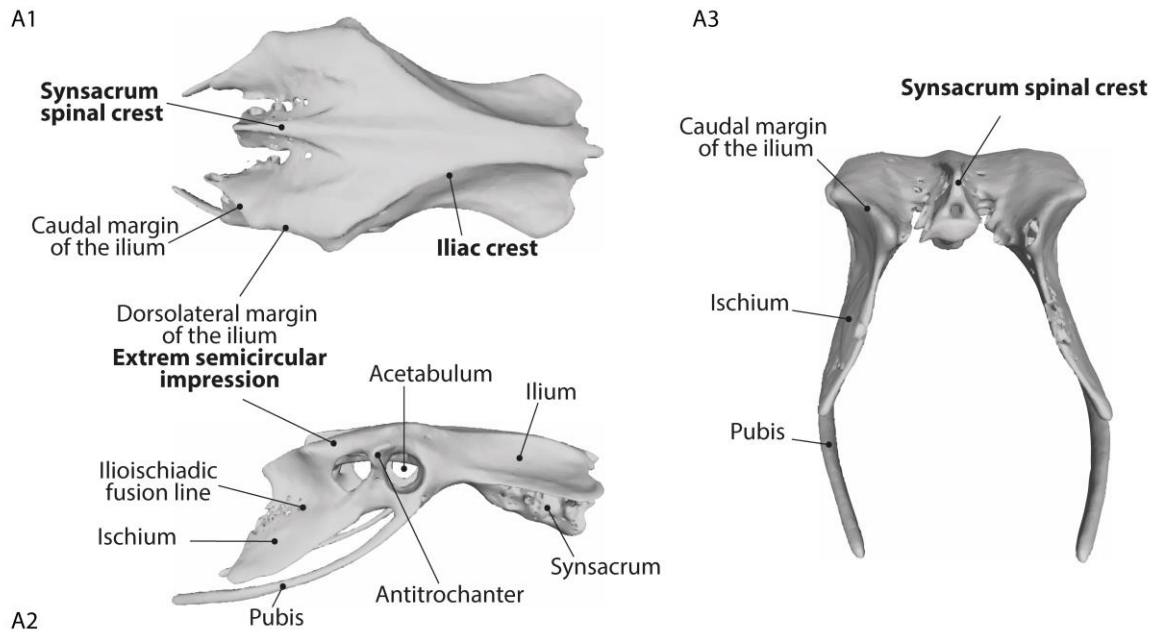


Figure 16 : Pelvic bone in dorsal view (A), right lateral view (B) and caudal view (C). Bold features are specific to the hoatzin and differ from those observed in most of other bird species; based on Livezey and Zusi (2007).

Ilium

The ilium forms the dorsal part of the pelvis above the synsacrum and extends caudally from the fifth thoracic rib to the acetabulum. The preacetabular ilium is concave and lateroventrally oriented. The ventral crest of the ilium from cranial to caudal is S-shaped. The ilium forms the cranial, dorsal and a part of the caudal border of the acetabulum. Dorsocaudal to the acetabulum, the dorsolateral margin of the iliac crest is rounded, distinct, and not projecting but still prominent (**C1866**). This iliac crest forms an enlarged semicircular impression on the dorsal face of the bone (**C1891**). The postacetabular part of the iliac alae is medioventrally oriented, whereas the spinal crista of the synsacrum becomes prominent caudally (**C1877**). Some intertransversal foramina are visible caudally and are very small.

Ischium

The ischium extends caudally from the acetabulum and ends just beyond the caudal end of the ilium. It lies ventral to the ilium and dorsal to the pubis. The cranial part is fused to the ilium and forms the caudal wall of the acetabulum, and the antitrochanter

dorsally. This fusion extends caudally into an ala which caudally forms the ilioischadic fusion line. The ilioschiadic foramen, just caudal to the acetabulum, is rounded.

Pubis

The pubic bone is the most ventral bone of the pelvic girdle. Its cranial end forms a small portion of the ventral border of the acetabulum. It is thin, long, rounded in cross section and curved. Its caudal extension, beyond the ischium, is curved medioventrally. There is no preacetabular tubercle. The ischiopubic fenestra is large, there is no contact between the pubis and the ischium ala.

Hind limb

Femur

The femur articulates proximally with the acetabulum, and distally with the tibiotarsus and the fibula (Figure 17 A). In medial view the femur has at its proximal end a prominent ball-like process, the acetabular articular facet. On the femoral acetabular articular facet, a fovea ligamentum capitis can be observed. Proximally, the acetabular articular facet is connected to the cranial trochanteric fossa and caudal obturator ridge which expands into the trochanter caudally and the trochanteric ridge cranially. At the distal extremity of the femur is a prominent medial condyle. The medial epicondyle is not prominent but present, medial to the medial condyle. The cranial projection of the medial condyle is very sharp-edged. In a lateral view, the lateral condyle is larger than the medial condyle. The lateral epicondyle appears as a long ridge on the lateral condyle. The fibular groove (fibular trochlea) lies between the lateral condyle and the lateral epicondyle and is delimited by divergent cristae (C2019). The intercondylar sulcus lies caudally between the lateral and medial condyles. The intercondylar sulcus extends to compose the rotular groove (trochlea) which lies cranially between the lateral and medial condyles. The rotula (patella) is not visible on the μ CT scans and collection specimen and possibly remains unossified. Only ligaments and muscular tendons connect the femur and tibiotarsus glides through the rotular groove. The popliteal fossa lies proximal to the intercondylar fossa.

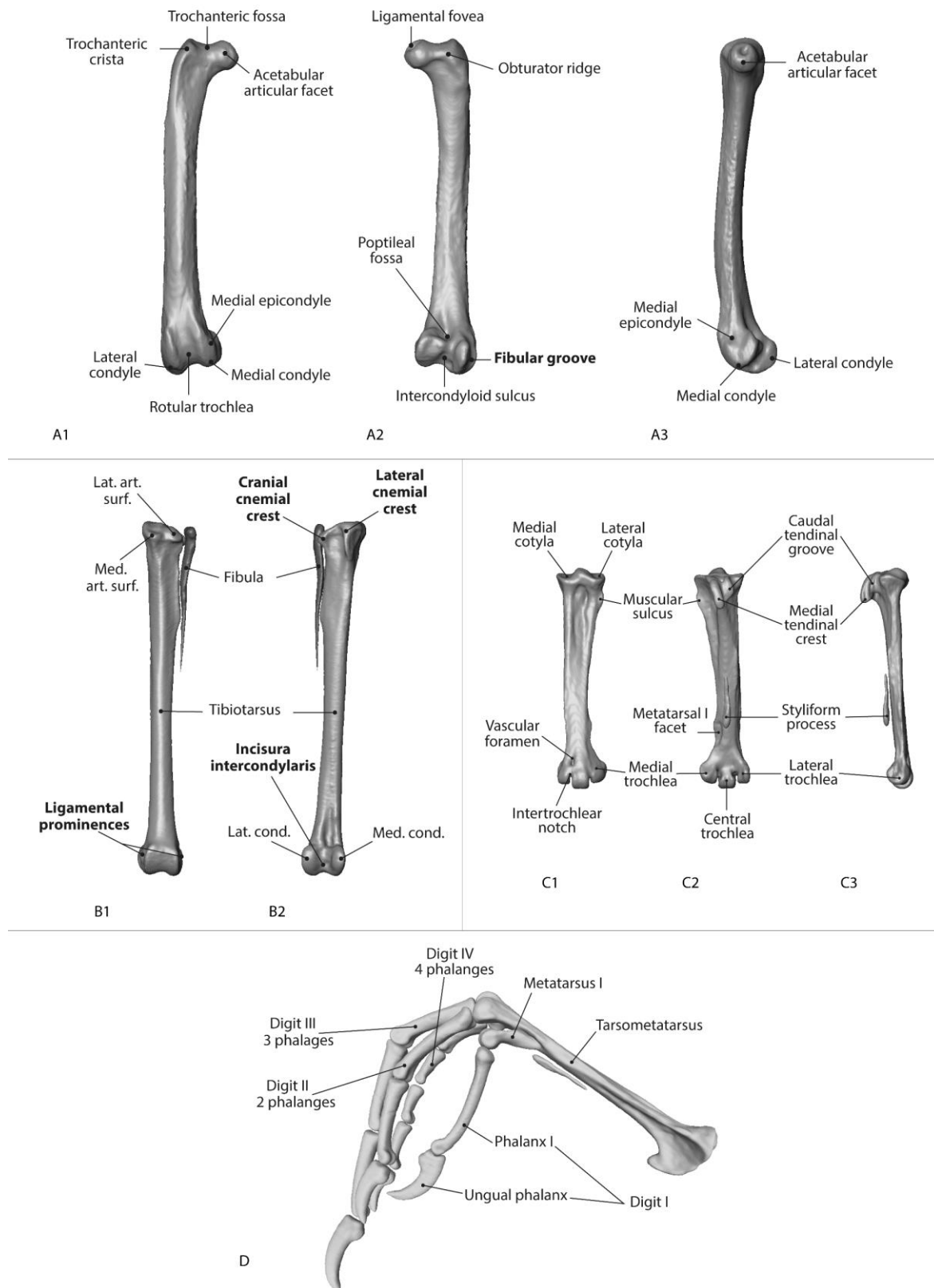


Figure 17 : Overview of the hindlimb bones. Right femur (A) in cranial view (1), caudal view (2) and medial view (3). Right tibiofibula (B) in caudal view (1) and cranial view (2); abbreviations: Caud.art.surf.: caudal articular surface; Lat.art.surf.: lateral articular surface; Lat.cond.: lateral condyle; Med.cond.: Medial condyle. Right tarsometatarsus (C) in cranial view (1), caudal view (2) and lateral view (3). Right foot bones (D) are represented in biological position in lateral view. Bold features are specific to the hoatzin and differ from those observed in most of other bird species; based on Livezey and Zusi (2007).

Tibiotarsus and Fibula

The tibiotarsus and the fibula are not fused (Figure 17 B). The tibiotarsus articulates proximally with the condyles of the femur and distally with the tarsometatarsus. The cranial cnemial crest is less developed than the lateral cnemial crest (C2098). The proximal part of the tibiotarsus is sharp-edged and is demarcated by a large rotular crest (patellar crest). Caudally, the lateral articular surface articulates with the lateral condyle of the femur and the medial articular surface articulates with the medial condyle of the femur. A smooth, distinct intermuscular line extends distally from the cranial cnemial crest on the shaft of the tibiotarsus to the proximal part and the lateral condyle. The fibula lies in the fibular crest of the tibiotarsus. At the distal extremity of the tibiotarsus, between the lateral and the medial condyles is an incisura intercondylaris (C2091). The supratendinal bridge (*pons supratendineus*), through which the tendon of the M. extensor digitorum pedis passes, is not visible. Laterally and medially, there is a poorly developed ligamental prominence (lateral and medial epicondylus) (C2150). The fibula is styliiform. The fibula extends distally one-third of the length of the tibiotarsus. The fibula is expanded cranially up to the fibular groove of the femur. It lies in contact with the fibular crest of the tibiotarsus along the proximal quarter of the tibiotarsus distally. The proximal fibular extremity bounds the tibiotarsus caudally to the lateral cnemial crest forming the lateral articular surface. The proximal part of the fibula extends cranially to the tibial articular surface and it articulates with the fibular groove of the femur.

Tarsometatarsus

The proximal part of the tarsometatarsus articulates with the lateral and medial condyles of the tibiotarsus (Figure 17 C). The proximal part of the tarsometatarsus has a marked dorsal infracondylar fossa. At its distal part, it has three trochleae for the articulation with the second, third and fourth digits. The hypotarsus (calcaneum) is a caudal ridged process extending from the proximal extremity to the shaft of the tarsometatarsus through the medial tendinal crest. In adult hoatzin, the hypotarsal ridge is not ossified (is not visible on μ CT scans and collection specimens) but the styliiform process is visible at its medial part. Distally, there are three trochleae, one for each of the three fused metatarsals: II, III and IV. Metatarsal I remains free. The metatarsal of digit I articulates medially and caudally just above the medial trochlea. Dorsally metatarsal I is narrowed

and lies in the articular fossa on the tarsometatarsus. Ventrally, it has a constriction and distally the articulation is as broad as the other trochleae at its articulation with the phalanx. The second and third trochleae have a similar shape but the lateral one is smaller than the central trochlea. The most medial trochlea is the smallest and articulates with digit II. The central trochlea articulates with digit III and the lateral trochlea with digit IV. Just proximal to the lateral intertrochlear notch, between the central and lateral trochlea, the large distal vascular foramen is positioned.

Digits I, II, III, and IV

All phalanges are convex dorsally and concave on their ventral surface (Figure 17 D). The ungual phalanx is claw-shaped and is typical for terminal phalanges of bird hind limb digits. The proximal articular fossa of the first phalanx is concave and enlarged. The distal articulating surface has two condyles, a lateral and a medial condyle, between which lies the intercondyloid sulcus. Digit I (hallux) is directed caudally and articulates with the free metatarsal I. It is composed of two phalanges: the first is a typical phalanx and the last is ungual. Digit II has two typical phalanges and one ungual phalanx. It is directed craniomedially. Its first phalanx articulates with the medial trochlea of the tarsometatarsus. Digit III has three typical phalanges and one ungual phalanx, is directed cranially and its first phalanx articulates with the third trochlea of the tarsometatarsus. Digit IV has four typical phalanges and one ungual phalanx. It is directed craniolaterally. Its first phalanx articulates with the lateral trochlea of the tarsometatarsus.

Discussion

By describing these four hoatzin specimens, we were able to highlight 28 original features of the hoatzin skeleton based on a comparison with the Livezey & Zusi (2007) matrix. We found the majority of these traits (14 of 28) on the scapular girdle and wing bones and the other features to be distributed in the skull (1 of 28), vertebrae (4 of 28), ribs (2 of 28), pelvic girdle and hind limb (7 of 28). Looking at the skull, the most important difference is the location of the lacrimal bone. Generally, this bone is completely fused with the frontal bone, posterior to the flexor zone between the braincase and the upper beak. In the hoatzin the lacrimal bone is fully fused to the nasal bone and is positioned anterior to the flexor zone. Moreover, the lacrimal projects a process into the jugal bone. The folivorous diet implies a particular shape of the quadratomandibular articulation, mainly for the quadrate bone. It has been suggested that the hoatzin is able to ‘masticate’ and it has been called a “chewing bird” (Korzoun, Erard, and Gasc, 2003). However, the articular bone of the lower jaw has a long and medially oriented process and a large retroarticular process which limit the opening movements of the lower jaw. Moreover, the medial condyle of the quadrate is sharp-edged and totally surrounded by the articular and prearticular bones of the lower jaw. The organization of the squamosal bone and the zygomatic process with the otic process of the quadrate is tight. Thus, the condyle shape and the articular part of the mandible could limit the lateral movement of the lower jaw. These movements should be more limited than dorsoventral movements as suggested by Dawson et al. (2011). However, the dorsoventral movements could be congruent with the processing of leaves as described by Korzoun et al. (2003) thanks to prominent keratinized ridges and protraction/retraction movements of the lower jaw.

The hoatzin has been described as strictly vegetarian, with a diet mainly based on young leaves (up to 85%, Grajal, 1995). This is the only known bird species with a foregut fermentation. As vertebrates do not produce the enzymes necessary to digest cellulose, herbivores show enlarged chambers to allow anaerobic microorganisms to degrade the cellulose making up the majority of plants. Ostriches and Emus are vegetarian but have a postgastric fermentation, as do horses, for example. In contrast, the hoatzin is the only known bird to have a pregastric enlarged fermentation chamber, analogous to what is observed in ruminants as the cow (Grajal, 1995). This

hypertrophied fermentation chamber, called the crop, is positioned ventral to the sternum complex. It lies on the cranial part of the scapular complex, in front of the fused furcula, coracoid and sternum bones (Figure 14 B). The crop is positioned on the pectoral muscles, under the skin and is housed in a concave depression of the sternum keel. It is surrounded by a tight membrane and the muscular wall is composed of several circular muscle layers (Grajal, 1995). The membrane could play a role into crop protection and its support. No information is provided about the origin and insertion of these muscle fibers (Perin, 1875). The hypertrophied crop can amount up to 7.5% of the hoatzin weight (Grajal, 1995). As it is placed in front of the pectoral muscles it likely impacts the shape of the pectoral girdle (Gadow, 1892; Grajal, 1995; Perin, 1875). The sternum carina is less developed on the cranial extremity and more developed in the caudal extremity. The caudal extremity of the carina is enlarged and concave, forming the resting pad used to support the trunk while engaged in 'sternal perching', a typical resting position of the hoatzin (Figure 7; Grajal, 1995). This resting pad arises from between the pectoral muscles and is covered only by keratinized unfeathered skin (Perin, 1875).

Another morphological particularity is the enlarged, flattened ribs without separate uncinat process and positioned close to one another. These particularities could help supporting the weight of the trunk (Gadow, 1892). The hoatzin spends 70-80% of the day roosting, sitting or in sternal perching. Consequently, sternal perching may represent a low-energy adaptation for long quiescent periods with a full crop (Müllner, 2004; Strahl, 1988). As such, the trunk weight could be supported by the "resting pad" of the sternum complex and the sternal ribs (Figure 13 and 14 B). This could potentially explain both the complete fusion of the sternum, furcula and coracoid bones and the enlarged robust ribs. Moreover, both coracoid bones are fused to one another and to the furcula, probably adding rigidity to the sternum complex (Figure 14 B). The complete fusion of the scapular girdle may, however, limit the flying ability of the hoatzin (Gadow, 1892; Grajal, 1995; J. M. Hughes and Baker, 1999; Parker, 1868). Indeed, it likely prevents the furcular spring action and coracoid movement which are important for energy recovery during wing beating (Jenkins et al., 2017).

The wing bones also show unusual features. For example, the humeral shaft is curved and somewhat S-shaped, especially the distal part which is laterally oriented.

This might also be linked to the resting position of the hoatzin. After field observations, we determined that to be able to put the resting pad on the branch, the bird may have to bend its legs with knees moving under the wings (Figure 7). Thus, the elbow joint should be a bit spread from the body. The curved shape of the humerus could allow the hoatzin to keep its wings into a closed position but with enough space for the knee. Moreover, the radial carpus is sharp-edged yet blunts dorsally (Figure 15 D2). The sulci for muscle tendons are smooth and undefined which could affect the wrist motion (Harvey, Kaiser, and Rosenberg, 1969). The metacarpus is an important bone for muscle insertions, including the extended pisiform process for alulae muscle insertions (Harvey, Kaiser, and Rosenberg, 1969). The hoatzin has marked insertion areas suggesting a robust *M. abductor digiti majoris* (Harvey, Kaiser, and Rosenberg, 1969). This muscle could be in association with the claws on the wing in the climbing young bird. Although the literature suggests that wing claws are completely absent in adult hoatzin (Olson, 1992; Strahl, 1988) we observed rounded and reduced bones corresponding to residual ungual phalanges at the tip of the digit II (alulae) and digit III (major) (Figure 15 D1). These residual bones seem not to have any muscle insertions in the adult bird. All digital phalanges are robust, suggesting large muscle insertions areas on the phalanges (Figure 15 D1; Stegmann, 1978).

The pelvic girdle also has some particularities. It has few pneumatic holes. The spinal crest is deeply concave, angular and prominent. This corresponds to the insertion area for the *M. levator caudae* (Gatesy and Dial, 1996) which has been described as well-developed in the hoatzin by Perin (1875). This group of muscles participates in the retraction of the caudal vertebrae (Baumel et al., 1993; Harvey, Kaiser, and Rosenberg, 1969) and plays a role in tail movement and body balance (Gatesy and Dial, 1996). The development of the spinal crest could be related to the locomotor behavior of the hoatzin. They use the tail for balance when they are overbalanced by the weight of their large crop when roosting on sternal perching (Strahl, 1988). The ilium bone is particularly sharp edged with a large crest (Figure 16). The most distinct is the dorsolateral margin of the iliac crest where the *Mm. ilirotrochanterici* insert. The well-developed iliac crest and the large semicircular impression enlarge the insertion area of these hip muscles (Figure 17). This might be explained looking at the sternal perching position with the knee positioned just below the shoulder resulting in a hyperflexed hip

(Figure 7). The stability of the hip could be reinforced both by the large insertion areas for hip muscles. The femur has a trochlea, which terminates as a sulcus, distinguished by a marked widening. The fibula lies into this lateral concave groove and is positioned higher than the tibiotarsus (Figure 17 B). This may help the joint to be more stable during resting (Cracraft, 1971b). On the tibiotarsus, we observed that the cranial and the lateral cnemial crests are poorly developed (Figure 17 B). These crests are the insertions areas of the *M. peroneus longus* and the *M. gastrocnemius* flexor and extensor of the ankle joint (Cracraft, 1971b; Harvey, Kaiser, and Rosenberg, 1969; Perin, 1875). The weak development of the crests may be related to the low level of locomotor activity observed of the hoatzins (Müllner, 2004; Strahl, 1988)

To conclude, in the present paper we described the skeletal features that make the hoatzin unusual. This is the first description of the whole skeleton of the hoatzin. The use of 3D data allows us to be as precise as possible while avoiding the destruction of these rare specimens. We attempted to provide plausible functional explanations. The cranial peculiarities may be related to the folivorous adaptations (Korzoun, Erard, and Gasc, 2003, 2001). Most of the post-cranial osteological features may be related to the crop hypertrophy and the sternal perching, a behavioral particularity linked to the unique diet and foregut digestion (Müllner, 2004; Strahl, 1988). However, we are aware that a part of these anatomical features could be linked to the phylogenetic heritage of the hoatzin, but the lack of detailed anatomical information on fossils prevents us from concluding further on this aspect. Future studies examining the muscles in relation to the skeletal elements described here will likely be particularly insightful in better understanding the unique anatomy of the hoatzin.

**Chapter 2 - Does bone preparation
impact its shape: consequences for
comparative analyses of bone
shape?**

Using the descriptive analyses of the whole hoatzin skeleton from the previous chapter, we highlighted that the scapular girdle of the hoatzin is the most peculiar part of its skeleton in comparison to other birds. Thus, we decided to focus all the further analyses on the scapular girdle of birds. To do so, we compared the morphology of each bone of the scapular girdle of the hoatzin to a large sample of birds with different diet and locomotor adaptations. Using 3D techniques, geometric morphometric methods and collection specimens, we quantitatively investigated evolutionary changes in the morphology of the scapular girdle of birds.

Nevertheless, before working on a large comparative dataset of the scapular bones, we needed to assess how the bone morphology could be impacted by several non-natural effects such as the preparation of the specimen. Indeed, several authors have described the effect of preparation processes on bones. In this following chapter, we decided to test the influence of the preparation process on the bone shapes from osteological collections. This study allowed us to assess the impact of bones preparation process on the shape of each bone of the scapula girdle using both intra- and inter-specific datasets of birds.

Does bone preparation impact its shape: consequences for comparative analyses of bone shape?

Fanny Pagès, Anne-Claire Fabre, Anick Abourachid

Accepted for publication in PeerJ

Abstract

Vertebrate osteological collections provide comparative material for morphological analysis. Before being stored in the collection and studied by researchers, specimens are treated by preparators or curators and are cleaned. The preparation protocol employed ideally should not damage the material. Here, we explore the potential deformation of bones due to preparation using geometric morphometric methods. We focus both on intraspecific and interspecific variability. Our data on the scapular girdle of birds show that at an intraspecific level, the effect of preparation on bone shape cannot be neglected. Paired and unpaired bones did not respond to the preparation process in the same way, possibly due to differences in function and their anatomical characteristics. Moreover, deformations due to preparation can be estimated by looking at the texture of the bone. At the interspecific level, we found no significant differences as the deformations induced by preparation are relatively small compared to differences between species. This study highlights the importance of carefully selecting preparation methods in order to avoid physical damage that could impact the shape of bones, especially for studies at the intraspecific level.

Introduction

Museum collections provide a rich source of anatomical material, often collected over the span of several centuries. These collections provide access to specimens, allowing for the study of a broad diversity and large number of animals from around the world. Before being added to collections, specimens are usually treated by preparators or curators. In order to prepare osteological material, common before the advent of computed microtomography facilities, specimens have to be cleaned using either natural (ranging from natural maceration, cleaning by boiling, to cleaning by bugs such as terrestrial isopods, marine isopods or dermestid beetles) or chemical (enzyme detergent soup, hydrogen peroxide or potassium hydroxide) treatments. Next, bones are dried using different techniques (natural drying lying on a flat surface or dried with artificial heat) allowing access to the bones (Fernández-Jalvo and Marin-Monfort, 2008). In theory, the preparation methods employed should not damage the integrity of the material. Thus, the protocol used should be adapted with products that are compatible with the material treated and must not interfere with possible future scientific studies. Possible consequences on the integrity of different skeletal elements depending on the preparation protocol used have already been studied and reported in several papers (Fernández-Jalvo and Marin-Monfort, 2008; Hahn, Vogel, and Delling, 1991; Lemoine, 2011). Such consequences can be somehow compared to morphological deformations induced by the processes of fossilization (i.e. taphonomy). Only few studies have attempted to characterize taphonomical processes and to develop approaches taking into account the deformation induced by these taphonomic effects (Denys, 2002; Fernández-Jalvo and Andrews, 2016; Lyman, 2010). Indeed, the consequences of preparation on bones often remain underestimated and poorly documented (López-Polín, 2012). However, a study of Fernández-Jalvo and Marin-Monfort (2008) evaluated the effect of preparation methods on bones using electron microscopy. They found that for a same bone, only two out of the twelve methods used could be recommended: burying and the use of enzymes with close control of the duration to minimize damage. Furthermore, another method was acceptable but not excellent: the use of potassium hydroxide (KOH) with careful control of the duration to avoid the risk of damage. This study highlights the importance of carefully selecting the preparation method in order to avoid physical damage that could impact the structure and shape of the treated bones.

Here, we decided to investigate variation in bone shape due to preparation given the large amount of variability observed in collection specimens. We predict that these deformations could be due to the preparation process using chemicals dissolving fat and proteins. However, some parts of the bone may also be more easily deformed (Fernández-Jalvo and Marin-Monfort, 2008; Hahn, Vogel, and Delling, 1991). We further predict that these deformations can have an impact for morphometric studies. Preparation deformations can cause and render more complex intra-individual and intra-species variability, modifying the bone shape depending of its composition, function, thickness or robustness (Lemoine, 2011).

We use geometric morphometric methods as these methods are commonly used to detect shape differences and are sensitive to small variations in shape. Shape variability can either be natural (natural variability including variability due to the functional role of a bone) or non-natural (due to preparation). We focused on the bones of the scapular girdle in birds. The scapular girdle is composed by two unpaired bones: the sternum and the furcula, and three paired bones: the scapula, the coracoid and the humerus (Figure 18). All these bones have an important role during locomotion, as muscles involved in wing movements are attached to them.

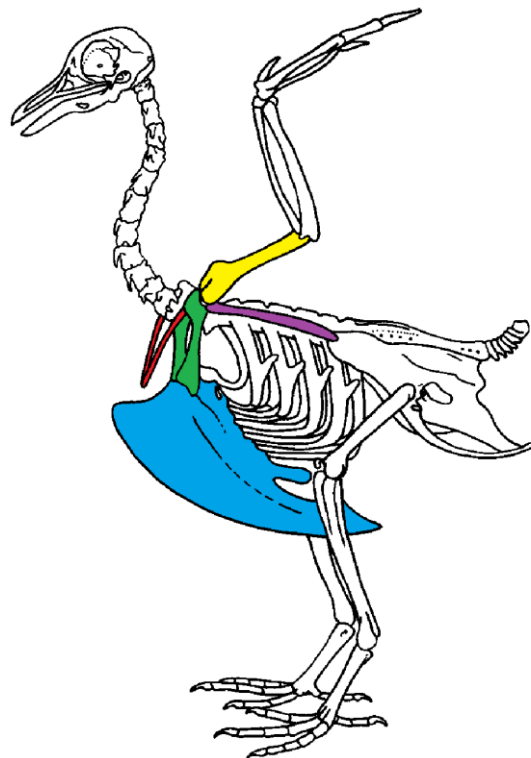


Figure 18 : Scapular girdle of bird. Drawing of a complete bird skeleton with scapular bones of interest highlighted in colors: furcula in red, sternum in blue, coracoids in green, scapula in purple, humerus in yellow. Modified from BIODIDAC.

Two types of functions in scapular girdle of birds were identified previously: 1) bones that need to resist the action of the muscles attached and that thus need to be robust and 2) bones that play a role of protection of the internal organs such as the heart and viscera. Both of these functions may also be related to bone flexibility, like the spring function of the furcula, which can absorb and return energy during the wingbeat (Goslow, Dial, and Jenkins, 1989; Kardong, 2012; Mitchell et al., 2017).

To assess the impact of preparation on bone, we analyzed the texture of the bone, its shape variation (disparity), and its asymmetry. The asymmetry was defined as significant differences in shape within a single specimen. We expect that the asymmetry should be higher if there is a preparation effect. To assess whether the observed deformations may impact subsequent analyses, we compared effects at the intraspecific and interspecific level.

Materials and methods

Material

We sampled 20 complete quail skeletons (*Coturnix coturnix*, Galliformes). These quail bones are housed in the research collection of A. Abourachid. All specimens were bred in captivity and prepared using the same protocol (see protocol below). In order to assess whether the intraspecific variability is lower than the interspecific one, we added several other species. We sampled one individual of six species from the collections of the Museum National d'Histoire Naturelle (Paris, France). Four are closely related to quails: *Meleagris gallopavo* (Galliformes), *Anseranas semipalmata*, *Chauna chavaria* and *Cygnus olor* (Anseriformes, sister group) and two share the same flight type: *Coua cristata* (Cuculiformes) and *Cariama cristata* (Gruiformes) (Table 1). We selected one individual per species for the interspecific dataset.

Table 1 : **Details of specimens used in the analyses.** Detailed family, order, species name and number of individuals included (N)

Family	Order	Species	Collection code	N
Anseriformes	Anatidae	Cygnus olor	MNHN-ZO-1871-420	1
Anseriformes	Anseranatidae	Anseranas semipalma	MNHN-ZO-2004-151	1
Anseriformes	Anhimidae	Chauna chavaria	MNHN-ZO-1921-255	1
Galliformes	Phasianidae	Meleagris gallopavo	MNHN-ZO-1873-174	1
Cuculiformes	Cuculidae	Coua cristata pyropyga	MNHN-ZO-1883-517	1
Gruiformes	Cariamidae	Cariama cristata	MNHN-ZO-1934-614	1
Galliformes	Phasianidae	Coturnix coturnix	Abourachid's scientific collection	20

Preparation protocol

The preparation protocol used for the quail data set is composed of ten steps. First, the birds are eviscerated and feathers, skin and viscera are removed. Then, large muscles are removed (defleshing). This is facilitated by carcass reduction (dismemberment and decapitation). Carcasses are then boiled for three hours and put into a lukewarm salt water bath with an addition of an enzyme (papain: cysteine protease enzyme; 1gr/L) for 48h at 60°C. At the end of this step, the bones are put into a lukewarm sodium perborate bath until chilled (for more than 24h). At that point, bones are well separated and free of flesh. Bones are rinsed and dried, lying on an absorbent surface (for 24 hours). Finally, if after drying step, traces of fat persist on the surface of the bones they are put in a bath of absolute alcohol for several days and the renewal of the bath is possible many times according to the state of saturation in bone fat (yellowish coloration). When bones appear no longer saturated a final drying step is necessary to evaporate the alcohol.

3D Data collection

We generated 3D surface scans with a white light fringe Breuckmann scanner (SmartSCAN) and its scanning software Optocat (<http://www.breuckmann.com>) at the 'plateforme de morphométrie' of the UMS 2700 of the MNHN. The scanner consists of a projector of white light fringes and two cameras that are positioned asymmetrically around the projector. Data on the surface of a bone are accurately captured and reconstructed by triangulation angles implemented in the Optocat software. It finally produces a high-resolution meshed 3D object which provides a representation of the surface of the bone only. For each specimen, we scanned eight bones: a sternum, a furcula, both coracoids (right and

left), both scapulae (right and left) and both humeri (right and left). Further processing is performed with the Geomagic Studio 2013 (<http://www.geomagic.com>) software package in order to obtain a surface on which data can be accurately acquired.

Methods

Shape quantification using geometric morphometric

In order to assess the effect of the deformations of the bone and its potential effect on shape analysis, we use 3D geometric morphometric analysis on our sample of seven species of birds. Geometric morphometrics allow a quantification of shape variation using Cartesian landmark coordinates. This approach permits to quantitatively study the shape variation of bones in relation to quantitative and qualitative traits. We created a set of landmarks in order to quantify morphological disparity.

Morphometric data were acquired on each surface scan of each bone using the IDAV Landmark software. For each bone, landmarks were chosen to accurately describe the complex geometry of each element. We used anatomical landmarks as well as sliding semi landmarks of curves and on surfaces to describe bone shape more accurately. Anatomical landmarks and sliding semi landmarks of curves were manually acquired on each scan by the same person (F.P.) whereas sliding semilandmarks on surfaces were semi-automatically projected onto the surface of each bone using the approach described below (see 3D sliding-landmarks procedures). To be able to compare the paired bones, we mirrored right bones into left bones, allowing to include all paired bones in the same comparative analysis. We kept the side information for each paired bone.

We defined a unique set of landmarks and curves for each bone. Furculae are described using 814 points, (17 landmarks, 70 curve points and 727 surface points; Table 2; Figure 19 A-B), the sternum shape with 3738 points (28 landmarks, 176 curve points and 3534 surface points; Table 3; Figure 19 C-D), the coracoids with 1080 points (8 landmarks, 87 curve points and 985 surface points; Table 4; Figure 19 E-F), the scapulae with 744 points (7 landmarks, 47 curve points and 690 surface points; Table 5; Figure 19 G-H) and the humeri with 813 points (22 landmarks, 29 curve points and 762 surface points; Table 6; Figure 19 I-J).

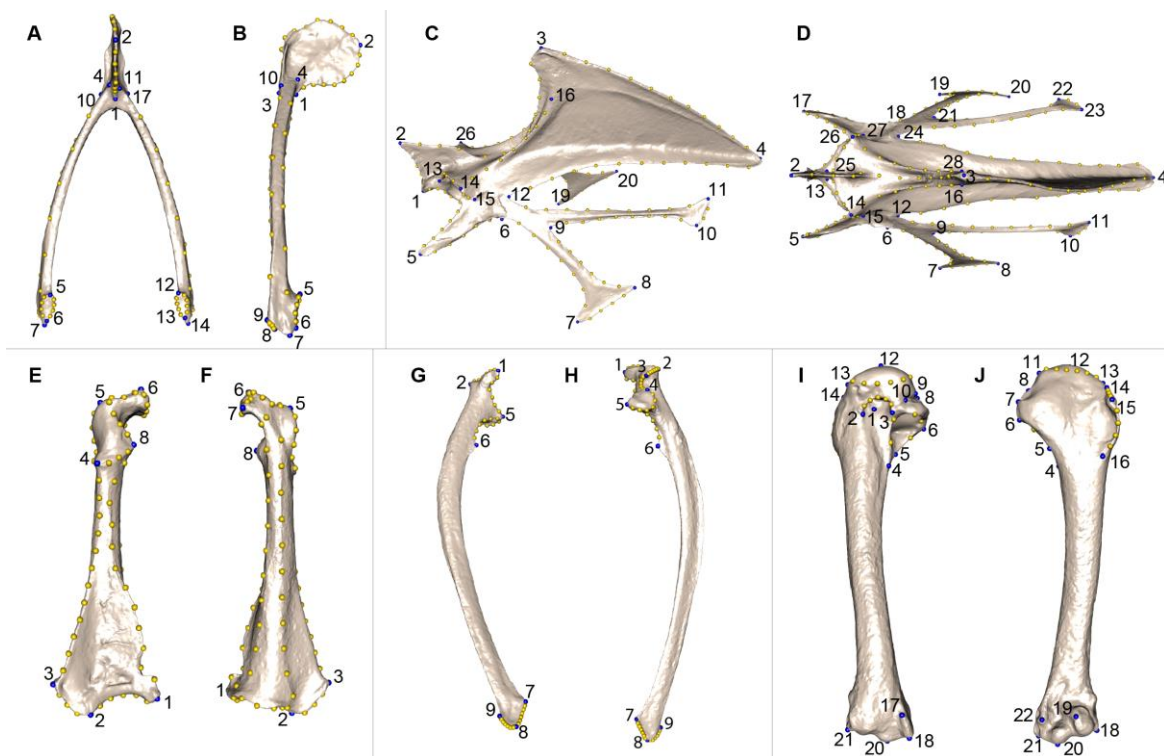


Figure 19 : Landmarks used in the analyses to quantify shape variation on scapular bones. Quail bones are presented. Furcula: (A) caudal view, (B) lateral view, see Table 2 for landmark definition. Sternum: (C) lateral view, (D) ventral view, see Table 5 for landmark definitions. Left coracoid: (E) dorsal view, (F) ventral view, see Table 4 for landmark definitions. Left scapula: (G) dorsal view, (H) ventral view, see Table 3 for landmark definitions. Left humerus: (I) medial view, (J) lateral view, see Table 6 for landmark definitions. Blue points represent landmarks and gold points represent semi-landmark curves.

Table 2 : Definition of the landmarks of the furcula used in the geometric morphometric analysis. See Figure 19 A-B for landmark position on the furcula.

Landmarks	Definition
1	dorsal extremity of the symphysis, cranial view
2	ventral extremity of the symphysis, caudal view
3	fusion point of the two clavicles
4	ventral point of the clavicle and symphysis fusion, right clavicle
5	rostral extremity of the acrocoracoidal articular facet, right clavicle
6	caudal extremity of the acrocoracoidal articular facet, right clavicle
7	most caudal point of the right clavicle
8	caudal extremity of the acromialis process, right clavicle
9	rostral caudal extremity of the acromialis process, right clavicle
10	dorsal point of the clavicle and symphysis fusion, right clavicle
11	ventral point of the clavicle and symphysis fusion, left clavicle
12	rostral extremity of the acrocoracoidal articular facet, left clavicle
13	caudal extremity of the acrocoracoidal articular facet, left clavicle
14	most caudal point of the left clavicle
15	caudal extremity of the acromialis process, left clavicle
16	rostral caudal extremity of the acromialis process, left clavicle
17	dorsal point of the clavicle and symphysis fusion, left clavicle

Table 5 : Definition of the landmarks of the scapula used in the geometric morphometric analysis. See Figure 19 G-H for landmark position on the scapula

Landmarks	Definition
1	medial extremity of the acromium
2	lateral extremity of the acromium
3	apex of the tuberculum coracoideum
4	dorsal extremity of the glenoid facet
5	ventral extremity of the glenoid facet
6	apex of the scapular tubercle
7	caudoventral extremity of the blade of the scapula
8	caudal extremity of the blade of the scapula
9	caudodorsal extremity of the blade of the scapula

Table 3 : Definition of the landmarks of the coracoid used in the geometric morphometric analysis. See Figure 19 E-F for landmark position on the coracoid

Landmarks	Definition
1	lateral extremity of the mediolateral angle
2	medial extremity of the sternal facet
3	medial extremity of the sternocoracoidal process
4	proximal extremity of the glenoid facet
5	proximal extremity of the procoracoid
6	apex of the acromium
7	apex of the brachial tuberosity
8	distal extremity of the procoracoid

Table 4 : Definition of the landmarks of the sternum used in the geometric morphometric analysis. See Figure 19 C-D for landmark position on the sternum.

Landmarks	Definition
1	cranial extremity of the dorsal manubrial spine
2	craniodorsal extremity of the manubrium
3	dorsal extremity of the cranial process of the keel
4	caudal extremity of the caudal process of the keel body
5	cranial extremity of the craniolateral process, left side
6	caudal extremity of the last sternal rib facet, left side
7	dorsal extremity of the first trabecula, left side
8	ventral extremity of the first trabecula, left side
9	junction point of the two trabeculae, left side
10	dorsal extremity of the second trabecula, left side
11	ventral extremity of the second trabecula, left side
12	junction point of the second trabecula and the sternum body, left side
13	medial extremity of the dorsolateral process of coracoidal articular facet, left side
14	ventral extremity of the dorsolateral process of coracoidal articular facet, left side
15	lateral extremity of the dorsolateral process of coracoidal articular facet, left side
16	ventral extremity of the lateral crest, left side
17	cranial extremity of the craniolateral process, right side
18	caudal extremity of the last sternal rib facet, right side
19	dorsal extremity of the first trabecula, right side
20	ventral extremity of the first trabecula, right side
21	junction point of the two trabeculae, right side
22	dorsal extremity of the second trabecula, right side
23	ventral extremity of the second trabecula, right side
24	junction point of the second trabecula and the sternum body, right side
25	medial extremity of the dorsolateral process of coracoidal articular facet, right side
26	ventral extremity of the dorsolateral process of coracoidal articular facet, right side
27	lateral extremity of the dorsolateral process of coracoidal articular facet, right side
28	ventral extremity of the lateral crest, right side

Table 6 : Definition of the landmarks of the humerus used in the geometric morphometric analysis. See Figure 19 I-J for landmark position on the humerus

Landmarks	Definition
1	distal point of the beginning of the central pneumatic fossa
2	end of the margo caudalis
3	apex of the bicipital crest
4	beginning of the dorsal crus
5	beginning of the ventral crus
6	end of the ventral crus
7	ventral extremity of the ligamental groove
8	lateral extremity of the capital groove
9	proximal extremity of the capital groove
10	medial extremity of the capital groove
11	ventral extremity of the head of the humerus
12	apex of the head of the humerus
13	dorsal extremity of the head of the humerus
14	proximal extremity of the deltoid crest
15	apex of the deltoid crest
16	distal extremity of the deltoid crest
17	proximal extremity of the entipocondyle, medial view
18	apex of the entipocondyle, medial view
19	distal extremity of the external epicondyle
20	apex of the ventral condyle
21	distal point of the medial epicondyle
22	proximal point of the dorsal condyle, lateral view

3D sliding-landmark procedures

The 3D sliding landmark procedure (Bardua et al., 2019; Bookstein, 1997; Gunz, Mitteroecker, and Bookstein, 2005) was used in this study. In this procedure, sliding landmarks are transformed into spatially homologous landmarks that can be used to compare shapes. They will slide along curves that are predefined on each surface. This operation is performed using the Morpho package in R (v3.5.0) (Schlager, 2017; Schlager, Jefferis, and Ian, 2019). Curves and surface sliding-landmarks are projected from the template onto each specimen for each data set. In this step, each new specimen is only defined by its landmarks and semi landmarks on curves. Next, the surface sliding-landmarks are projected onto the predefined curves and the surface of the new specimen using a template. Finally, spline relaxation was performed minimizing the bending energy criterion.

Generalized Procrustes Superimposition

Generalized Procrustes Superimposition or GPA (Rohlf and Slice, 1990) allows the comparison of an object's shape by removing size, orientation, and position relatively to the origin of coordinate system. We computed the first step which was an operation of translation

of all the objects, allowing the superimposition on their center of gravity. The second step was an operation of normalization; all the objects were scaled and end up having the same scale. During this operation, all the coordinates of each object were divided by the centroid size which was the square root of the summed squared distances of each landmark to the centroid (Bookstein, 1991). Finally, each conformation was rotated by minimizing the summed square distances between all the landmarks. We performed the GPA using the function ‘gpagen’ in Geomorph R package (Adams and Otárola-Castillo, 2013).

After superimposition, each object was defined by Procrustes coordinates and rescaled. Thus, differences in conformation or objects shape could be studied and were simply represented by changes in the proportion of structures. After this operation has been performed for each data set, the landmarks of all specimens were comparable.

Statistical analysis

All the statistical analyses below were done in R (v.3.5.0; <https://www.r-project.org/>)

Principal component analysis

In order to explore the distribution of the specimens in the morphological space (morphospace) and to reduce the number of dimension of our dataset, we performed a principal component analysis (PCA) using the function plotTangentSpace of “geomorph” package in R (Adams and Otárola-Castillo, 2013).

Difference of bone shape depending of bone texture

We wanted to compare, for each bone, the external appearance as a proxy for deformation due to preparation. Each bone was categorized depending on its external appearance, from oily to powdery. We created three categories: oily for yellow and shiny bones meaning lot of fat remained, powdery for bones that are very white and dusty representing little fat, and neutral for the other bones. We tested for shape differences depending on these qualitative categories using a multivariate analysis of variance (MANOVA) on the principal component scores (PC) accounting for 95% of the overall variance of each bone (furcula: 10 PCs representing 95.5%, sternum: 11 PCs representing 95.7%, coracoid: 22 PCs representing 95.5%, scapula: 18 PCs representing 95.4% and humerus: 23 PCs representing 95.1% of the overall variance).

Visualizing shape similarities using a neighbor joining tree

We computed neighbor joining trees on the Euclidean distances using at least 95% of the overall variance in order to obtain unrooted trees.

Quantification of asymmetry to assess the impact of bone preparation using t-test

In order to quantify the preparation effect, we tested the presence of asymmetry using a paired student test comparing right and left parts of the bones (Kharlamova et al., 2010). We used the `t.test` function in basic package in R. In the same way, we compared symmetrized and non-symmetrized shapes.

Quantification of disparity for each bone shape

We also calculated morphological disparity of each bone in both datasets thanks to the D index which give us a numerical value showing how different bones are between each other using the `morphol.disparity` function in “geomorph” package in R (Zelditch et al., 2004).

Assessing a possible effect of bone preparation on interspecific morphological studies

Finally, we performed a PCA and disparity analyses on the interspecific data set in order to compare it to the intraspecific variability. It allows to assess a possible effect of bone preparation on interspecific morphological studies. If the impact of bone preparation is low, we expect to see a clustering of all the *C. coturnix* in the same part of the morphospace, whereas the other species should occupy a larger part of the morphospace. We also expect that the disparity of *C. coturnix* will be lower than those of all the other species combined.

Results

Intraspecific level

Shape differences depending on texture or color

The results of the MANOVAs showed that powdery bones are significantly morphologically different from neutral and oily bones (p-value below 0.01; Figure 20, Table 7). Powdery bones in comparison to neutral and oily ones are characterized by furculae with narrower clavicles, sterna with dorsolateral and caudolateral processes that are more distant from the central part, coracoids with a thinner shaft, scapulae with a thinner blade, and humeri with a more gracile shaft. No shape differences were found between oily and neutral bones.

Table 7: Results of the MANOVAs testing for shape differences depending of the texture for each bone. Significant differences are indicated in bold.

Bone PC1 scores	Oily	Neutral	Powdery
Furcula	x	x	0.01
Sternum	x	x	<0.01
Coracoid	x	x	<0.01
Scapula	x	x	<0.01
Humerus	x	x	<0.01

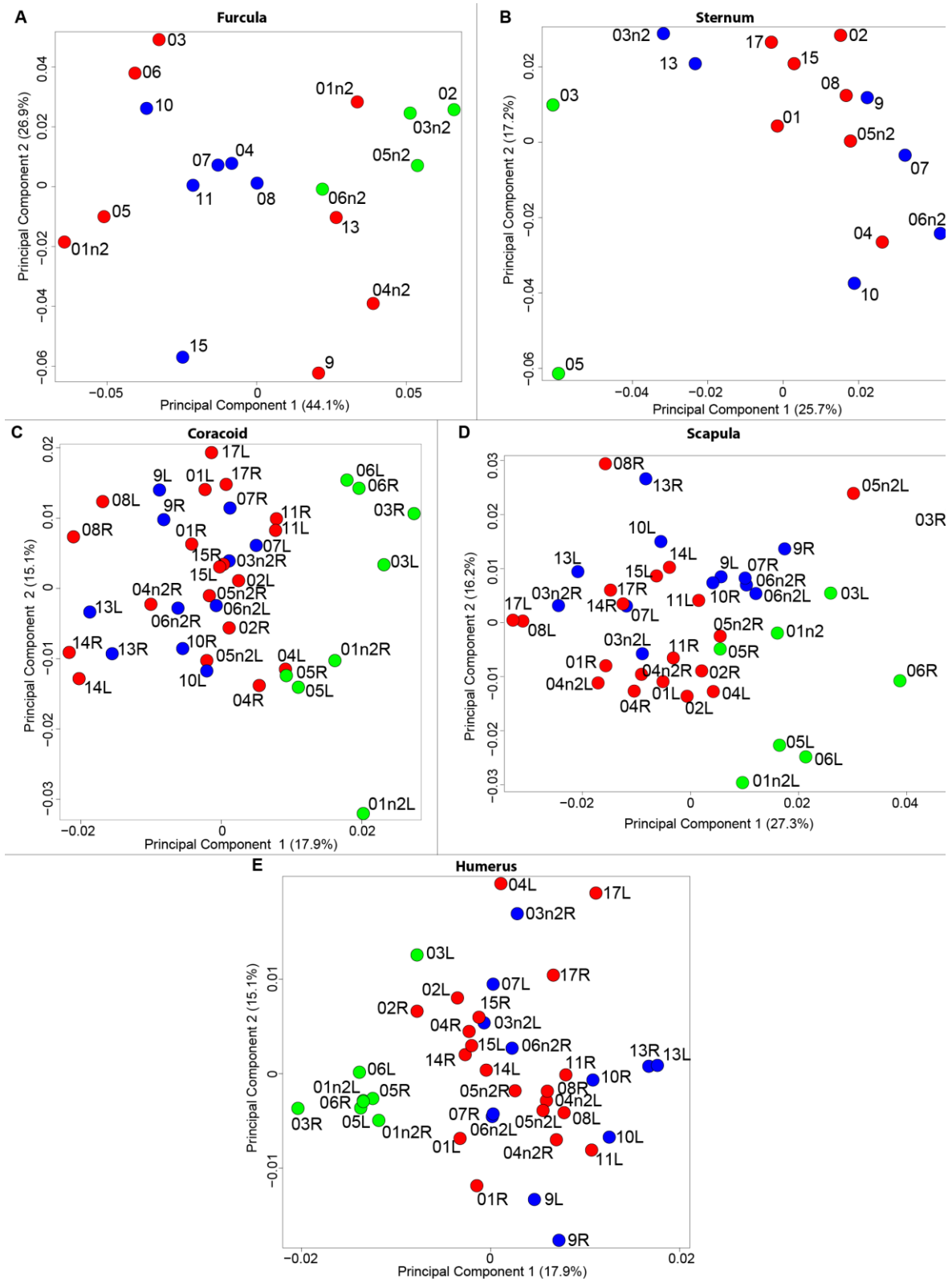


Figure 20 : Overview of the results of Principal Component Analyses (PCA) performed on quails bone shapes. Colors represent bone texture: green is for powdery bones, blue is for neutral bones and red is for oily bones. Each individual is identified thanks to a unique code, for paired bones we add the information of the side: L left and R right. furcula (A), sternum (B), coracoid (C), scapula (D), humerus (E).

Furcula

We computed the consensus shape of the furcula. The points on each side were very dispersed which means that there is considerable shape variation in the furculae (Figure 21 A). The four first axes of the intraspecific PCA explained 83.5% of the total variance (PC1 = 44.1%, PC2 = 26.9%, PC3 = 7.4% and PC4 = 5.1%; Figure 21 B). Two types of shapes were distinguished along the first axis. The negative axis was represented by a furcula with the clavicles being more distant from one another and a rounded caudally oriented symphysis. On the contrary, narrow clavicles and elongated dorsally oriented symphysis were situated towards the positive side of the axis.

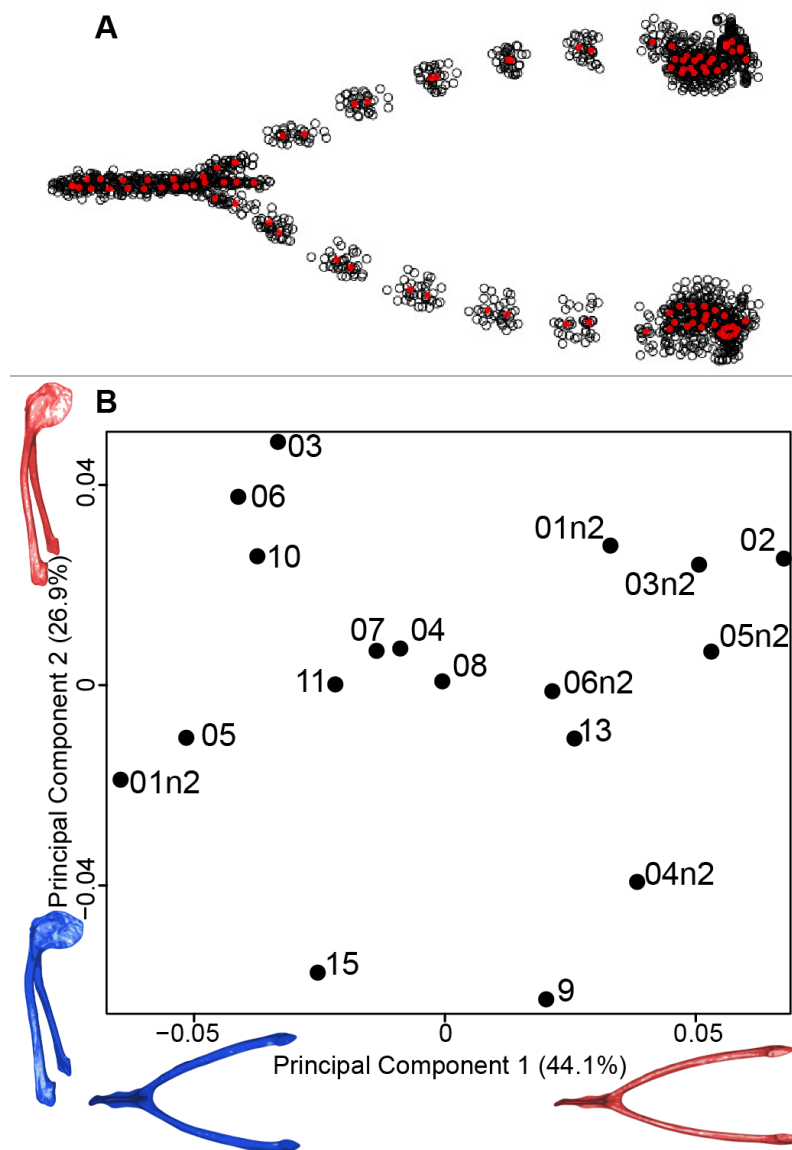


Figure 21: Overview of the analyses of the quail furculae. Consensus shape plot of the quail furculae (A). Consensus shape is shown in red points, all shapes observed are in black points. Principal Component Analysis performed on quail furcula shapes (B). Maximum theoretical shapes are shown in red and minimum theoretical shapes are in blue. Each individual is identified thanks to a unique code.

Sternum

We found the same pattern for the sternum as observed for the furcula (Figure 22 A). Thin parts on each side were very variable in orientation and shape. However, both the center part and the keel, showed little deformation. The four first axes of the PCA explained 65.3% of the total variance (PC1 = 25.7%, PC2 = 17.2%, PC3 = 12.0% and PC4 = 8.7%; Figure 22 B). Two types of shapes were distinguished along the first axis. The negative part was represented by a sternum with dorsolateral and caudolateral processes more distant from the central part of the sternum. The second axis showed differences in the anterior part of the sternum with the coracoid joint and the craniolateral process which were more prominent on the negative part of the axis compared to the positive part.

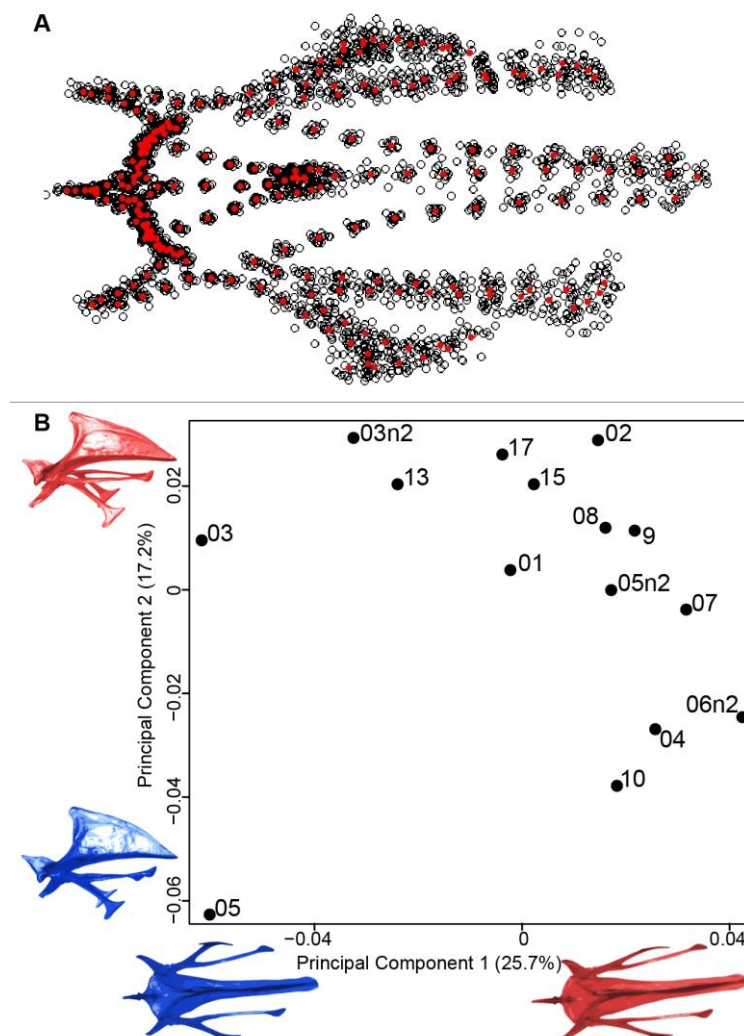


Figure 22: Overview of the analyses of the quail sternums. Consensus shape plot of the quail sternum (A). Consensus shape is shown in red points, all shapes observed are in black points. Principal Component Analysis performed on quail sternum shapes (B). Maximum theoretical shapes are shown in red and minimum theoretical shapes are in blue. Each individual is identified thanks to a unique code.

Coracoids

For the coracoid bone, which is a paired bone, the consensus shape showed that all the landmarks overlapped (Figure 23 A). This was confirmed by the fact that all right and left coracoids were each other's closest neighbors in the neighbor joining trees (Figure 23 B). The four first axes of the PCA explained 54.3% of the total variance (PC1 = 17.9%, PC2 = 15.1%, PC3 = 12.0% and PC4 = 9.3%; Figure 23 C). Two types of shapes could be distinguished along the first axis. The positive part was represented by a coracoid with angular sternocoracoidal process. The second axis showed differences on the anterior part of the coracoid with the acromion and the clavicle facet being more prominent on the positive part of the axis than on the negative part of the axis.

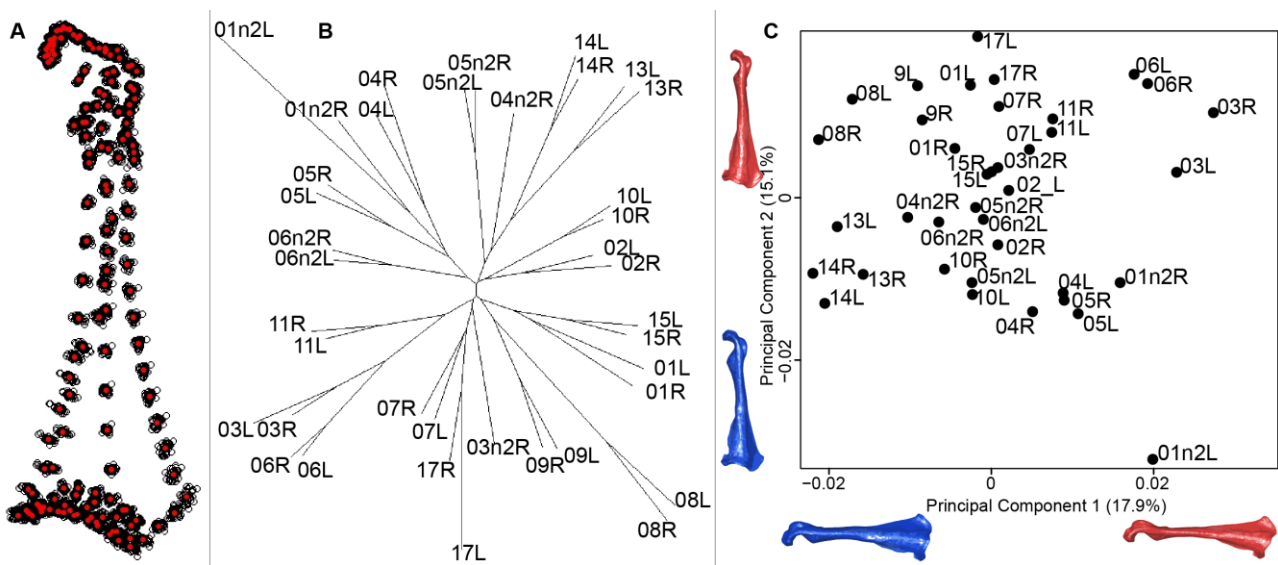


Figure 23 : Overview of the analyses of the quail coracoids. Consensus shape plot of the quail coracoids (A). Consensus shape is shown in red points, all shapes observed are in black points. Quail coracoid shapes neighbor joining tree (B). Each individual is identified thanks to a unique code, L: left side and R: right side. Principal Component Analysis performed on quail coracoid shapes (C). Maximum theoretical shapes are shown in red and minimum theoretical shapes are in blue.

Scapula

Scapula consensus shape showed that all the landmarks overlapped (Figure 24 A). Yet, not all right and left scapulae were each other's closest neighbors in neighbor joining trees (Figure 24 B). The four first axes of the PCA explained 67.8% of the total variance (PC1 = 27.3%, PC2 = 16.2%, PC3 = 14.2% and PC4 = 10.1%; Figure 24 C). Along the first axis, the positive part was represented by a gracile scapula with the anterior part of the blade being enlarged. The second axis showed differences on the global robustness of the blade on the positive part of the axis and a more gracile and curved blade on the negative part.

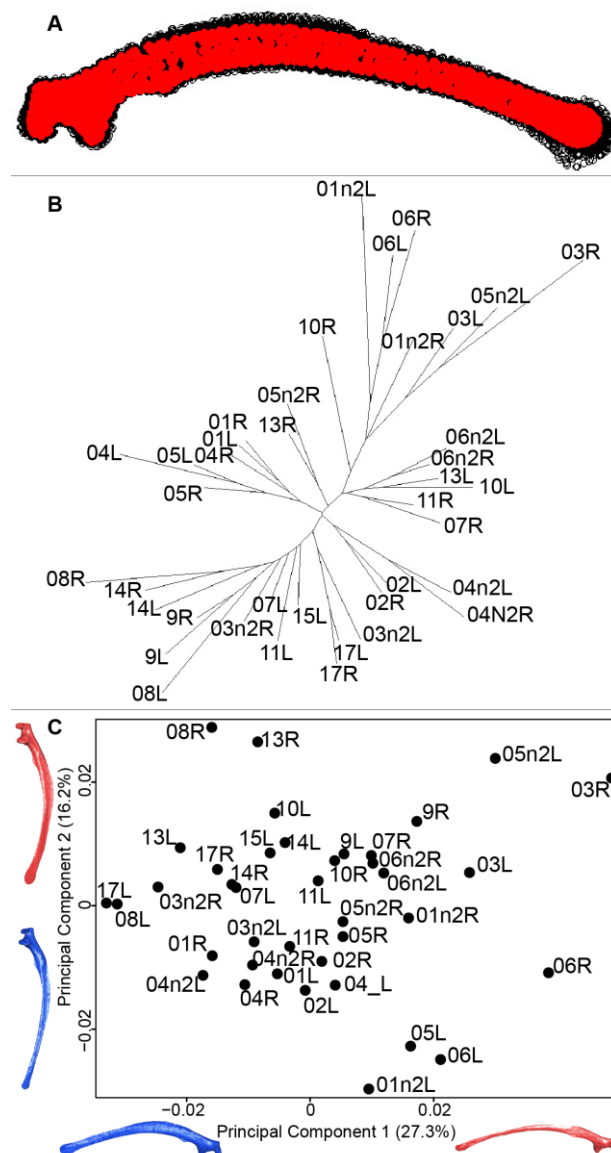


Figure 24 : Overview of the analyses of the quail scapulae. Consensus shape plot of the quail scapulae (A). Consensus shape is shown in red points, all shapes observed are in black points. Quail scapula shapes neighbor joining tree (B). Each individual is identified thanks to a unique code, L: left side and R: right side. Principal Component Analysis performed on quail scapula shapes (C). Maximum theoretical shapes are shown in red and minimum theoretical shapes are in blue.

Humerus

For the humerus, the consensus shape showed that all the landmarks overlapped (Figure 25 A). This seemed to be congruent with the neighbor joining tree where almost all right and left humeri were each other's closest neighbors (Figure 25 B). The four first axes of the PCA explained 51.7% of the total variance (PC1 = 17.9%, PC2 = 15.1%, PC3 = 10.2% and PC4 = 8.5%; Figure 25 C). The positive part was represented by a robust humerus with a large shaft and articulation. In contrast, gracile humeri with long and thin shaft were associated with the negative part of the axis. The second axis highlighted a difference in the head length on the anterior part of the humerus with a longer head at the negative part of the axis.

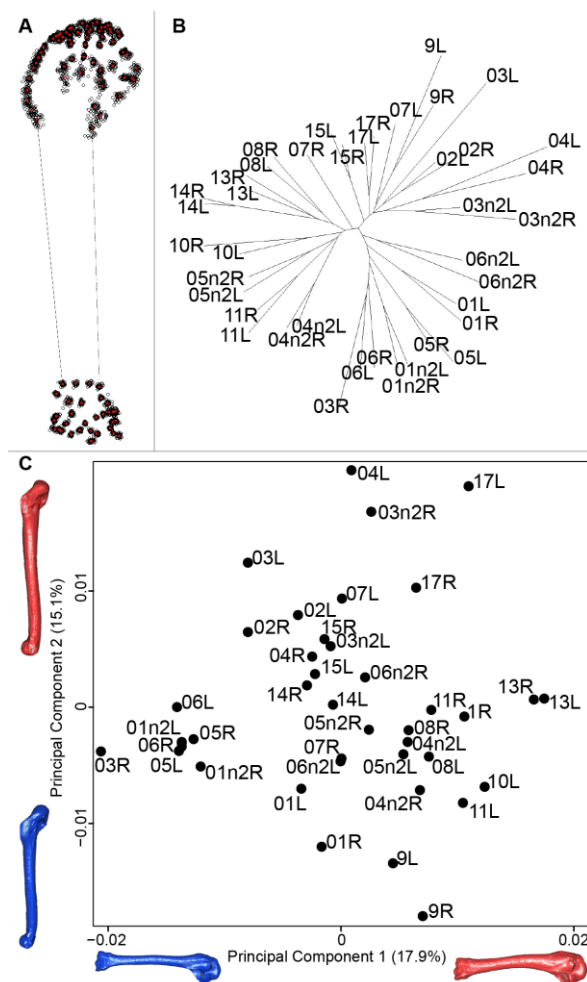


Figure 25 : Overview of the analyses of the quail humeri. Consensus shape plot of the quail humeri (A). Consensus shape is shown in red points, all shapes observed are in black points. Quail humerus shapes neighbor joining tree (B). Each individual is identified thanks to a unique code, L: left side and R: right side. Principal Component Analysis performed on quail humerus shapes (C). Maximum theoretical shapes are shown in red and minimum theoretical shapes are in blue.

Disparity and symmetry

Unpaired bones, furcula and sternum, had a higher disparity than paired bones (Table 8). Symmetry tests showed that the bones have different patterns of symmetry (Table 9). Unpaired bones, such as the furcula and the sternum, seemed to be less symmetrical than paired bones such as the coracoid, scapula and the humerus. Among the paired bones, the results showed that the sternum seemed to be more asymmetrical than the furcula. These symmetry test results were congruent with the disparity tests.

Table 8 : Results of the morphological disparity test for each bone. (x100,000)

Bone / Sampling	Intraspecific level	Interspecific level
Furcula	333	2024
Sternum	822	6382
Coracoid	83	699
Scapula	95	301
Humerus	38	187

Table 9 : Results of the symmetry tests performed on each bone for the intraspecific dataset. Significant differences are indicated in bold.

Bone	Student T value	Student test P-value
Furcula	-29.1	<0.01
Sternum	-48.3	<0.01
Coracoid	-1.4	0.16
Scapula	<0.001	1
Humerus	<0.001	1

Interspecific level analyses to assess the impact of bone deformation in a broader context

Furcula

The first four axis of the interspecific PCA explained 91.8% of the total variance (PC1 = 67.4%; PC2 = 12.3%; PC3 = 8.5%; PC4 = 3.6%; Figure 26 A). The quail specimens group together whereas the other species are spread in the morphospace. The disparity calculation showed a larger disparity between species than among quails (Table 8).

Sternum

The interspecific PCA fourth axis explained 95.9% of the total variance (PC1 = 83.2%; PC2 = 7.1%; PC3 = 3.5%; PC4 = 2.1%; Figure 26 B). Quail specimens grouped together whereas the other species were widespread in the morphospace. The disparity calculation which showed an eight times larger disparity at the interspecific level compared to the intraspecific level (Table 8).

Coracoid

The four first axes of the PCA computed on the sternum shapes explained 86.6% of the total variance (PC1 = 64.9%, PC2 = 10.3%, PC3 = 6.8% and PC4 = 4.6%; Figure 26 C). In this morphospace, all the quails were packed and well differentiated from other species. Again, disparity calculations supported this result (Table 8).

Scapula

The four first axes of the PCA computed on the coracoid shapes explained 79.8% of the total variance (PC1 = 39.2%, PC2 = 20.4%, PC3 = 12.9% and PC4 = 7.3%; Figure 26 D). Quails were clustered together, yet, *Coua cristata* overlapped with the quails on the first two axes. The disparity calculation confirmed that there was less disparity among quails than at the interspecific level (Table 8).

Humerus

The four first axes of the PCA computed on the scapula shapes explained 81.7% of the total variance (PC1 = 52.9%, PC2 = 17.3%, PC3 = 7.5% and PC4 = 4.0%; Figure 26 E). Quail bones clustered together and were well separated from other species, which corresponds to the disparity estimates (Table 8).

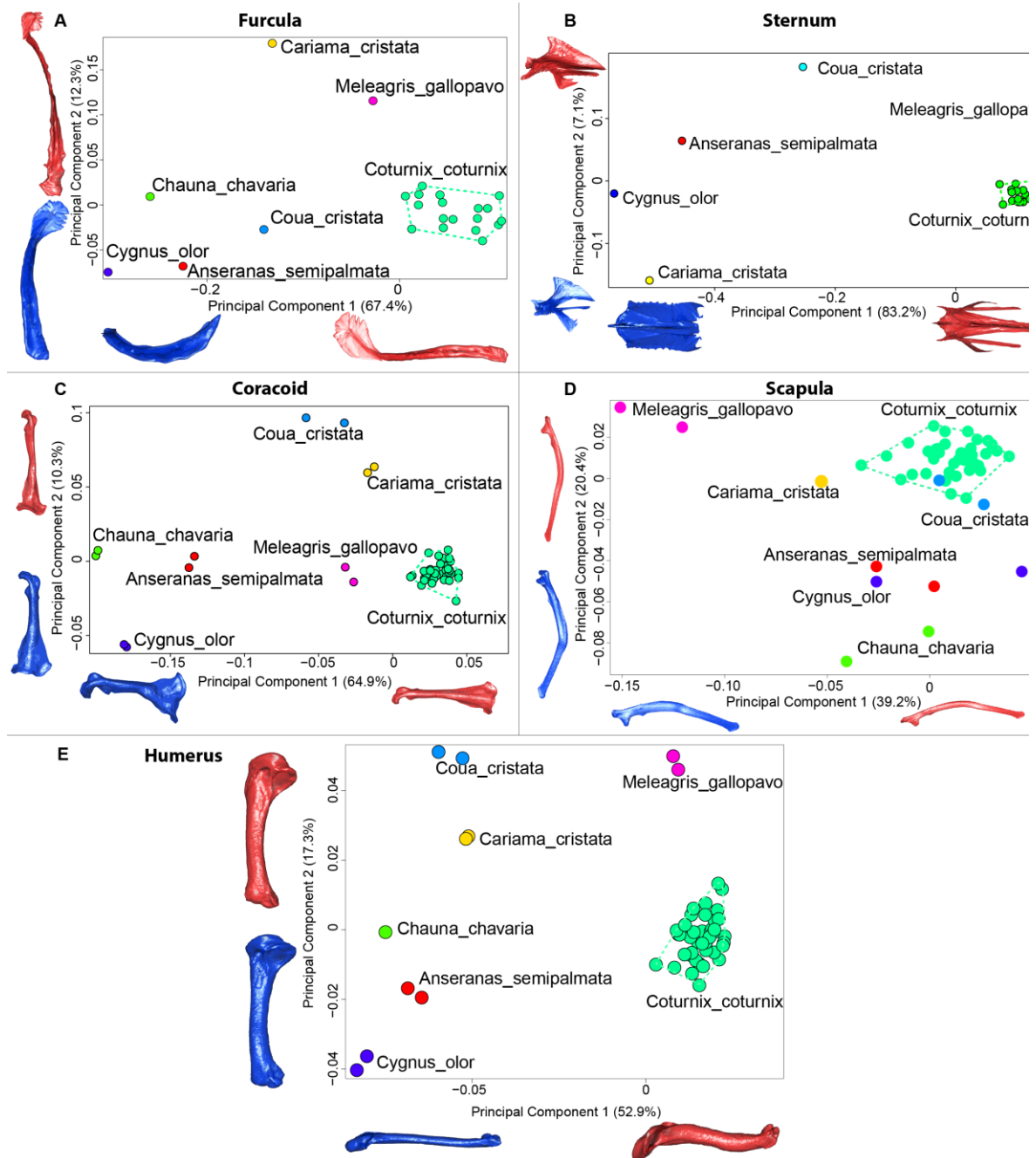


Figure 26 : Overview of the results of Principal Component Analyses (PCA) performed on interspecific dataset of bone shapes. Colors represent each species. *C.coturnix* specimens are linked together. (A) furcula, (B) sternum, (C) coracoid, (D) scapula, (E) humerus. Maximum theoretical shapes are shown in red and minimum theoretical shapes are shown in blue.

Discussion

The preparation process is an obligatory step in the preparation of bones for collections. It is, however, important to be able to quantify potential effects of preparation on the morphology of the treated bone as this may impact subsequent comparative studies. Some effects have been reported, such as modified microstructure and modification of the chemical composition of the bone (Fernández-Jalvo and Marin-Monfort, 2008; Hahn, Vogel, and Delling, 1991; Lemoine, 2011). In practice, there appears to be no specific preparation protocol for bird bones. Yet, birds bones are pneumatic and this characteristic should be taken into account during preparation (Baumel et al., 1993; Fernández-Jalvo and Marin-Monfort, 2008; Novitskaya et al., 2017; Pennycuick, 1967; Ritzen, 1978). Moreover, the preparation protocol with enzymes used for our bones is one of two best protocols studied by Fernandez-Jalvo and Marin-Monfort (2008) to avoid physical damage.

What is the impact of deformation due to preparation on the bone shape at the intraspecific level?

Differences in shape depending on the color and texture.

The results of the MANOVAs performed on each bone show significant shape differences depending on the texture. The main differences are between powdery bones and other types of bone (Figure 20; Table 7). Powdery bones appear to have a wider distribution in the morphospace for each bone. Considering extreme bones shapes shown in the PCA for each bone, most of the time the gracile shapes match the powdery bones. This suggests a direct impact on the thickness and the composition of the bone because of the preparation process.

Looking more specifically at the concerned individuals, some individuals have powdery bones for all the paired bones. A powdery texture is not found on all the bones of the same specimen, which suggest that this characteristic may not be individual-specific. It could be linked to the type of preparation, more specifically to the removal of the fat. Preparators are used to evaluate the fat saturation by looking at the bone texture directly after an obligatory first bath. There are three possibilities during preparation: 1) the fat saturation of the bone looks low and the treatments are stopped; 2) the fat saturation of the bone is still too important so the renewal of this step is decided or 3) the first bath treatment itself may be too aggressive for the bone and texture is already powdery after the initial fat removal step. It is

known that the bird furcula is composed of Haversian bone for a large part of the fused part of the clavicle (Cubo et al., 2005; Mitchell et al., 2017; Ponton et al., 2007). This particular bone formation may result in a different reaction when treated with the chemicals used in the preparation protocol (Lemoine and Guilminot, 2011). For this reason, preparation protocols have to be adapted to the specific bones (Hahn, Vogel, and Delling, 1991). Because all individuals and bones may differ in internal composition, length, width, weight and thickness, using the same quantity of chemicals or the same time of processing for all bones could impact the bone. The external appearance of the bone appears to be a good indicator of the impact of preparation and as such a good proxy for preparation deformation. It would be interesting in future studies to perform histological analyses to be able to detect the effect of chemicals on the preparation on the bones.

Furcula

The analysis of the furcular shape shows that the main shape modifications occur on the clavicles and their symphysis. Considering the results of the principal component analysis and shape differences depending on the texture, the deformation appears to result in a flatter furcula with narrower and straighter clavicles and with an elongated and more dorsally oriented symphysis (Figure 21). These shape modifications could be explained by a modification of the Haversian bone, which is specifically located in this area of the furcula. Indeed, furcula bone composition is known to be different from the other bird bones (Mitchell et al., 2017). Furthermore, wing beats during locomotion have been shown to induce cyclic deformations, with bone remodeling replacing damaged bone with Haversian bone (Ponton et al., 2007). This bone type seems more likely to be affected by the chemical preparation process compared to the non-Haversian bone.

Sternum

The main parts of the sternum shape affected by preparation are the lateral processes, the thicker parts of the sternum which appear more distal from the central part (Figure 22). The central part of the sternum has a protection function and provides support for the carina. This part of the sternum is thick and robust to hold the pectoral muscles and to withstand their force (Baumel et al., 1993; Harvey, Kaiser, and Rosenberg, 1969). The cranial and central part is involved into the coracoid joint area, its functional constraint could explain the light amount of deformation. The lateral thin parts of the sternum are inter-connected with fasciae and aponeuroses of the flat oblique abdominal muscle (Goslow, *et al.*, 1990). Moreover, these

abdominal muscle forces may deform the bone during wingbeats to keep the unity of the trunk (Jenkins, Dial, and Goslow, 1988). Jenkins et al. (1988) showed that the sternum also exhibits cyclical movements with each wingbeat. During down-stroke the sternum ascends and retracts caudodorsally, and then during the subsequent upstroke it descends and protracts cranio-ventrally. As in the furcula, flexible parts of the sternum involved in wingbeats seem to be more easily affected by the preparation process.

Coracoid

Coracoid bones display less shape variation than unpaired bones. The main shape modification seems to be the gracile conformation of the bone. The shaft is sharper, the distal part is sharp-edged and the proximal part is more curved. These deformations look like a slight contraction of the whole bone on itself. Coracoids have an important function during flight, as they act as a pulley for the pectoral muscles, which are the biggest muscles involved in the wing upstroke. Coracoids have to be robust enough to support and transmit muscles forces without deforming (Beaufrère, 2009; Nesbitt et al., 2009). Its crucial role in force transmission could be a strong constraint on both shape and robustness (George and Berger, 1966; Shufeldt, 1901, 1909). This result seems to be confirmed by the neighbor joining tree, showing that both right and left coracoids are well paired for each individual (Figure 23). This result supports the hypothesis of strong solidity of this bone (George and Berger, 1966; Gordon et al., 2008).

Scapula

The neighbor joining tree performed on the shape data of the scapula shows some morphological variation between the right and left bones for each individual. Natural asymmetry is not expected to be higher within individuals than between individuals, thus, these differences could be due to the preparation process. This result is supported by the wide distribution in the morphospace, especially on the positive part of the first axis which is characterized by a gracile and low scapula (Figure 24). This suggests that these morphologies may not be due to natural asymmetries but more likely due to the preparation process (Hahn, Vogel, and Delling, 1991; Lemoine, 2011).

Humerus

In contrast to the results obtained for the scapula, the neighbor joining tree of the humeri shows that left and right bones belonging to the same individual cluster together. This suggests that the preparation process may have less impact on the humerus. Looking at the PCA, a group of bones seems more isolated from the others. Their shape is gracile, the deltoid crest is less prominent and the distal extremity is less robust (Figure 25). As for the scapula, extreme humerus bone shapes have a more gracile morphology than the mean bone shapes. Moreover, the humerus is known to be not significantly loaded in direct tension or compression, which implies no particular ossification or solidification of this bone (Pennycuik, 1967). Again, it suggests a non-natural deformation and thus could be due to preparation process affecting the thickness of the whole bone (Hahn, Vogel, and Delling, 1991; Lemoine, 2011).

In general, powdery paired bones are more gracile than neutral and oily bones. It seems that the last step of the preparation protocol, the fat removal which can be repeated several times, is the main factor causing bone shape deformation.

Disparity and asymmetry

We observed that unpaired bones display a greater disparity than paired ones and the same pattern is found in interspecific analyses (Table 8). This could mean that unpaired bones are more easily deformed by preparation than paired bones. This could be explained by two factors: 1) paired bones can easily be dried in a specific position. For unpaired bones, the most convenient method is to put it on its side. Thus, this position can induce a morphological deformation only on one side due to the fact that the bones have to support their own weight. This way of drying can lead the bone to have a directional drying asymmetry; 2) all vertebrates display a bilateral symmetry, yet are not perfectly symmetric. Many factors can impact symmetry including lateralisation (Galatius and Jespersen, 2006; Klingenberg, 2003; Mays, Steele, and Ford, 1999; Palmer, 2004). This phenomenon should, however, impact paired and unpaired bones similarly. However, the symmetry tests show a significant difference between right and left sides for unpaired bones, such as furculae and especially sterna, whereas the differences are not significant for paired bones. Given that one side is

always significantly different from the other one this suggests an impact of the drying process on bone asymmetry.

What is the impact of deformation due to preparation on shape analysis at the interspecific level?

The interspecific dataset demonstrates that, despite the large morphological disparity observed within the quail dataset, analyses conducted at an interspecific level are not impacted by the effect of bone preparation (Table 8). It suggests that, even if there are some deformations due to the preparation protocol, at an intraspecific dataset level of analyses, these deformations are too small to be significant.

Conclusions

In summary, it appears that flexible bones and bones with thin parts such as the blades of the sternum and scapula are more likely deformed by the preparation process. However, the central part of the sternum and the keel which provide protection and have large muscle insertions or the coracoid with its robust pulley function are not deformed. Symmetry tests show that shape variations cannot be natural because they are located mainly on unpaired bones and are not equally distributed between the two sides of the bone. Thus, the drying process could induce some deformations on unpaired bones. Moreover, for paired bones, the more gracile bone shape with a powdery texture appeared to be a direct consequence of the preparation process. We showed that these preparation deformations can influence intraspecific analysis and lead to functional erroneous conclusions, especially when studying the effect of symmetry on bones. Finally, these deformations due to the preparation have little effect at the interspecific level. This study highlights the importance of carefully selecting preparation methods in order to avoid physical damage that could impact the shape of the treated bones. To more accurately understand the effect of preparation on the deformation of bones, future studies need to be done comparing X-ray computed tomography of specimens before and after preparation.

**Chapter 3 - Does flight type
constrain the shape of the scapular
girdle in birds? Inferences on the
flying ability of the hoatzin
(*Opisthocomus hoazin*)**

The results of the previous chapter have shown that at an intraspecific level, the effect of the bone preparation on the shape of each bone of the scapular girdle of birds cannot be neglected. Moreover, deformations due to preparation can be estimated just by looking at the texture of the bone. However, we found no significant differences at the interspecific level as the deformations induced by preparation are negligible in comparison to shape differences between species. Following these results, we decided to select collection specimens carefully in further studies.

In order to test the hypothesis from the literature about the poor flying abilities of the hoatzin, we used a comparative dataset composed of fifty-nine species for which the locomotor behaviour is well known. We used shape analyses for each bone of the scapular girdle to determine if the unique sternum shape of the hoatzin, especially the reduced carina, were the direct responsible of the poor flying abilities of the hoatzin. We first tested for shape differences for each bone of the scapular girdle depending on flight type in this large dataset of birds with different locomotor strategies. Then, when shape differences were found, we performed assignation tests on the bones impacted by locomotor factors in order to assess the flight type of the hoatzin.

Does flight type constrain the shape of the scapular girdle in birds? Inferences on the flying ability of the hoatzin (*Opisthocomus hoazin*)

Fanny Pagès, Anick Abourachid, Anne-Claire Fabre

In progress

Abstract

The hoatzin (*Opisthocomus hoazin*) is a strictly folivorous bird with a unique digestive physiology. Due to its foregut fermentation, the crop is hypertrophied causing modifications of the scapular girdle. It has been hypothesized that this could have functional implications by greatly reducing the sternal carina, thus reducing the insertion area for the flight muscles. However, this hypothesis remains to be tested. We quantified the morphology of bones that are functionally important during flight: the sternum, the scapular girdle, and the humerus. To do so, a 3D-surface geometric morphometric study was performed on these bones for 59 species of birds with different locomotor abilities. Morphological differences in relation to flying ability were explored using a principal component analysis, multivariate analysis of variance, and regressions taking into account phylogeny. Our results show morphological differences for the bones of the scapular girdle depending on the type of flight suggesting that bone shape can be used to infer flight type. Overall, the shape of the scapular girdle of birds seems a very good indicator of flight adaptations with its shape capable of distinguishing good from poor flyers. In contrast to what has been suggested in the literature the shape of the bones of the scapular girdle in the hoatzin are not dramatically different from those of other birds and resemble those of gliders. Future studies exploring the shape of the bones of the scapular girdle in closely related extinct species might help to better understand the locomotor evolution in this group.

Introduction

Many animals have independently colonized the aerial environment resulting in different anatomical specializations to flight. Among vertebrates, the most iconic group of flying animals is undoubtedly represented by birds. They are the most successful among tetrapods with the highest number of species (Lecointre, Le Guyader, and Visset, 2016) and have successfully colonized a diversity of habitats (from aerial to aquatic) around the globe ranging from the poles to the equator (Hawkins et al., 2007, 2006). As a consequence of their adaptation to these habitats, birds display a tremendous morphological diversity (disparity) of form and function (MacArthur and MacArthur, 1961) involving unique morphological specializations such as the modified forelimb and feathers (Mariani and Martin, 2003). Thus, their morphology is highly variable and specialized, ranging from swimming animals with an aerodynamic body (penguin), over animals with insect-like flight types (hummingbird), to an almost complete reduction of the forelimbs (kiwi) (Abourachid, Castro, and Provini, 2019; Viscor and Fuster, 1987).

In this context, the origin and evolution of birds, and more particularly the origin of flight remain key questions in evolutionary biology. One of the often-used models to compare to and to make inferences on extinct species of early birds is the iconic hoatzin (*Opisthocomus hoazin*). As its chicks retain claws on their wing the hoatzin is often used by paleontologists as an extant analogue for the locomotor mode of fossil taxa (Feduccia, 1993; Gatesy and Dial, 1996; Serrano et al., 2018). Nevertheless, the hoatzin is an unusual species that remains poorly studied. The few studies done (Grajal, 1995; Grajal et al., 1989; Parker, 1891; Strahl, 1988) have suggested that the hoatzin is a poor flyer due to its unique digestive physiology and the hypertrophy of its crop inducing modifications of the sternum. Indeed, it has been hypothesized that the reduction of the sternal carina involves a reduction of the attachment area of the flight muscles. Furthermore, the few *in vivo* observations describe the hoatzin as a species with a very non-agile flight (del Hoyo, Elliott, and Sargatai, 1993; Grimmer, 1962; Müllner, 2004).

However, in order to make any solid inferences on the flying ability of the hoatzin it is essential to understand the interplay between the morphology of the bones of scapular girdle and flight ability in a large and comprehensive sample of extant birds.

The scapular girdle is an important anatomical structure in birds as it allows the attachment of the flight muscles. Thus, it is likely a good proxy of locomotor adaptations and flight type in birds. The scapular girdle is composed of five bones: the sternum, the furcula, the coracoid, the scapula and the humerus. Some of the bones have been modified and are fused such as the clavicles which form the furcula. The furcula is the only bone of the scapular girdle that has been studied intensively in the context of locomotion in birds. Previous studies have described it as the main driver of the flight type in birds (Close and Rayfield, 2012; Hui, 2002; Mitchell et al., 2017). It has also been shown that its morphology is closely related to flight type with a U-shaped furcula in soaring birds and a V-shape in swimming birds (Hui, 2002). Furthermore, the degree of curvature of the furcula seems to differentiate swimming birds from birds of prey, for example (Close and Rayfield, 2012; De Margerie et al., 2005; Hui, 2002; Voeten et al., 2018). For the other bones of the scapular girdle, the coracoids have been described as being mobile during the beating of the wings as they support the furcula (Baier, Gatesy, and Dial, 2013; Jenkins, Dial, and Goslow, 1988). Concerning the scapula and the humerus, their roles and shapes have been rather poorly studied in relation to flight mechanics or flight type. Finally, the sternum, and more specifically its carina, forms the main and largest area of attachment for the flight muscles (Kardong, 2012). The presence or absence of the carina has been suggested as being characteristic for flight ability (Gill, 2007). For example, flightless birds such as the ratites have a sternum that does not display any carina whereas bird of prey have a high carina (Cano, 2012; Gussekloo and Cubo, 2013).

The aim of this study is to explore the relationships between locomotor specialization and the shape of the bones of the scapular girdle in birds. This allows us to i) test for shape differences depending on flight type, ii) to better understand which bones are good proxies of flying ability in birds, and iii) to infer the flying ability of the hoatzin in light of the observed shape of the bones of the scapular girdle. We predict to find shape differences depending on locomotor specialization for each bone of the scapular girdle. More specifically, we expect that the furcula will be more U-shaped in soaring birds whereas it will be V-shaped in aquatic birds (Hui, 2002). We also expect that the sternum will have a less developed carina in flightless birds in comparison to flying ones (Gill, 2007). We also expect to find shape differences in the humerus according to the locomotor type. We expect that the coracoids and scapulae will be less

developed in flightless than in flying birds. Finally, we predict that the bones of the scapular girdle of the hoatzin should be similar to those of poor flyers as suggested in previous studies (Grajal et al., 1989; Strahl, 1988).

Material and methods

Data collection

Sample

Fifty-nine species from the collections of the Muséum National d'Histoire Naturelle were selected in order to represent a broad locomotor diversity across a phylogenetically diverse sample of birds (Annex A). For each specimen, eight bones were selected: the sternum, the furcula, both coracoids (left and right), both scapulae (left and right) and both humeri (left and right). For smaller specimens (bones measuring less than twenty centimeters of length), the 3D surfaces were acquired using a white light fringe Breuckmann scanner (SmartSCAN) and its scanning software Optocat (<http://www.breuckmann.com>) at the “plate-forme de morphométrie” of the UMS 2700 of the MNHN. Larger specimens (bones measuring more than twenty centimeters of length) were scanned at the “plateforme Surfacus” of the MNHN using a laser scanner RANGE 7 (Konica Minolta; <https://www.konicaminolta.com>) and the associated RangeViewer (v. 2.00) and Rapidform (v. XOR) software packages. Further processing was performed with the Geomagic Studio 2013 (<http://www.geomagic.com/>) software package in order to obtain a surface on which shape data can be accurately acquired.

Locomotor data sampling

We collected locomotor data on the species used in this study from the Handbooks of the birds of the world (del Hoyo, Elliott, and Sargatai, 1991) (Annex A). We defined flight type as the type of flight most commonly used by a species during steady, level flight (Close and Rayfield, 2012). These definitions do not take into account behaviors such as takeoff, landing, or maneuvering (Close and Rayfield, 2012). Data about the flight types were collected from the literature (Close and Rayfield, 2012; Hui, 2002; Mitchell et al., 2017; Viscor and Fuster, 1987). In order to keep enough statistical power for analyses, we defined only broad categories describing the main flight types used. Six categories were defined: flapping birds, gliding birds, poor flyers, birds which are unable to fly, semi-aquatic birds, and finally swimming birds (Table 10).

Table 10 : Definitions of the different flight types used in this study

Flight type	Definition
Flapping	Flapping requires constant, regular wing beats occurring in the air and without prolonged soaring (Hui, 2002)
Gliding	Gliding and soaring were grouped together to represent a flight type which requires only series of wingbeats separated in time by long periods without and where the wings are extended. Anatomical adaptations may exist to help maintain wing extension (Hui, 2002).
Poor flyers	Poor flyers or 'burst-adapted' fliers, a category which gathers species that are only capable of very short-range flights (to escape a predator), and cannot maintain flight for prolonged periods (Close and Rayfield, 2012)
Semi-aquatic	Semi-aquatic species use their wings for locomotion in both air and water. Adaptations must meet the requirements of both subaqueous and steady aerial flight (Hui, 2002).
Swimming	Swimming species only use their wings for swimming. The increased profile drag due to the higher density of water may require increased wing protraction (Hui, 2002).
Flightless birds	Birds which are not able to fly

Shape quantification using geometric morphometrics

In order to accurately quantify the shape of each bone of the scapular girdle we used a 3D geometric morphometric analysis. Morphometric data were digitized on the surface scans using the IDAV Landmark software (v. 3.0.0.6). For each bone, landmarks were chosen to accurately describe the complex geometry of each element. Each set of landmarks is detailed below for each studied bone (Tables 11-15, Figure 27). For our analyses, we use sliding semi landmarks on curves between landmarks and a patch of points to more accurately define bone shape.

We defined a unique set of landmarks and curves for each bone. Furculae were described using 814 landmarks (10 anatomical landmarks, 108 curve landmarks and 1417 surface landmarks), the sternum shape was quantified using 5723 landmarks (13 anatomical landmarks, 295 curve landmarks and 5415 surface landmarks), the coracoid shape was described by 2376 landmarks (10 anatomical landmarks, 170 curve landmarks and 2196 surface landmarks), the scapulae were described with 1065 landmarks (7 anatomical landmarks, 150 curve landmarks and 908 surface landmarks) and humeri were described using 2172 landmarks (18 anatomical landmarks, 205 curve landmarks and 1949 surface landmarks) (see Figure 27 and Tables 11-15 for a detailed description of the landmarks).

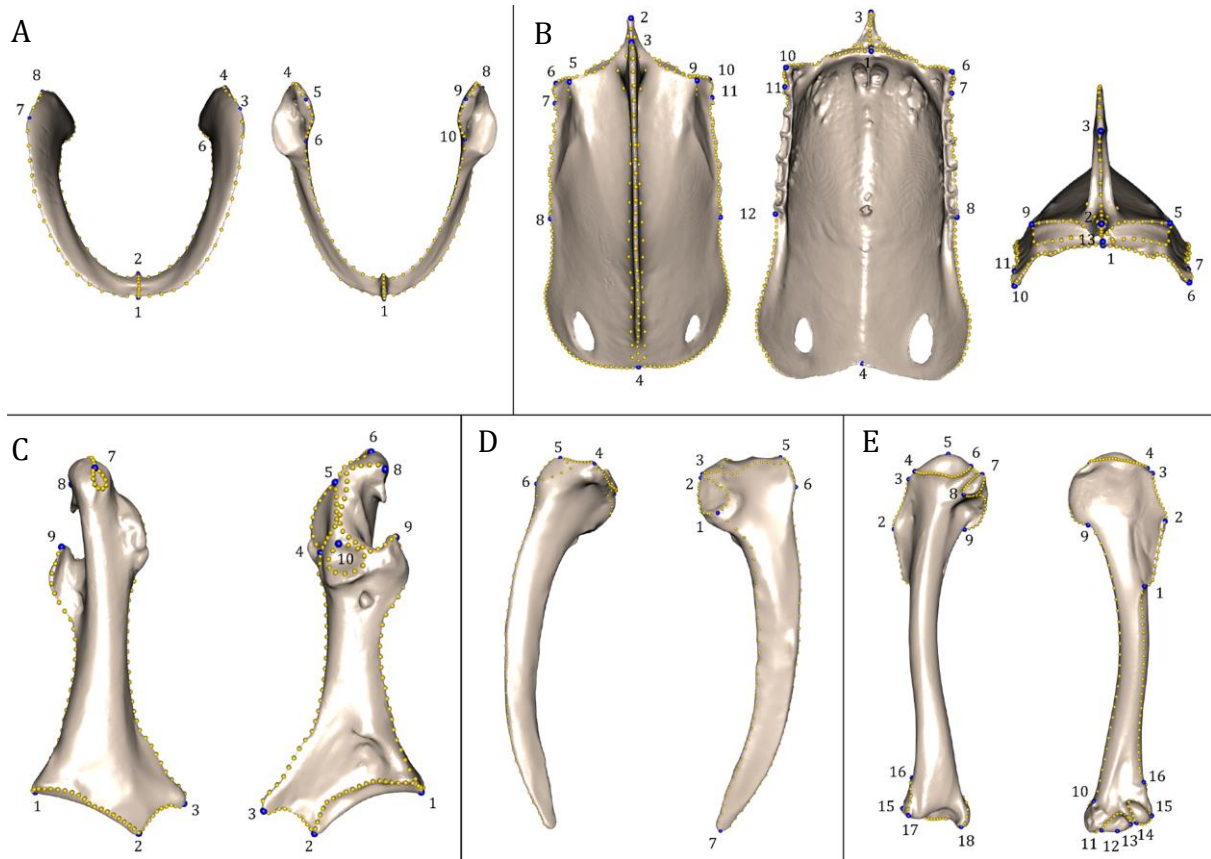


Figure 27 : Landmarks used in the analyses to quantify shape variation on scapular bones. Northern goshawk (*Accipiter gentilis*) bones are presented. Furcula: (A) caudal view, (B) lateral view, see Table 13 for landmark definition. Sternum: (C) lateral view, (D) ventral view, see Table 12 for landmark definitions. Left coracoid: (E) dorsal view, (F) ventral view, see Table 11 for landmark definitions. Left scapula: (G) dorsal view, (H) ventral view, see Table 14 for landmark definitions. Left humerus: (I) medial view, (J) lateral view, see Table 15 for landmark definitions. Blue points represent landmarks and gold points represent semi-landmark curves

Table 11 : Definition of the landmarks of the coracoid used in the geometric morphometric analysis. See Figure 27 E-F for landmark position on the coracoid

Landmarks	Definition
1	lateral extremity of the mediolateral angle
2	medial extremity of the sternal facet
3	medial extremity of the sternocoracoid process
4	proximal extremity of the glenoid facet
5	proximal extremity of the procoracoid
6	apex of the acromion and the brachial tuberosity fusion
7	distal extremity of the furcular process
8	distolateral extremity of the caudal facet of the acromion
9	distal extremity of the procoracoid
10	distal extremity of the scapular facet in caudal view

Table 13 : Definition of the landmarks of the sternum used in the geometric morphometric analysis. See Figure 27 C-D for landmark position on the sternum

Landmarks	Definition
1	cranial extremity of the dorsal manubrial spine
2	craniodorsal extremity of the manubrium
3	dorsal extremity of the cranial process of the keel
4	caudal extremity of the caudal process of the keel body
5	extremity of the dorsolateral process of coracoidal articular facet, left side
6	cranial extremity of the craniolateral process, left side
7	cranial extremity of the first sternal rib facet, left side
8	caudal extremity of the last sternal rib facet, left side
9	extremity of the dorsolateral process of coracoidal articular facet, right side
10	cranial extremity of the craniolateral process, right side
11	cranial extremity of the first sternal rib facet, right side
12	caudal extremity of the last sternal rib facet, right side
13	medioventral extremity of the coracoidal articular facet

Table 12 : Definition of the landmarks of the furcula used in the geometric morphometric analysis. See Figure 27 A-B for landmark position on the furcula

Landmarks	Definition
1	dorsal extremity of the symphysis, cranial view
2	ventral extremity of the symphysis, caudal view
3	maximum of curvature, right clavicle
4	beginning of the joint with the coracoid, right clavicle
5	most caudal point of the right clavicle
6	end of the joint with the coracoid of the right clavicle
7	maximum of curvature, left clavicle
8	beginning of the joint with the coracoid, left clavicle
9	most caudal point of the left clavicle
10	end of the joint with the coracoid of the left clavicle

Table 14 : Definition of the landmarks of the scapula used in the geometric morphometric analysis. See Figure 27 G-H for landmark position on the scapula

Landmarks	Definition
1	Distal extremity of the glenoid facet
2	Proximal extremity of the glenoid facet
3	Ventral extremity of the coracoidal tubercle
4	Ventral extremity of the acromion
5	Dorsal extremity of the acromion
6	Distal extremity of the furcula articular facet
7	Proximal extremity on the blade

Table 15 : Definition of the landmarks of the humerus used in the geometric morphometric analysis. See Figure 27 I-J for landmark position on the humerus

Landmarks	Definition
1	distal extremity of the deltoid crest
2	apex of the deltoid crest
3	proximal extremity of the deltoid crest
4	dorsal extremity of the head of the humerus
5	apex of the head of the humerus
6	ventral extremity of the head of the humerus
7	Lateral extremity of the ventral tubercle
8	Medial extremity of the ventral tubercle
9	Distal extremity of the ventral crus
10	proximal point of the ventral epicondyle
11	Ventral extremity of the ventral condyle
12	Apex of the ventral condyle
13	Dorsal extremity of the ventral condyle
14	Ventral and distal extremity of the dorsal condyle
15	Dorsal and distal extremity of the dorsal condyle
16	Apex of the dorsal supracondylar process
17	Apex of the dorsal epicondyle
18	Apex of the flexor process

Each specimen is only defined by its landmarks and sliding landmarks on curves. Next, surface landmarks are projected from a template onto each specimen using a semi-automated method (Bardua et al., 2019). In this procedure, the surface sliding-landmarks are projected onto the surface of the new specimen using a template that was created following the protocol described in Souter *et al.* (2010). Finally, landmarks were slid to minimize the bending energy (Bookstein, 1997; Gunz, Mitteroecker, and Bookstein, 2005; Gunz and Mitteroecker, 2013) thus transforming sliding-landmarks into spatially homologous landmarks that can be used to compare shapes. This operation was performed using the Morpho package in R (v3.5.0; Schlager, 2017). For each bone, a separate generalized Procrustes superimposition (Rohlf & Slice, 1990) was performed in order to compare the shape (Bookstein, 1991). This step was performed using the 'gpagen' function in Geomorph R package (Adams and Otárola-Castillo, 2013). After superimposition, each object is defined by its Procrustes coordinates (shape) and centroid size (size). Thus, size and shape parameters for each bone can be studied independently but also pooled to analyze the form as a whole.

Statistical analysis

All the statistical analyses were performed in R (v.3.5.0; <https://www.r-project.org/>).

Principal component analysis

A principal component analysis (PCA) was performed on each bone data set in order to explore the distribution of the species in the morphological space (morphospace). To do so, we used the function 'plotTangentSpace' of the R 'geomorph' package (Adams and Otárola-Castillo, 2013). As a PCA allows a reduction of dimensionality, we further used the principal component scores (PCs) representing 95% of the overall variance as input for all further analyses. Theoretical shapes were computed using maximum and minimum data of the PC axes.

Shape differences depending on flight types

For each bone of the scapular girdle, we tested for shape differences depending on flight types using multivariate analyses of variance (MANOVA), and phylogenetic MANOVA. We used as input the principal component scores (PCs) accounting for 95% of the overall shape variance. These tests were done using respectively both the 'procD.lm' and 'procD.pgls' functions of the 'geomorph' package. Univariate ANOVAS and subsequent Tukey post-hoc tests were performed with Bonferroni correction on the first three PCs separately. Only bones being significantly different between flight types in the MANOVAs were used in the ANOVAs.

Inferring flight type of the hoatzin based on its morphology

In order to assess the flight type of the hoatzin, we performed a K nearest neighbour classification test (Ripley, 1996) using the R library 'class' (Venables and Ripley, 2002) on the shape data of each bone of the scapular girdle that was significantly different in the MANOVAs. To do so, we used as input for each bone the PCs accounting for 95% of the overall shape variance. The algorithm then predicted the classification of the hoatzin according to the K nearest neighbour classification. Each assigned classification was finally assessed statistically through a cross-validation test for each bone separately. For all of our tests the K value that provided the best assignation result is K=1. This parameter has been used in other morphometric studies (Baylac and Frieß, 2005; Cornette et al., 2015; Guillaud, Cornette, and Béarez, 2016). We know that the hoatzin is not a swimming bird, nor a semi aquatic nor a flightless bird based on the literature. Thus, to maximize the statistical power of the classification test, we performed the classification test using three biologically possible flight types: flapping flight, gliding flight, and poor flier.

Results

Principal Component analyses

Furcula

The first three PCs account for about 70% of the overall shape variation. The overall morphospace of the second and third axes tends to separate the aquatic and semi aquatic species from the others (Figure 28). It is worth noting that the poor flyers are clustered. The shape of the furcula in flapping birds tends to be flattened and horizontally oriented whereas it appears more rounded and vertically oriented in poor flyers, semi-aquatic, and swimming birds. It is interesting to note that no pattern is distinguishable for any flight type on the scatterplot described by the first two axes of the PCA. The furcula shape of the hoatzin in this morphospace falls slightly outside that of flapping and gliding birds.

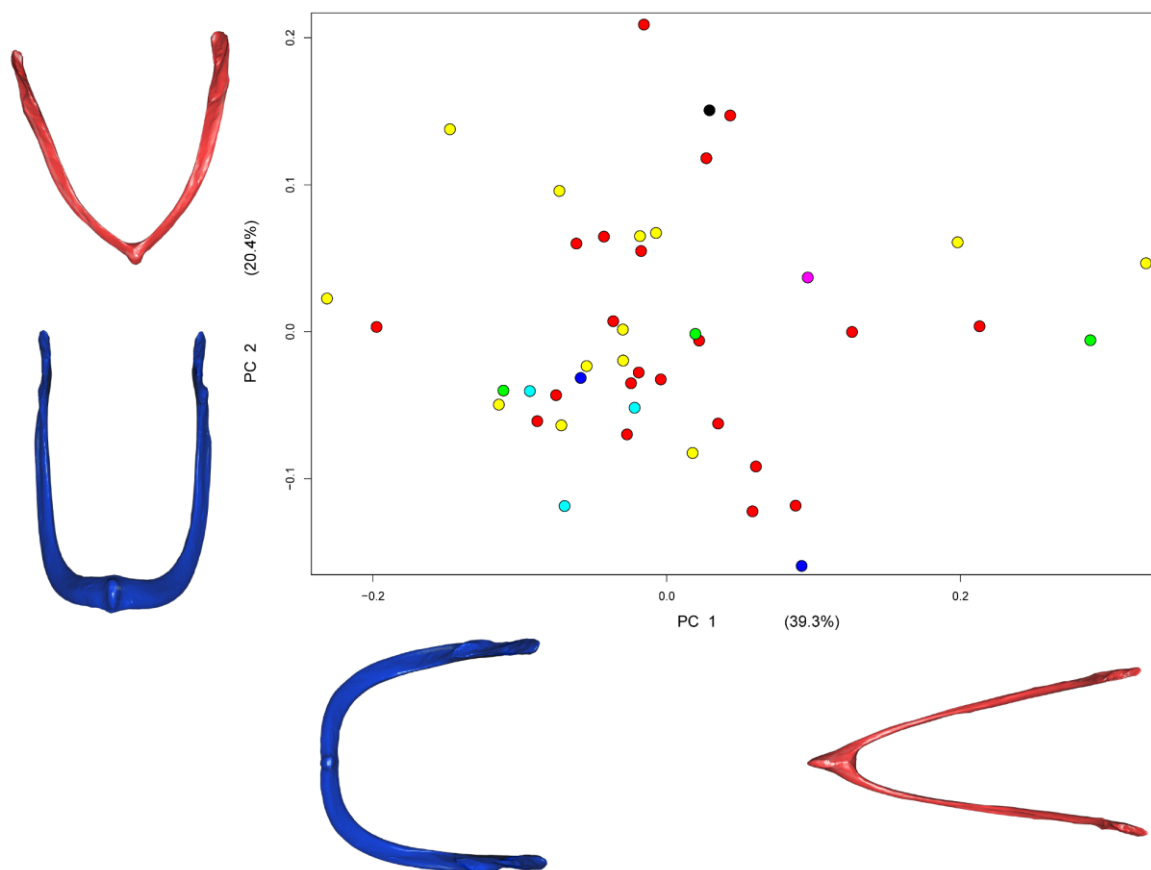


Figure 28 : Principal Component Analyses (PCA) performed on furcula shapes. Colors represent flight types: red is for flapping flight, yellow is for flapping flight, green is for poor flyers, light blue is for semi-aquatic species, dark blue is for swimming birds, pink is for flightless birds and finally black is for the hoatzin with no flight type associated. Red and blue shapes are theoretical furcula shapes computed from the maximal and minimal part of the principal components (PC).

Sternum

The first three PCs account for about 70% of the overall shape variation. The first axis tended to differentiate the poor flyers and flightless species on the one hand from flapping, gliding, and swimming species on the other hand. The second axis tended to differentiate flightless, gliding and some flapping species from poor flyers, some flapping and gliding species, and swimmers (Figure 29). The third axis separates the flightless and semi-aquatic birds from all the other flight types. Flapping birds tend to have a carina that is displaced to the front. Gliding birds appear to have an enlarged sternum body and a small carina. Poor flyers have a backward position of the carina on the sternum with a thin sternum body. Semi-aquatic birds have a long, thin and flattened sternum body associated with well-developed carina, whereas flightless birds have a reduced or nearly absent carina. In these scatterplots, the hoatzin tended to fall in the morphospace of the poor flyers.

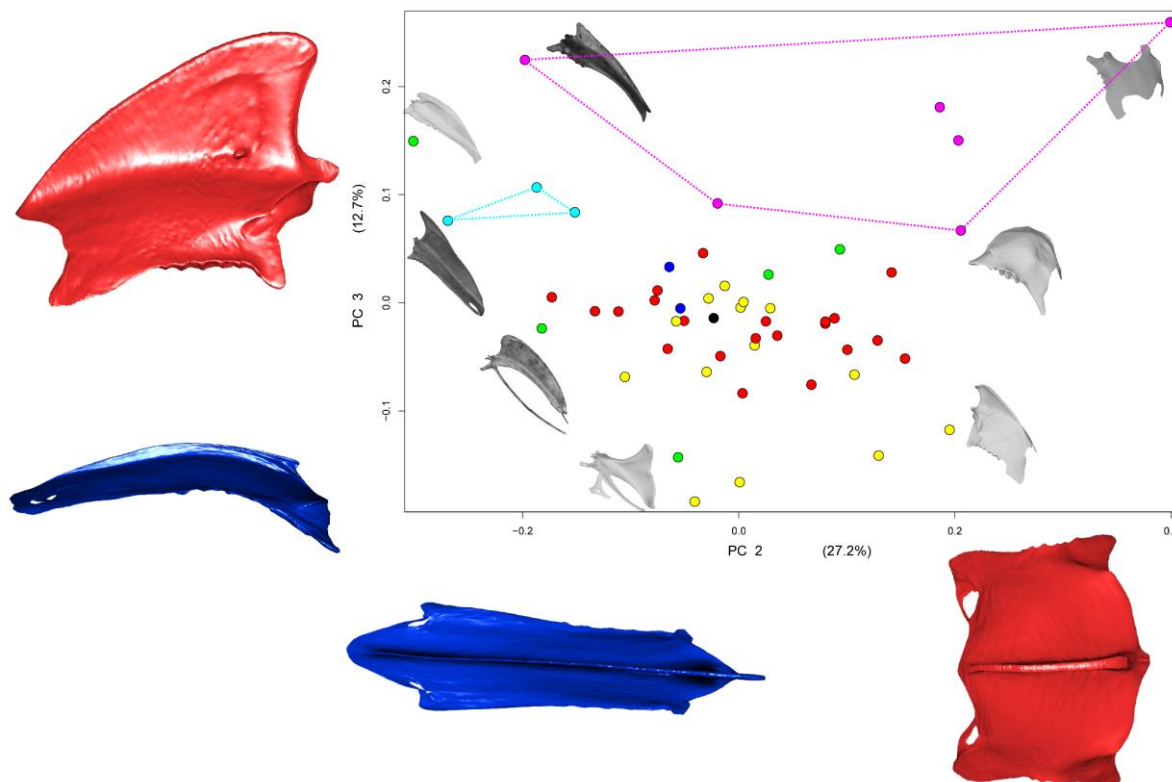


Figure 29 : Principal Component Analyses (PCA) performed on sternum shapes. Colors represent flight types: red is for flapping flight, yellow is for flapping flight, green is for poor flyers, light blue is for semi-aquatic species, dark blue is for swimming birds, pink is for flightless birds and finally black is for the hoatzin with no flight type associated. Red and blue shapes are theoretical sternum shapes computed from the maximal and minimal part of the principal components (PC). Dotted lines represent flight type groups which are significantly different from other flight types. Flightless birds and semi-aquatic birds have different sternum shapes compared to other flight types. Sternum shapes inside the PCA are extracted from the 3D models used in the study. From left and up to right and down: *Rhynchotos*, *Apteryx*, *Psophia*, *Uria*, *Struthio*, *Crypturellus*, *Meleagris*, *Diomedea*.

Coracoid

The first three PCs account for about 60% of the overall shape variation. In the morphospace described by the first two axes gliding and flapping species tend to occupy the entire morphospace (Figure 30). The second axis tends to separate semi-aquatic and aquatic species from the poor flyers. Flapping and gliding birds appear to have a compromised coracoid, between robust and gracile with a wide range of sternal joint curvature. Semi-aquatic birds have robust coracoids and a smooth procoracoid process with linear sternal joint. Swimming birds have a short, flattened and enlarged shaft and small epiphyses. Poor flyers have slender bones with a thin and elongated shaft and small epiphyses associated with a well-developed and sharp procoracoid process. In this morphospace the hoatzin tends to fall in the morphospace of the poor flyers.

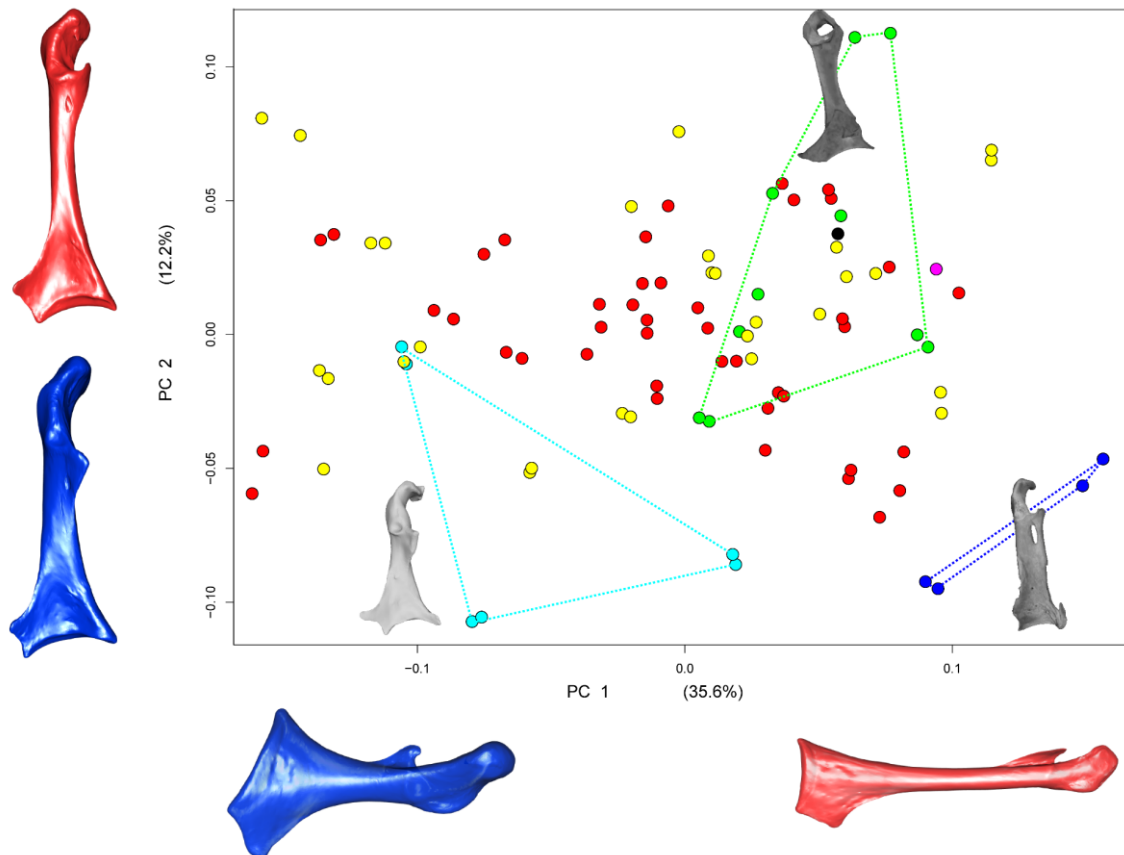


Figure 30 : Principal Component Analyses (PCA) performed on coracoid shapes. Colors represent flight types: red is for flapping flight, yellow is for flapping flight, green is for poor flyers, light blue is for semi-aquatic species, dark blue is for swimming birds, pink is for flightless birds and finally black is for the hoatzin with no flight type associated. Red and blue shapes are theoretical coracoid shapes computed from the maximal and minimal part of the principal components (PC). Dotted lines represent flight type groups which are significantly different from other flight types. Poor flyer birds, swimming and semi-aquatic birds have different coracoid shapes compared to other flight types. Coracoid shapes inside the PCA are extracted from the 3D models used in the study. From left and up to right and down: *Tauraco*, *Uria*, *Eudyptes*.

Scapula

The first three PCs account for ~55% of the overall shape variation. In the morphospace of the first two axes, all flight types overlap (Figure 31). Nevertheless, some groups of species tend to cluster together depending on their flight type such as the swimming species, the poor flyers, and the semi-aquatic species. Flapping and gliding birds have a scapula with a thin blade. Poor flyers displayed a flattened scapula with a large head and a thin blade. Semi aquatic birds are characterized by a curved head and gracile blade. Swimming birds have straight and very enlarged blade associated with reduced head. In this morphospace, the hoatzin falls with the flapping and gliding species, close to the morphospace occupied by the poor flyers.

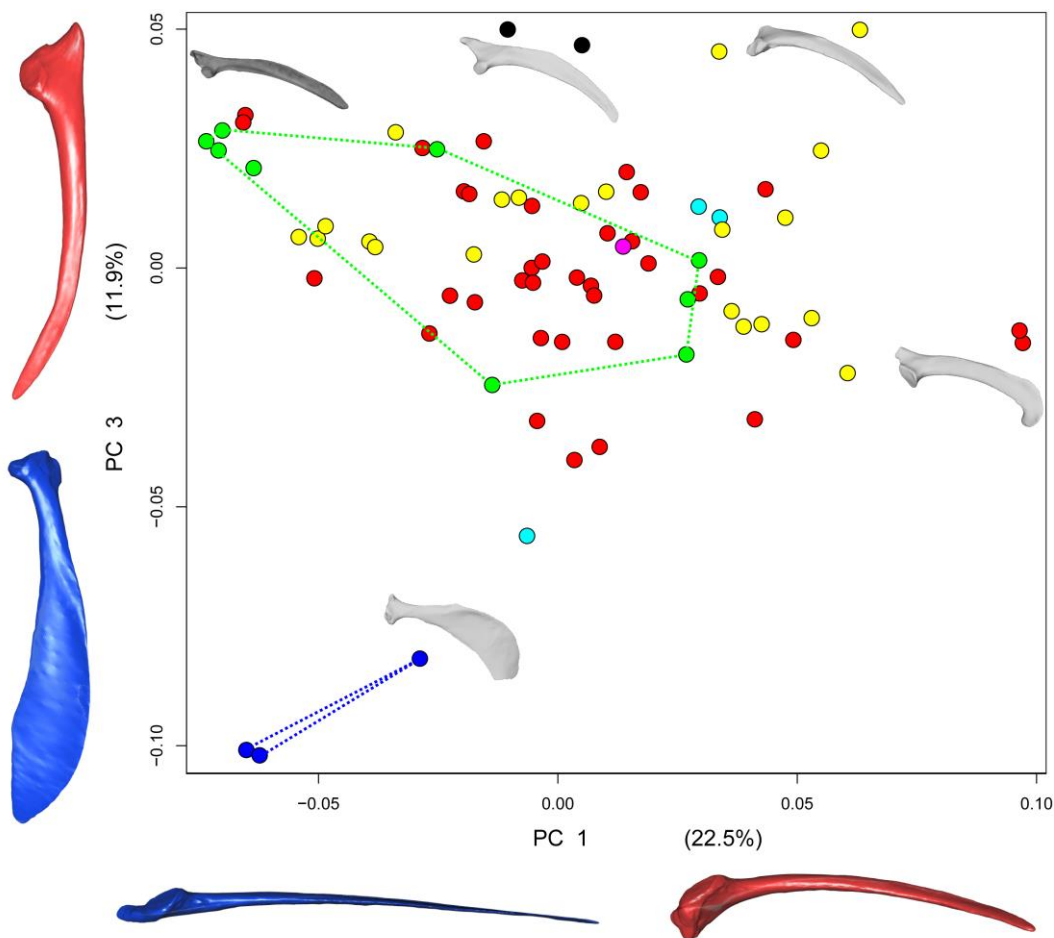


Figure 31 : Principal Component Analyses (PCA) performed on scapula shapes. Colors represent flight types: red is for flapping flight, yellow is for flapping flight, green is for poor flyers, light blue is for semi-aquatic species, dark blue is for swimming birds, pink is for flightless birds and finally black is for the hoatzin with no flight type associated. Red and blue shapes are theoretical scapula shapes computed from the maximal and minimal part of the principal components (PC). Dotted lines represent flight type groups which are significantly different from other flight types. Poor flyer birds and swimming birds have different scapula shapes compared to other flight types. Scapula shapes inside the PCA are extracted from the 3D models used in the study. From left and up to right and down: *Gavia*, *Opisthocomus*, *Vultur*, *Dryocopus*, *Aptenodytes*.

Humerus

The first three PCs account for roughly 70% of the overall shape variation. The morphospace describing the first two axes tended to separate the swimming birds from all the others (Figure 32). It is worth to note that species tended to cluster depending on their flight type. Swimming birds have a very short, flattened and robust humerus while other flight types have more rounded and elongated humeral shaft. Flightless birds have a humerus that is more flattened with small epiphyses. Semi-aquatic birds have enlarged epiphyses with large insertions sites for muscles. In this morphospace, the hoatzin tends to fall in the morphospace of the gliding and flapping species.

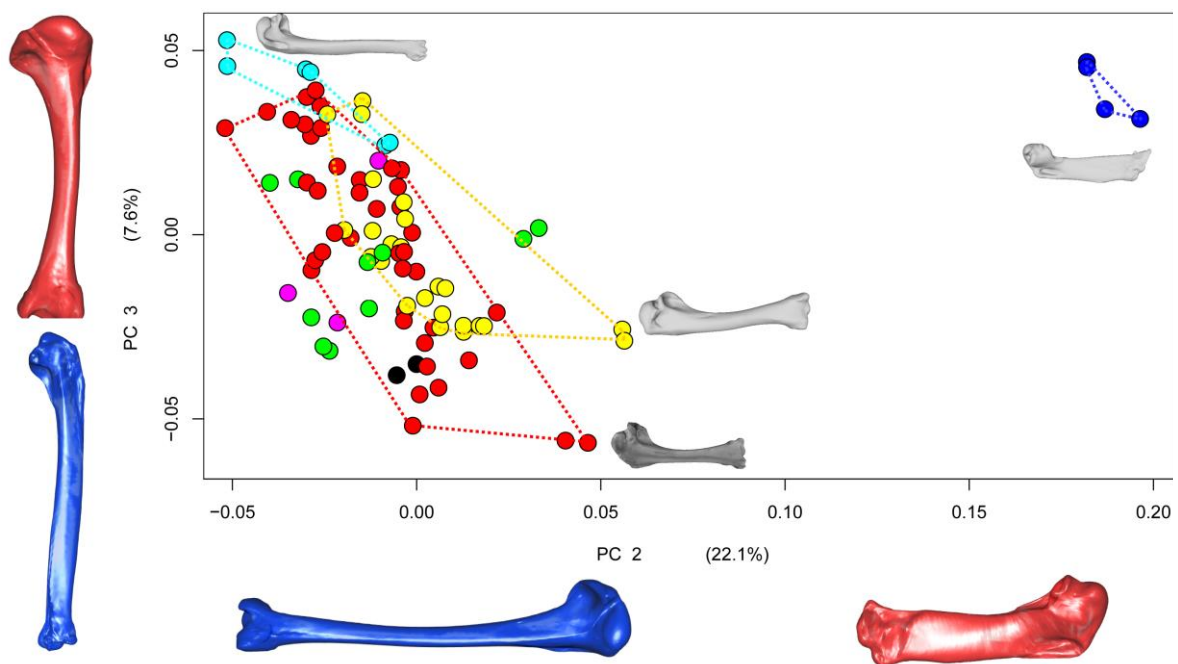


Figure 32 : Principal Component Analyses (PCA) performed on humerus shapes. Colors represent flight types: red is for flapping flight, yellow is for flapping flight, green is for poor flyers, light blue is for semi-aquatic species, dark blue is for swimming birds, pink is for flightless birds and finally black is for the hoatzin with no flight type associated. Red and blue shapes are theoretical humerus shapes computed from the maximal and minimal part of the principal components (PC). Dotted lines represent flight type groups which are significantly different from other flight types. Flapping, gliding, swimming birds and semi-aquatic birds have different humerus shapes compared to other flight types. Humerus shapes inside the PCA are extracted from the 3D models used in the study. From left and up to right and down: *Uria*, *Aptenodytes*, *Meleagris*, *Ducula*.

Shape differences depending on flight type using (M)ANOVAs and phylogenetic (M)ANOVAs

The results of the MANOVA demonstrated shape differences depending on flight type for all bones except the furcula (Sternum: $F_{51}= 2.94$, $P = 0.001$; Coracoid: $F_{93}= 3.22$, $P = 0.001$; Scapula: $F_{44}= 2.04$, $P = 0.001$; Humerus: $F_{89}= 5.37$, $P = 0.001$; Furcula: $F_{43}= 1.23$, $P = 0.15$). When taking into account the phylogeny, the results remained significant only for the coracoids, scapulae and humeri (Coracoid: $F_{93}= 1.66$, $P = 0.02$; Scapula: $F_{44}=1.54$, $P = 0.025$; Humerus: $F_{89}= 2.35$, $P = 0.007$). No shape differences were found for the furcula and the sternum (Sternum: $F_{51}= 1.19$, $P = 0.2$; Furcula: $F_{43}= 0.89$, $P = 0.6$).

Subsequently, we tested for shape differences on each PC axis for each bone of the scapular girdle for which the MANOVAs were significant (sternum, coracoid, scapula and humerus). The results of the ANOVAs performed for the first three PCs separately were all significant (Table 16).

Table 16 : Results of the ANOVAs performed on the first three PCs. Df: degrees of freedom. Significant differences are indicated in bold.

Bone	Principal Component 1			Principal Component 2			Principal Component 3		
	Df	F-stat	P-value	Df	F-stat	P-value	Df	F-stat	P-value
Sternum	51	3,145	0,0105	51	4,199	0,00316	51	14,62	<0,001
Coracoid	93	5,145	<0,001	93	8,244	<0,001	93	3,079	0,0131
Scapula	74	2,413	0,0448	74	3,087	0,0142	74	16,15	<0,001
Humerus	89	2,853	0,0198	89	76,97	<0,001	89	7,114	<0,001

Post-hoc tests performed on the sternum showed significant shape differences between flightless birds and semi-aquatic species ($P = 0.001$) on the second PC. On the third PC we found significant sternal shape differences between gliding and semi-aquatic species ($P = 0.002$), flightless and gliding species ($P = 0.001$), flightless and flapping species ($P = 0.001$), and flightless species and poor flyers ($P = 0.001$).

Post-hoc tests performed on the coracoid showed significant shape differences between swimming and semi-aquatic birds ($P = 0.002$), as well as swimming and gliding species ($P = 0.003$) on the first PC. Differences between flapping and semi-aquatic species ($P = 0.001$), flightless and swimming species ($P = 0.0002$), and gliding and semi-aquatic

species ($P = 0.0002$), and semi-aquatic species and poor flyers ($P = 0.0007$) were found on the second PC. On the third PC we found no significant coracoid shape differences.

Post-hoc tests computed on scapula shapes showed significant shape differences between semi-aquatic species and swimmers ($P = 0.0001$), flapping and swimming species ($P = 0.0001$), flightless and swimming species ($P = 0.0007$), gliding and swimming birds ($P = 0.00001$), and poor flyers and swimming species ($P = 0.0001$) on the third PC only.

Post-hoc tests performed on humeral shapes showed significant shape differences between swimming and semi-aquatic birds ($P = 0.0001$), flightless and swimming birds ($P = 0.0001$), flapping and swimming birds ($P = 0.0001$), poor flyers and swimming birds ($P = 0.001$), and gliding and swimming birds ($P = 0.0001$) on the second PC. The third PC showed shape differences between swimmers and poor flyers ($P = 0.002$), semi-aquatic species and poor flyers ($P = 0.0002$), semi-aquatic and gliding species ($P = 0.0005$), and semi-aquatic and flapping birds ($P = 0.001$).

K nearest neighbour classification and cross-validation test

The results of the cross-validation test of the K nearest neighbour algorithm classified the hoatzin sternum, coracoid, and humerus with those of gliding birds (Table 17). The scapula is the only bone that is classified as similar to that of poor flyers. The furcula was not used as this bone does not display morphological differences depending of flight type.

Table 17 : Results of the K-nn assignation tests performed on each bone of the hoatzin

Bone	Dimensions	Correct assignation	Result of hoatzin classification
Sternum	15	67,50%	Gliding
Coracoids	24	97,50%	Gliding
Scapulae	19	78,80%	Poor flier
Humeri	28	90,70%	Gliding

Discussion

Our results show that shape differences can be found in the scapular girdle of birds that appear to depend on flight type. Interestingly, these shape differences were not found for all bones for all flight types suggesting that not all bones are good proxies of locomotor behaviour in birds. In contrast to the literature, our results suggest that mainly the humerus, scapula, coracoid and the sternum tend to be good proxies of flight type in birds. Unexpectedly, our results show that the most important functional signal was not detected on the furcula, in contrast to previous studies (Close and Rayfield, 2012; Hui, 2002). However, in these studies the authors used different methods including linear measurements (Hui 2002) and 2D geometric morphometrics (Close and Rayfield, 2012) as well as a different sample of birds. Based on our 3D shape analysis and species included in the analysis flight types could not be discriminated based on the shape of the furcula. This difference can be explained either by the different methods used between studies or by the lack of statistical power in our study as we have some locomotor categories represented by only a few species (e.g. swimming birds). However, our results show that all the other bones of the scapular girdle are capable of discriminating between flight types.

For the sternum, our results confirmed our prediction and it differentiated flightless birds from all the other flying birds with shape differences mainly driven by the presence/absence of the carina (Cano, 2012; Gussekloo and Cubo, 2013). Our results quantitatively confirmed that sternum shapes without carina were associated to flightless birds such as the ratites in our sample. Nevertheless, the carina shape is more complex than just its presence or absence. In this study, we demonstrated that the position of the carina tends to be different in addition to differing in orientation or height depending on the locomotor behaviour. More specifically, a backward positioned carina tended to characterize poor flyers and flightless birds. By moving the carina backwards, the insertion of the flight muscles such as the supracoracoideus and the pectoral muscles is effectively reduced. In contrast, a forward placed carina tended to be associated with flappers and gliders and may allow a greater area of insertion for the flight muscles (Grajal et al., 1989; Kaiser, 2007). Interestingly, semi-aquatic birds tended to have a higher carina than other birds, which could be related to larger flight muscle attachments (such as supracoracoideus and the pectoral muscles) allowing both

upstroke and downstroke of the wing during flight in a dense medium like water and also a powerful wing beat needed to take-off from the water (Kaiser, 2007). Moreover, the shape of the sternum body also showed a great variability depending on flight type, ranging from very large to narrow; short to elongated, and curved to flattened. These differences tended to differentiate semi-aquatic birds from other types of flight. The narrow sternum body in these birds could be related to a more hydrodynamic shape of their body needed to reduce the drag profile during swimming (Kaiser, 2007). Another advantage of having an elongated sternum can be the protection of the viscera. For example, a previous study has shown that an elongated sternum could be linked to the protection of the egg in the Auk (Kaiser, 2007).

The coracoid displayed also shape differences depending on flight type. All aerial birds (flapping, gliding birds, as well as poor flyers) showed robust coracoids with a short shaft and large epiphyses whereas all semi-aquatic and fully aquatic birds displayed an elongated one. This difference in shape can be related to the biomechanical role of this bone as it needs to act as a pulley (Baier, Gatesy, and Dial, 2013; Jenkins, Dial, and Goslow, 1988). Its robustness may be related to a greater area of support for the supracoracoideus muscle responsible of the abduction of the wing which goes through the coracoid and lies on the procoracoid process. A robust and shortened shape as in aerial birds could be associated with higher forces needed during the upstroke of the wing. On the contrary, an elongated coracoid such as that observed in semi-aquatic and fully aquatic birds may provide greater leverage for animals moving in a dense medium like water (Kaiser, 2007). Kaiser (2007) also showed that elongated coracoids were found in aquatic species and robust ones in aerial birds and explained these results as a consequence of the higher drag forces in the water than in the air (Kaiser, 2007). Another anatomical characteristic of the coracoid is located at its sternal joint. Aquatic and semi-aquatic birds tended to have a curved sternal joint whereas poor flying birds have a more linear one. The presence of this curvature can potentially be related to the coracoid movement during wing beating (Baier, Gatesy, and Dial, 2013). Indeed, aquatic birds may need a more solid structure to support the muscle forces during wing beats than aerial ones. A more curved articular facet could limit the range of abduction/adduction and thus avoid energy loss (Baier, Gatesy, and Dial, 2013).

The procoracoid process tended to be different depending on flight type as well. The procoracoid process is an important element allowing the pulley function of the coracoid. Furthermore, the muscles responsible for the abduction of the wing run across this process. In our sample, swimming birds and poor flyers tended to have a more developed procoracoid process. It has been hypothesized that this morphology allows for a better stabilization of the supracoracoideus muscle and thus helps keep the wing adducted along the body which can be important during swimming or running (Keneisenuo et al., 2019). On the contrary, semi aquatic birds, which can both swim and fly, have shortened procoracoid process. Although it is unclear to date why this is the case, future studies exploring the covariation between the wing abductor muscles and the procoracoid process may shed further light on this issue.

Our results for the scapula showed that aquatic birds have very enlarged blades compared to other birds. The main functional role of the scapula is to stabilize the shoulder with its muscular fixation to the vertebral column (Dial, 1992; Kaiser, 2007). Thus, the enlarged blade of the scapula found in aquatic birds may allow a larger surface of attachment of the muscles (rhomboideus and serratus muscle complexes) allowing the stabilization of the shoulder, thus providing higher resisting forces when moving the wings under water (Baumel et al., 1993). On the opposite, flapping birds, gliding birds and poor flyers have a scapula with a very thin blade and appear not to require a strong stabilization of the shoulder. The elongation of this bone suggests that it may be useful in flight by redistributing stresses across the tops of the ribs (Kaiser, 2007). Semi-aquatic birds have a scapula with a thin and curved blade possibly allowing it to be retracted along the ribs more quickly.

The humeri of gliding and flapping birds have large proximal epiphysis for flight muscle insertions (supracoracoideus and pectoralis muscles). The distal epiphysis seems more developed in gliding species than in flapping species, which could be related to the full wing stabilization needed in gliding birds. Both gliding and flapping species have a rounded and curved shaft which has been suggested to reduce the stresses by transferring flight forces towards the joints (Kaiser, 2007). On the contrary, swimming birds have very short and flat humeri. A flattened bone might contribute to decreased drag by presenting a thinner cross-section as the wing passes through the water (Kaiser, 2007). Moreover, a flat bone is designed to cope with large stresses generated by wing

movement through a dense medium like water if the orientation of the forces is predictable (Kaiser, 2007). Semi-aquatic birds also have a flattened humeri, probably due allowing a decrease in drag forces when swimming. They also displayed a well-developed proximal epiphysis allowing a greater area of insertion for the supracoracoideus and pectoralis muscles. Flightless birds also displayed a flattened humerus, but in contrast to aquatic birds it is elongated. The humerus is generally described as a curved bone as this allows the transfer of stresses towards the joints (Kaiser, 2007). Our results show that the proximal part of the humerus can have various curved morphologies depending on flight types. The head of the humerus that articulates with the shoulder is distinctly curved in flapping, gliding and semi aquatic species such that most of the wing stroke can occur below the horizontal (Kaiser, 2007). The physics of flight suggest that the lower part of the wing stroke is the most important because its power is vectored inward and downward against the other wing, instead of dispersing outward (Baier, Gatesy, and Dial, 2013; Dial, 2003; Goslow, Dial, and Jenkins, 1990; Kaiser, 2007).

To conclude, our results tended to indicate that shape differences can be detected for nearly all bones of the scapular girdle, except for the furcula, at least in our sample of birds. The sternum, the scapula, the coracoid and especially the humerus appear to be excellent proxies of flight type allowing to differentiate aquatic and semi-aquatic birds from flying birds. Flightless birds tended to have a different shape of the bones of the scapular girdle, sometimes with a mosaic of morphological features ranging from those observed in aquatic birds to those observed in poor flyers. These results indicate the importance of studying as many skeletal elements as possible in relation to function, as they may not be all informative for the same types of locomotion. Using the results obtained in this study and only the bones showing shape differences depending on locomotor behaviour (sternum, scapula, coracoid and humerus), our results of the K nearest neighbour classification and cross-validation show that the hoatzin can be generally assigned to the gliding species with the exception of the scapula which places it with the poor flyers. These results suggest that either the shape of its bones does not reflect its flying ability or that this species is not a poor flyer as has been suggested in the literature. Clearly more and especially *in vivo* studies are needed to better understand the flying abilities of this enigmatic bird. Some morphological characteristics unique to the hoatzin such as the complete fusion of the sternum, furcula and coracoids

are not included in this analysis and may influence its flight type. This study is the first to include a comprehensive number of skeletal elements of the scapular girdle. Nevertheless, adding more species to each locomotor category will be necessary in order to increase the statistical power of the analysis. Finally, in order to improve our understanding of the functional morphology of flight in birds, further studies on postcranial skeleton in relation to muscle anatomy and function are needed.

**Chapter 4 - Preliminary
description of the hoatzin
development: ossification
sequence, focus on scapular girdle
and cranial musculature**

Finally, the results obtained in chapter 3 allowed us to conclude that the shape of the sternum of the hoatzin seems not to be the main reason of its poor flying abilities. Furthermore, it appeared that the shape of scapular bones of the hoatzin were similar to those of gliding species. These results didn't allow us to understand why previous authors considered the hoatzin as a poor flyer when studying its skeletal elements. Further integrative studies need to be done to better understand the impact of other factors (such as the development or combination of function) on the unique skeletal morphology of the hoatzin.

In this last chapter, we aimed to better understand the impact of development of the unique morphology of the hoatzin. More precisely, we focused on the ontogenic origin of the sternum complex shape in hoatzin. As the description of the ossification sequence and its comparison with other species could be informative on the understanding of the anatomy of the hoatzin, we used a complete 3D skeleton dataset of a developmental series of the hoatzin. This developmental series allow us to describe the overall morphological changes in embryos and juveniles, with a special focus on the scapular girdle. We also described the muscles development of the masticatory system in embryos and juveniles.

Preliminary description of the hoatzin development: ossification sequence, focus on scapular girdle and cranial musculature

Fanny Pagès, Nadia Toumani, Anthony Herrel, Anne Claire Fabre, Anick Abourachid

Preliminary work

Introduction

The previous chapters have identified traits of the Hoatzin that appear to be unique and that are derived to those commonly observed in other birds. However, to better understand the origin of the differences in shape and form of these structures we need to explore the development thereof. However, developmental series of birds are relatively rare (Maxwell, 2008a; Maxwell and Harrison, 2008) and most commonly focus on a single organ system, bone, or muscular system or document the general ossification sequence of the skeleton (Maxwell, Harrison, and Larsson, 2010). Through collaborators in Venezuela, we were able to obtain a unique series of embryos in addition to four juveniles and two adults that were CT-scanned and subsequently segmented.

The objectives of this preliminary study were 1) to identify the ossification sequence of the hoatzin to explore whether the unusual adult morphology is caused by differences in ossification sequence; 2) explore whether the unusual shape of the sternum is formed during development or whether it already has its adult shape at the earliest stages of development which would suggest a genetic determinism of the shape of the sternum; 3) to explore the condensation and differentiation of the cranial muscles to better understand the origins of the cranial muscle.

To do so, we first describe the ossification sequence of the entire skeleton. We then compared the hoatzin ossification sequence with that reported for other bird species including nidifugous and nidicolous species (Atalgin and Kürtül, 2009; Carril and Tambussi, 2017; Maxwell, 2008b, 2008c; Maxwell and Harrison, 2008; Maxwell and Larsson, 2009; Mitgutsch et al., 2011). By means of contrast-enhanced μ CT scans we examined specifically the scapular girdle and the cranial muscles. This allowed us to visualize the cartilaginous parts of the scapular girdle and thus to describe the early shape of the sternum. Finally, we explored how the cranial muscles develop and differentiated in the hoatzin as these muscles are derived compared to other birds in relation to their unusual folivorous diet (Korzoun, Erard, and Gasc, 2003, 2001).

Material and methods

Specimens

The analyzed specimens are comprised seven hoatzin embryos at different development stages, four juveniles and two adults. The specimens were collected in nests along the Cojedes River of Venezuela during August 2015. The ontogenetic series were obtained from eggs which were collected by our Venezuelan collaborators and incubated for different periods of time. They were preserved in a 5% aqueous formaldehyde solution and then transferred to a 70% ethanol solution or RNA later. Adults and juveniles were collected in the field (material transfer agreement number: SJ MNHN 518-14) and were preserved in a 10% formaldehyde solution for 48 hours, rinsed and transferred to a 70% aqueous ethanol solution. Embryos and juveniles ages are not known but were estimated using the feather apparition sequence in quails (Ainsworth, Stanley, and Evans, 2010).

CT-scanning

Specimens were scanned at Ghent University (www.ugct.ugent.be) using a PerkinElmer detector at 120 kV and amperage of 60 W with a 1mm aluminum filter. The two adult hoatzins were scanned at a 170 μ m voxel size. For each specimen, a series of 698 projections of 728 pixels and 1820 slices was recorded covering 360 degrees. The four juveniles were scanned following the same parameters with a voxel size between 65 and 89 μ m. The embryos were scanned with a voxel size of around 20 μ m. The raw data were processed and reconstructed using the in-house developed CT software 'Octopus' (Vlassenbroeck et al., 2007). Each bone was segmented and separated in Avizo v8.1 (FEI Visualization Sciences Group). The skeletal descriptions are based on the 3D slices and segmentations. To be able to visualize non-ossified parts of the bones as well as the soft tissues, embryos, juveniles, and adult hoatzins were stained with PMA (phosphomolybdic acid) for periods ranging from several days to several months and were scanned again following the same parameters except the voxel resolution which was ten times higher (Descamps et al., 2014).

Results

In the description below we describe the different specimens from the youngest to the oldest, with ages being assigned based on the feather apparition sequence (Ainsworth, Stanley, and Evans, 2010). Juvenile developmental order was defined on the field such as P4 is the younger, then P1, P2 and finally P3 is the older one.

Table 18 : Developmental order and corresponding ages of the hoatzin embryos.

Embryos	Age (days)
E2	17
D2	19
2i	21,5
3i	22
J2	22
4i	23
K	23

Complete skeleton – μ CT scans

E2

The braincase is still almost completely cartilaginous (Figure 33-34-35). Only the squamosal and the frontal bones are already ossified at their lateral parts. The beak is discernable as the central part of the nasal bones has started to ossify. The premaxilla is already almost fully ossified as are parts of the maxilla, the jugal and quadratojugal which are ossified proximally. The palatine is almost completely ossified, as are the pterygoid bones. Concerning the mandible, the dentary, angular, splenial and prearticular bones are nearly completely ossified but not yet fused. For the hyoid apparatus, only the distal part of the ceratobranchial is ossified. The vertebrae and ribs are not ossified. The scapular girdle is at this point during development only composed of the furcula where the hypocleidum is present but short. The clavicles are already well developed and very large. The scapula is almost completely cartilaginous and only a small section of the central diaphysis is ossified. The humerus, radius, ulna, metacarpus III, and IV have their central parts ossified. No digits are visible. None of the pelvic bones are ossified yet. The femur, tibia, fibula, metatarsal II, III, IV bones begin to ossify at the central part of the diaphysis. None of the toes are present.

D2

The occipital complex starts ossifying: the central part of the exoccipital is visible (Figure 33-34-35). The parasphenoid complex appears and the basisphenoid is largely ossified. The squamosal is elongated towards the frontal bone, the parietal is very thin on its lateral border and the frontal is thicker than in the previous stage but not longer. The lacrimal is ossified on its lateral and medial parts but not its center. The premaxilla is now fused to the maxilla. The rostral part of the vomer appears. The jugal is almost fully ossified and start fusing with the quadratojugal which is almost fully ossified. The pterygoid is elongated. The dentary bones of the left and right side start to fuse, yet some holes are still present rostrally. The mandibular bones are thicker but still not fused. The ceratobranchial starts ossifying dorsally. The scapulae are elongated but still very thin. The coracoids are visible through their ossified shaft. The shafts of the long bones start to ossify. The first phalanx of the alulae is ossified and has a ring-shape. In the pelvic girdle, the ilium is ossified in its central part and at its thin caudo-dorsal border. The pubis ossification starts but is very thin at its distal part. The long bones of the hind limb elongate their shafts. The first and second phalanges of the toe I, the first phalanx of the toes II, III and IV are ossifying and form ring-shaped bones.

2i

The lateral parts of the supraoccipital are fused to the now thicker exoccipital (Figure 33-34-35). The parasphenoid complex is enlarged and the right and left parts of the lamina start to fuse. The basisphenoid is robust. The frontal ossifies towards its anterior part. In the upper beak, the nasal elongates ventrally and the central part is filled with bone. The premaxilla is elongated towards the posterior side and the maxillary process is developed. The maxilla elongates dorsally and is fused to the jugal. The jugal is fused to the maxilla and almost fused to the nearly completely ossified quadratojugal. The central part of the quadrate is ossified. For the lower jaw, the right and left parts of the dentary are fully fused, the holes are reduced and the bone is thicker. The mandibular bones are thicker and more robust, especially the prearticular but their fusion is not complete. The thin centrae of the thoracic and the synsacrum are ossifying. The scapulae, coracoids, and long bones of the arm have an elongated ossified shaft. The furcula hypocleidum becomes longer. Metacarpal bones III and IV have their central part ossified. Phalanx I of the digit II and phalanges I and II of the digit III are ossifying in a

ring shape. The ilium is largely ossified at its central part as are the ischia. The pubis is ossifying from the distal part towards the proximal part. The long bones of the leg elongate their shaft. The distal part of the fibula is fully ossified while the proximal part is still absent. Metatarsal bones I, II, III and IV have an elongated shaft. All phalanges have ring-shaped ossification.

3i

The occipital complex is elongated and enlarged towards the foramen magnum (Figure 33-34-35). The parasphenoid complex and basisphenoid are fully ossified and fused. The squamosal is now fused with the frontal forming the border of the eye and the squamosal is also fused to the enlarged parietal which is now ossifying towards the back of the skull, above the supraoccipital. The frontal is fused to the nasal which is still thin. The premaxilla is robust and fused to the nasal and the maxilla which is thick and robust. The jugal is fully fused to the quadratojugal with no visible fusion line. The palatine is fully fused to the upper beak bones and completely ossified. The vomer's bifid tip is ossified but its rostrum is not yet complete. The central part of the corpus of the quadrate is enlarged. The dentary, supra-angular, angular, splenial, and prearticular are fully formed, ossified and fused. Cervical, thoracic and synsacral centra extend. The cervical arch and the thoracic transverse processes are developing. The dorsal ribs are ossifying the central part of their shaft. The furcula is thinner, yet other bones of the arm are longer. On the feet, claws on the toe I, phalanx IV on toe III and phalanx V on toe IV are now visible.

4i

The braincase is ossifying and the orbitosphenoid is appearing (Figure 33-34-35). The squamosal, parietal and supraoccipital are not yet fused. The sphenoid complex is almost fully fused. The basioccipital and the exoccipital bones are robust. The upper beak and especially the premaxilla are thicker and enlarged. The quadrate shaft is almost complete. The vomer is now fused to the sphenoid complex through its rostral part. The mandible is enlarged but still not completely fused and is lacking the articular bone. The vertebral centra are ossifying on the cervical, thoracic and synsacral parts. Vertebral ribs are developing and cervical ribs appear. The furcula is elongated. The scapulae, coracoids and arm long bones have their diaphysis almost completely ossified. Wing phalanges are longer and wing claws are visible on the alulae and major digits. The

ilium is almost fully ossified but right and left sides are not fused to the vertebrae yet. Ilium, ischium and pubis are not fused. Leg long bones have almost the complete shaft that is ossified. All phalanges and claws are visible and ossifying.

P4

The braincase is ossifying dorsally but all bones are not yet fused (Figure 33-34-35). The mesethmoid is ossifying from the rostral part of the frontal to the back. The upper jaw is almost completely ossified and fused but not fused to the braincase yet. The vomer is completely ossified. The mandible is fully ossified, fused and robust, except for the articular bone. The articular bone is starting to ossify. The ceratobranchials are almost fully ossified and are still the only bone of the hyoid complex that are visible. The vertebral ribs are elongated but the sternal parts are still not ossified. Cervical, thoracic, and synsacral vertebrae are almost fully ossified. Only the cervical vertebrae have their neural arch completely ossified. Caudal vertebrae do not yet have fully ossified centra. The pygostyle shows some ossification holes and is long and thin. The scapular girdle is characterized by the apparition of laterocranial and laterocaudal processes of the sternum. Long bones are growing. Metacarpal II is ossifying in a ring shape. The pelvic bones and long bones are growing. Metatarsal I is elongated.

P1

The lateral border of the braincase is now fusing (Figure 33-34-35). The orbitosphenoid bone is thicker and larger. The mandible starts fusing its dorsal bones, the articular is not in contact with the main part of the mandible. Vertebral ribs are ossifying for the vertebrae towards the ventral side of the body. Cervical vertebrae are complete, thoracic and synsacral vertebrae are lacking neural arches and caudal vertebrae start ossifying their vertebral centra. The furcula is elongated and thinner, the posterior part of the sternum is ossifying. Wing and leg long bones are thicker and more robust.

P2

The braincase is still not fully fused (Figure 33-34-35). The lacrimal bone projects a process that is now fused to the jugal bone. All vertebral ribs are now ossified. Thoracic neural arches are still incomplete. Caudal centrae are small and caudal neural arches are not ossified yet. The pygostyle is triangular and thin. The body of the sternum

starts ossifying from the latero-caudal processes towards the cranial part of the sternum. The pelvic bones are still not fused.

P3

The braincase bones start ossifying on the top but around the foramen magnum there is still no ossification or bone fusion (Figure 33-34-35). Vertebral ribs are complete. Vertebral centra are ossified but thoracic neural arches are still lacking ossification. Caudal vertebrae are completely ossified. The pygostyle is developing and has a near-adult shape. The metacarpal II is more robust but metacarpal bones II, III and IV are not fused yet. Phalanges are enlarged. Wing claws are still present. The pelvic long bones are starting to ossify their epiphyses.

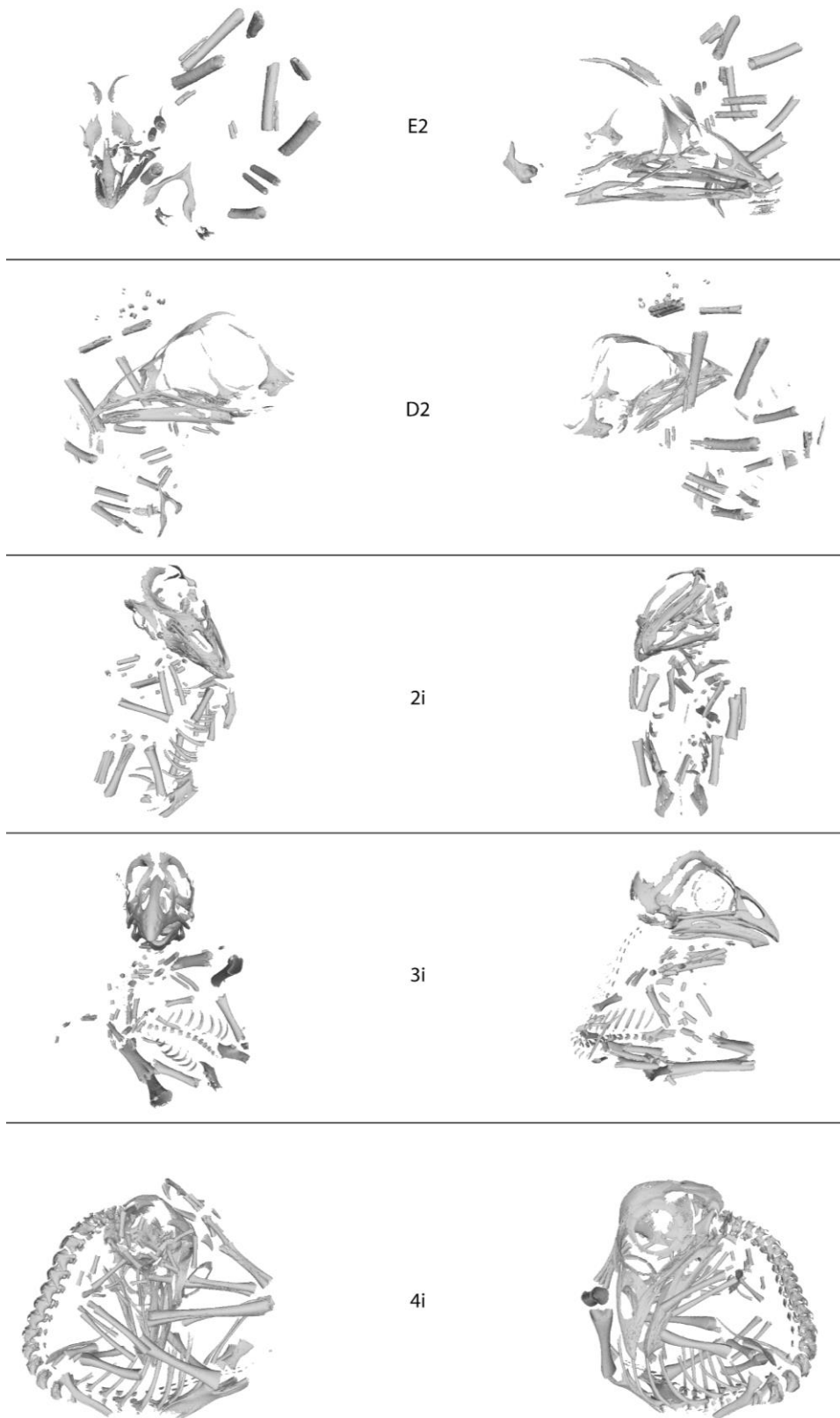
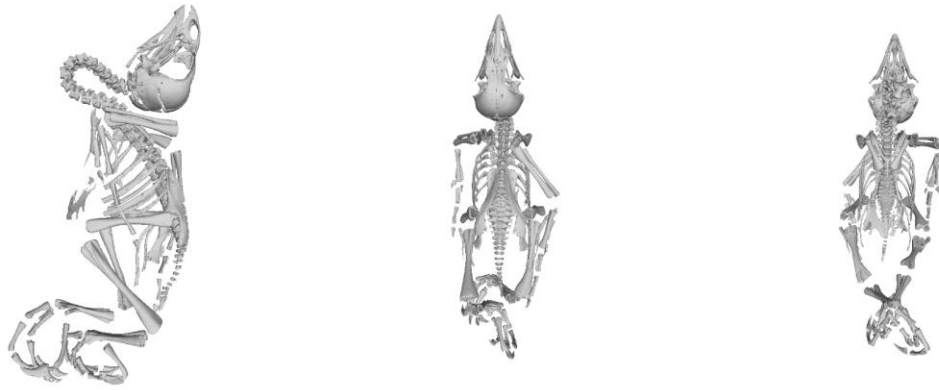


Figure 33 : Complete ossified skeleton of hoatzin embryos segmented from μ CT scans. Order of appearance respects the developmental order. Specimen code is specified.

P4



P1



P2



P3



Figure 34 : Complete ossified skeleton of hoatzin juveniles segmented from μ CT scans. Order of appearance respects the developmental order. Specimen code is specified. From left to right: lateral view, dorsal view and ventral view.

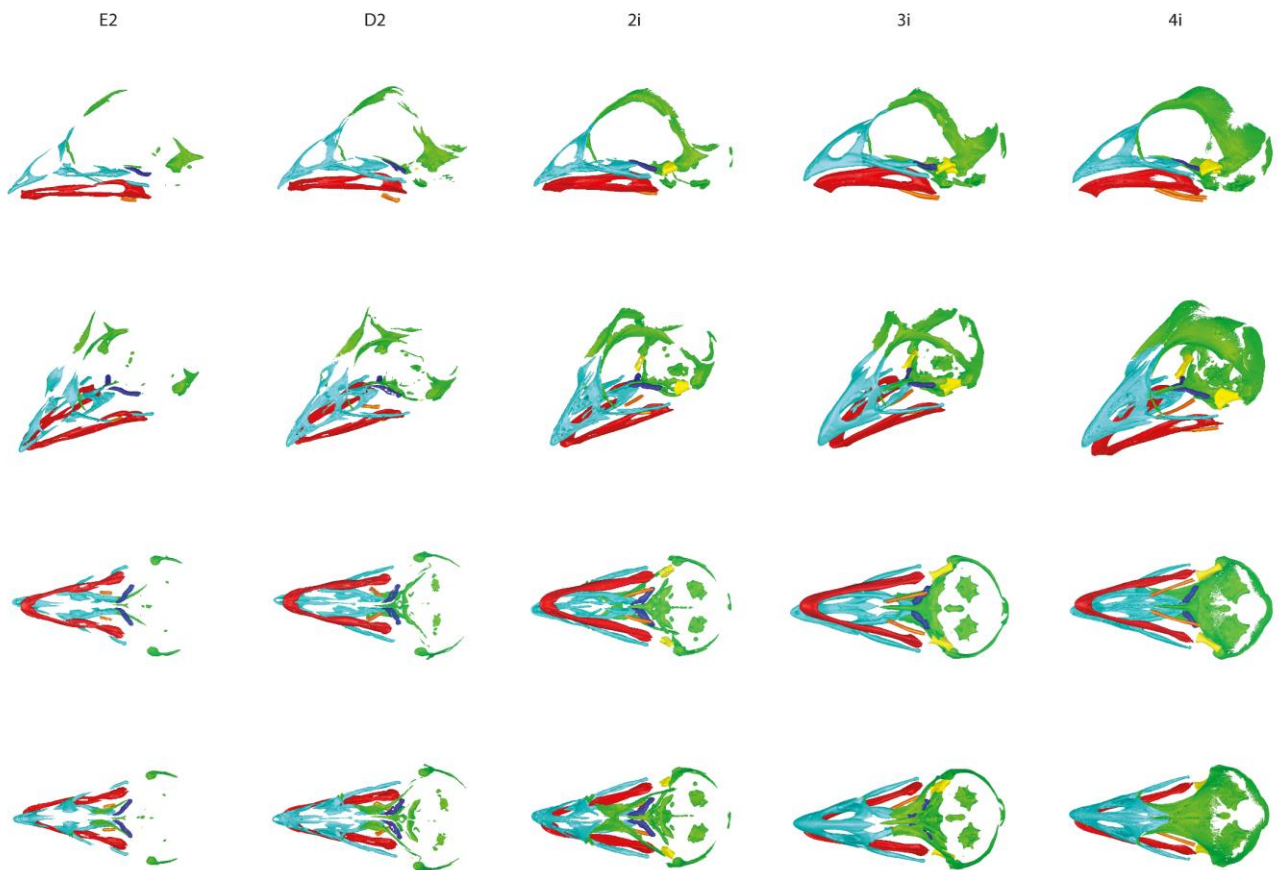


Figure 35 : Skull ossification in hoatzin embryos. Ontogenetic order is respected. Colors represent each part of the skull. Green is for the braincase, light blue is for the upper jaw, red is for the lower jaw, yellow is for the quadrate, dark blue is for the pterygoid, orange is for the hyoid complex. From top to bottom: left lateral view, oblique frontal view, caudal view and cranial view.

Comparative ossification sequence

The comparative dataset is available in Annex B.

Skull

The frontal, lacrimal, nasal and premaxillary (face bones) bones start ossifying earlier in the hoatzin compared to *Myiopsitta monachus* and especially *Dromaius novaehollandiae*. The caudal bones of the skull (sphenoid complex) ossify earlier in the hoatzin than in *Myiopsitta monachus*, *Struthio camelus*, *Dromaius novaehollandiae*, *Coturnix coturnix*, and *Meleagris gallopavo*. The laterosphenoid ossifies later in *Myiopsitta monachus* than in the hoatzin and the cervical ribs ossify later in *Rhea Americana* than in the hoatzin. The mesethmoid ossification is early in the hoatzin, *Coturnix coturnix*, *Dromaius novaehollandiae* and *Rhea americana* compared to other birds.

Axial skeleton

No difference was found in the development of the vertebrae. The vertebral ribs appear to develop before the vertebrae in *Meleagris gallopavo*, *Gallus gallus*, *Coturnix coturnix* and *Larus argentatus* which is different from other birds, including the hoatzin.

Scapular skeleton

The furcula and scapular bones ossify earlier in the hoatzin than in all the other birds. For other bones, no differences were observed.

Pelvic skeleton

The three bones of the pelvis: ilium, ischium, and pubis ossify in the same stage in the hoatzin. It is possible that the time lag between our stages E2 and D2 is too large to be able to detect a delay. For other species, some develop the pubis later (*Larus ridibundus* and *Larus canus*), some the ischium later (*Gallus gallus*), and some others the ilium later (*Cairina moschata*, *Struthio camelus*). The long bones do not show any difference in their ossification sequence. Metatarsal I ossifies earlier in the hoatzin compared to *Anas platyrhynchos*, *Stercorarius skua*, *Larus ridibundus* and *Cairina moschata*. Foot phalanges ossify early in the development of the hoatzin. In *Myiopsitta monachus* they ossify at later stages.

Scapular girdle development

By using contrasted-enhanced μ CT scans we are able to visualize both the cartilaginous and ossified parts of the scapular girdle in the embryos (Figure 36-37). This technique allows us to see the observed the shape of the developing sternum. Juveniles (P-specimens) and late embryos (4i and K specimens) are not fully represented because some bones were missing or were damaged during the extraction of bone elements for another study.

D2

The sternum already appears to have its near-adult shape. The ventral process known as the “resting pad” is already formed. The latero-caudal and latero-dorsal processes are not yet present. The sternum body is more laterally curved than in the adult bird and more rounded. The furcula is fused to the sternum and is leaning forward on the sternum. The coracoids look like the adult ones but are not fused to the sternum. The scapular heads are well formed but the blade is strongly curved and the caudal tip is sharper. The humeri have marked insertion areas at their proximal and distal extremities. The humerus shaft is curved distally.

J2

The sternum is more rectilinear than in D2, the resting pad is less developed and lateral borders are shorter. The furcula is less inclined but a bit more curved and thinner. The coracoids are positioned more upward. The scapular heads are smoother than in D2. The blades are less curved but thinner. The humeri are smoother too and seem less developed.

4i

The sternum has a more developed and sharper resting pad process. Fused lateral processes appear. The sternum body is less dorsally curved than before. The furcula is longer and thinner. Coracoids are longer. The scapular head is more arched, the blade is curved and the distal tip sharper. The humeri are distally curved.

K

The lateral processes are not visible on this specimen. The borders of the sternum are rounded and the furcula is thinner. The coracoid heads are larger. The scapular blades are straighter but still curved at the middle of the blade. The humerus shaft is twisted.

P4

The youngest juvenile has a sternum body that is less curved. The lateral processes are formed and independent. The resting pad is larger at its tip. The furcula is thinner and elongated. The coracoid heads are less large but have more marked muscle insertion areas. The scapular blades are straighter and start looking like adult scapula. The humerus is adult-shaped.

P1

The resting pad is more developed and the lateral processes are larger. The furcula is adult-shaped. The coracoid shafts are larger and the scapulae are adult-shaped.

P2-P3

The resting pad is longer and appears more robust. The furcula is thinner. The coracoids are adult-shaped.

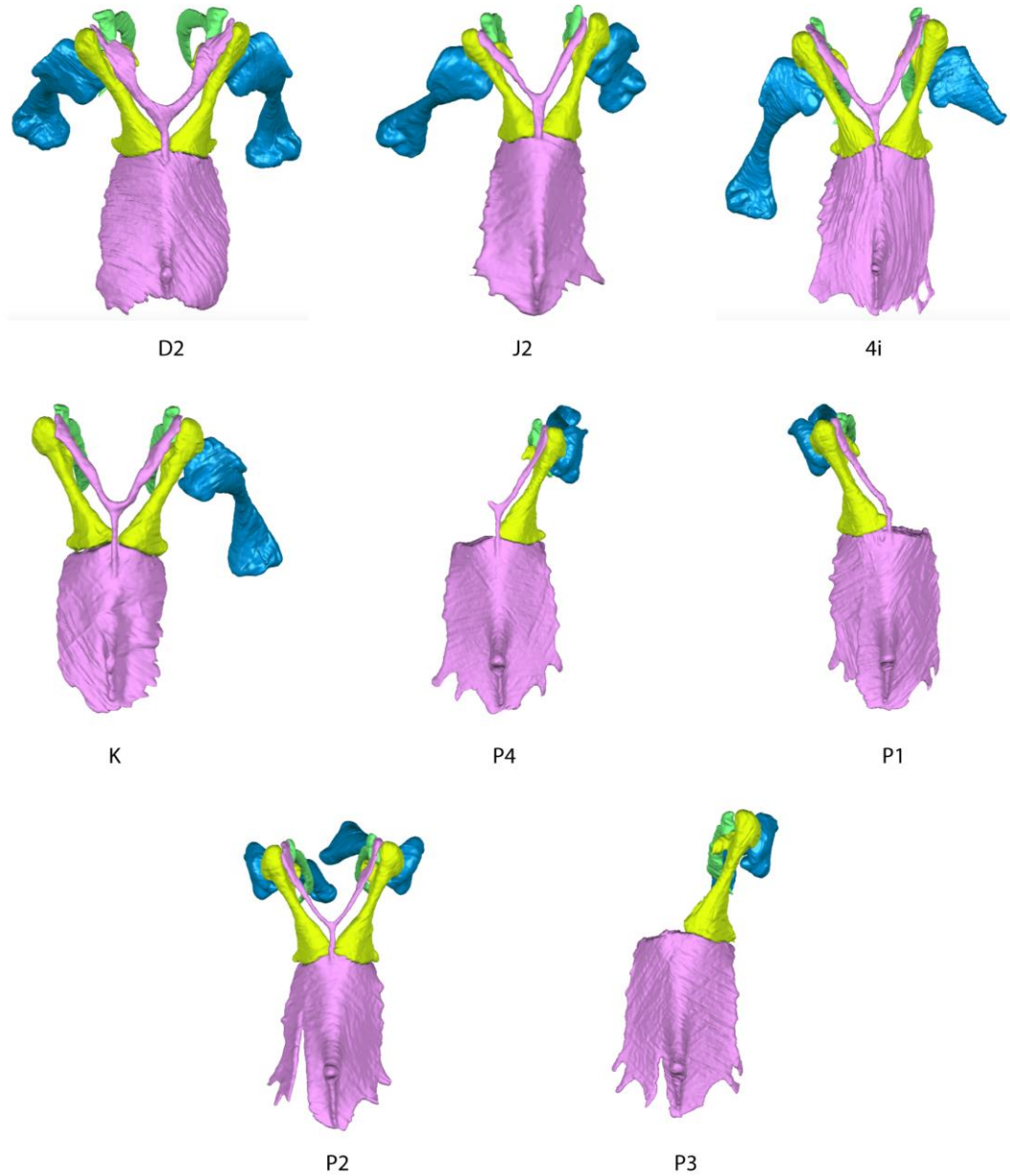


Figure 36 : Scapular bones of the hoatzin embryos and juveniles segmented from contrasted enhanced μ CT scans in ventral view. Ontogenetic order is respected. Colors represent each bone: pink is for the sternum – furcula fused complex, yellow is for coracoids, green is for scapulae and blue is for humeri.

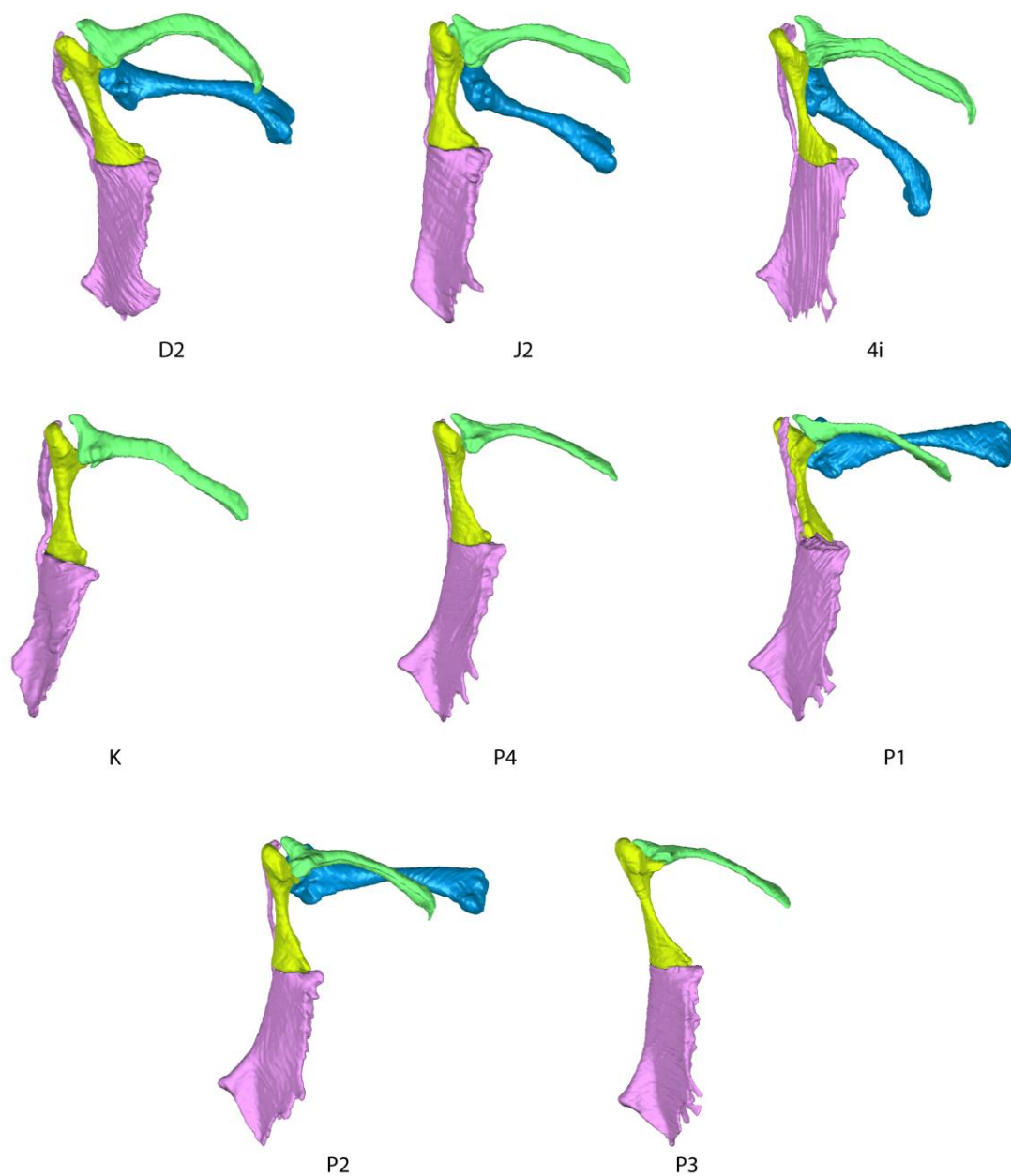


Figure 37 : Scapular bones of the hoatzin embryos and juveniles segmented from contrasted enhanced μ CT scans in left lateral view. Ontogenic order is respected. Colors represent each bone: pink is for the sternum – furcula fused complex, yellow is for coracoids, green is for scapulae and blue is for humeri.

Cranial musculature

Using contrast enhanced μ 3D scans, we segmented the skull and the muscle implied in the masticatory system of the hoatzin (Figures 38-39-40-41 and Table 19). From the D2 embryo onwards the depressor mandibulae is well developed. The opening of the mandible is thus already possible. The external adductor of the mandible and the pseudotemporalis muscle are present and so the closing of the mandible is possible too. The muscles responsible for the elevation of the premaxilla (upper beak) are formed. Of the upper beak retractors only the dorsal and ventral lateral pterygoideus muscles are differentiated. The retractor palatini and the dorsal and ventral medial pterygoideus are not yet differentiated but a muscle precursor is present. The retractor bulbi is already differentiated and allows eye movements. In the J2 stage we can identify the rostral external adductor of the mandible which participate to the closing of the mandible. The precursor of the retractor palatini and pterygoideus is visible and not yet differentiated. The lateral pterygoideus muscles are not visible as separate entities in this embryo. The K embryo has a broken pseudotemporalis of which a part appears attached to the rostral part of the quadrate. The retractor bulbi is not visible but should be present. The lateral pterygoideus muscles are not differentiated. The 4i embryo has more strongly developed muscles. The mandible depressor, pseudotemporalis and ventral external adductor of the mandible are enlarged. The lateral ventral and dorsal pterygoideus muscles are visible and differentiated. The precursor of the retractor palatine and medial pterygoideus muscle is enlarged but not yet differentiated. In the juveniles the dorsal medial pterygoideus muscle is differentiated only in the oldest specimen. It seems that this muscle complex is the last to differentiate. This suggests that forceful retraction of the premaxilla may not be necessary for feeding in juveniles. The lateral dorsal and ventral pterygoideus muscles appear to enlarge later in the development. At the adult stage, the external ventral adductor attachment parts are larger than in previous stages. The pseudotemporalis is well developed too. The mandible depressor seems shorter and more rounded than the jaw adductor muscles.

Table 19 : Color code for cranial musculature figures

	Mandible depressor
	Precursor of retractor palatini + medial / dorsal / ventral pterygoideus
	Retractor palatini + medial / dorsal / ventral pterygoideus (A1 only)
	Exterior rostral adductor of the mandible
	Exterior ventral adductor of the mandible
	Pseudotemporalis + Exterior rostral adductor of the mandible (P2 only)
	Pseudotemporalis
	Probable pseudotemporalis (K specimen)
	Retractor bulbi
	Protractor quadrati
	Lateral dorsal pterygoideus
	Lateral dorsal and ventral pterygoideus (P4 only)
	Lateral ventral pterygoideus

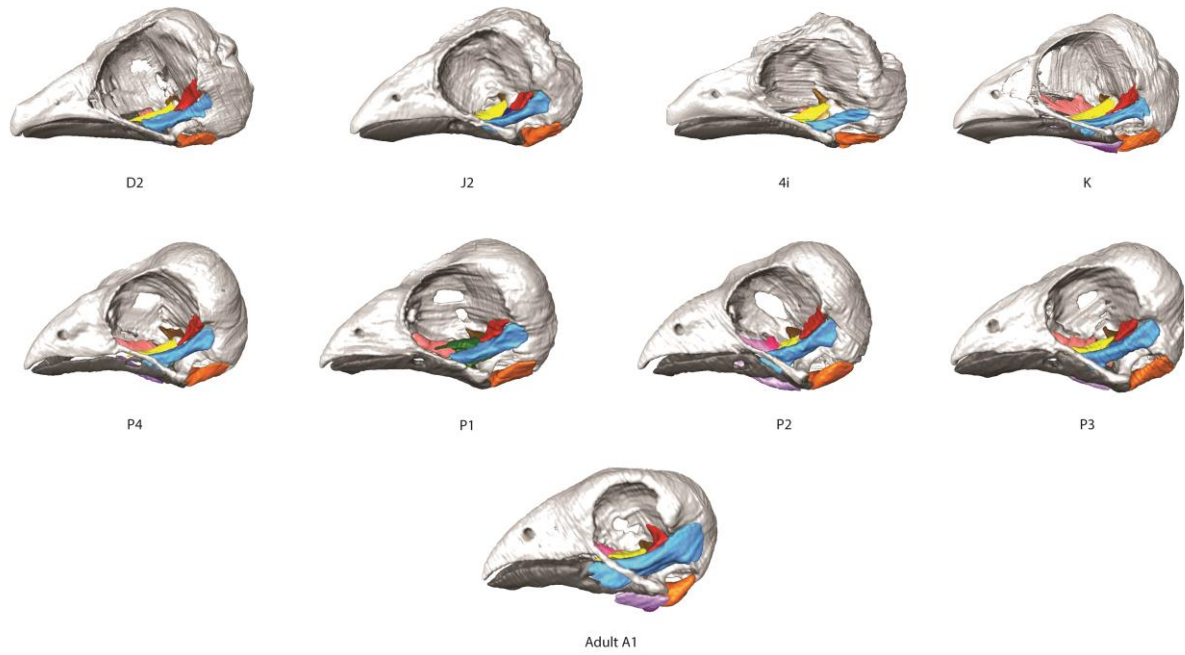


Figure 38 : Left lateral view of skull obtained after segmentation of contrasted enhanced μ CT scans. Developmental order is respected. Skull is in light grey and lower jaw is in dark grey. For muscle color code see Table 19.

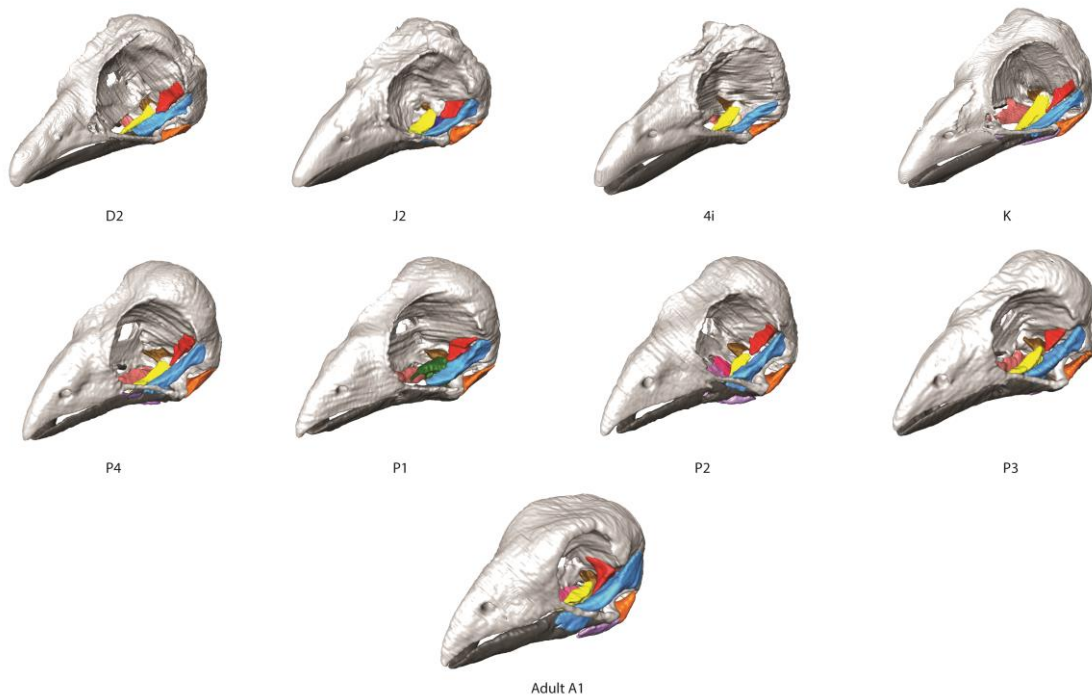


Figure 39 : Oblique frontal view of skull obtained after segmentation of contrasted enhanced μ CT scans. Developmental order is respected. Skull is in light grey and lower jaw is in dark grey. For muscle color code see Table 19.

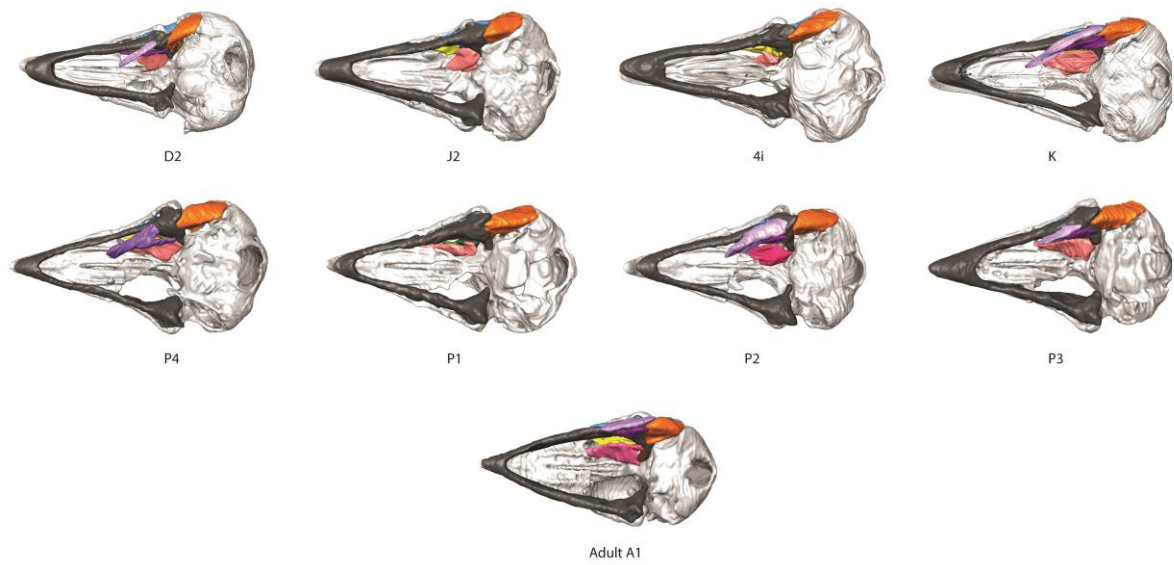


Figure 40 : Caudal view of skull obtained after segmentation of contrasted enhanced μ CT scans. Developmental order is respected. Skull is in light grey and lower jaw is in dark grey. For muscle color code see Table 19.

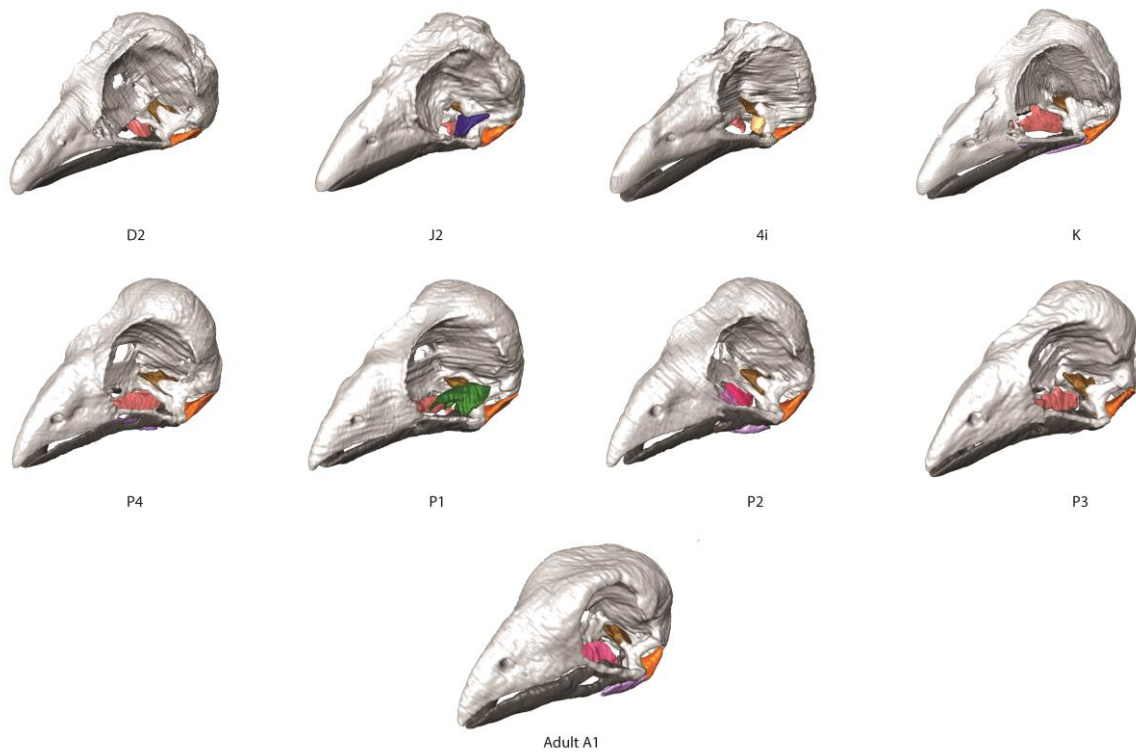


Figure 41 : Oblique frontal view of skull obtained after segmentation of contrasted enhanced μ CT scans. The superficial muscle layer has been removed. Developmental order is respected. Skull is in light grey and lower jaw is in dark grey. For muscle color code see Table 19.

Discussion

These preliminary data highlight that the ossification sequence in the hoatzin is not dramatically different from that in other birds. Yet, some interesting differences can be noticed such as the early ossification of the sphenoid complex which takes place earlier than in precocial birds. However, no clear difference can be detected in the ossification of the phalanges of the wing skeleton compared to other birds despite the functional wing in juvenile hoatzin (Abourachid et al., 2019). Contrast-enhanced scans allowed us to observe that the sternum shape is already determined in the earliest stages of development of the specimens at our disposition. The fusion of the furcula to the sternum is already present in our earliest embryo while the complete fusion of the coracoid to the sternum happens only in the adults. Contrast-enhanced scans further show that the opening of the mandible and the elevation of the premaxilla are functional early during embryonic development. Jaw closing appears fully functional before hatching yet the forceful retraction of the premaxilla appears to be possible only in older juveniles and adults that actively feed on leaves. The premaxillary retraction has been suggested to help cut parts of leaves in the hoatzin (Korzoun, Erard, and Gasc, 2003) and as such it makes sense that the muscles responsible become functional only late during the development.

General discussion

General discussion

The aim of the present thesis was to improve our understanding of the functional anatomy of a unique bird, the hoatzin, *Opisthocomus hoazin*. Despite the unusual nature of the hoatzin and its use as a functional analogue of fossil birds, its skeletal anatomy remains only partly known. Descriptions have remained partial and have mainly focused on some parts of the skeleton (Mitchell, 1896; Parker, 1891; Shufeldt, 1918). Based on the literature, the hoatzin appears to be the only bird with fully folivorous diet implying morphological and physiological adaptations (Grajal et al., 1989). The hoatzin skull shows some adaptations related to its specialized diet such as the particular shape of the quadratomandibular articulation. It has been suggested that the hoatzin is able to ‘masticate’ and it has been called a “chewing bird” (Korzoun, Erard, and Gasc, 2003). The shape of the quadrate condyle and the articular part of the mandible could limit the lateral movement of the lower jaw. These movements should be more limited than dorsoventral movements as suggested by Dawson et al. (2011). However, the dorsoventral movements could be congruent with the processing of leaves as described by Korzoun et al., (2003) thanks to prominent keratinized ridges and protraction/retraction movements of the lower jaw. Contrast-enhanced scans further show that the opening of the mandible and the elevation of the premaxilla are functional early during embryonic development. Jaw closing appears fully functional before hatching, yet the forceful retraction of the premaxilla appears to be possible only in older juveniles and adults that actively feed on leaves. The premaxillary retraction has been suggested to help cut parts of leaves in the hoatzin (Korzoun, Erard, and Gasc, 2003) and as such it makes sense that the muscles responsible become functional only later during the development which is congruent with the long chick feeding period (2 months according to Müllner, 2004).

Another consequence of the enlarged crop is the modification of the sternum and especially the carina thereof. The hoatzin has been described as the only strictly vegetarian bird, and to be able to digest leaves hoatzins use pregastric foregut fermentation, analogous to what is observed in ruminants (Grajal, 1995; Grajal et al., 1989). This crop thus acts as a hypertrophied fermentation chamber and is positioned

ventral to the sternum. As the crop is enlarged it is housed in a concave depression of the sternum keel (Parker, 1891). The crop is positioned on the pectoral muscles, under the skin. It lies on the cranial part of the scapular complex, in front of the fused furcula, coracoid and sternum bones (Grajal, 1995). Both coracoid bones are fused to each other and to the furcula, probably adding rigidity to the sternum complex. Contrast-enhanced scans allowed us to observe that the sternum shape is already determined in the earliest stages of development of the specimens at our disposition. The fusion of the furcula to the sternum is already present in our earliest embryo while the complete fusion of the coracoid to the sternum happens only in the adults. Contrast-enhanced scans allowed us to observe that the sternum shape is already determined in the earliest stages of development of the specimens at our disposition. The fusion of the furcula to the sternum is already present in our earliest embryo while the complete fusion of the coracoid to the sternum happens only in the adults. An additional particularity of the hoatzin sternum is the enlarged and flattened pad at the distal part of the sternum keel. This “resting pad” is used by the hoatzin while perching for long periods (Parker, 1891). Sternal perching may represent a low-energy adaptation for long quiescent periods with a full crop (Müllner, 2004; Strahl, 1988). These particularities on the sternum could thus help support the weight of the trunk (Gadow, 1892). Again, this anatomical particularity seems to be already present in early embryos but its ossification happens in late juveniles.

Thus, the scapular girdle of the hoatzin has a unique suite of features more so than observed for the rest of the whole skeleton in comparison to a large sample of birds. The morphological analysis of the complete skeleton showed that the scapular girdle appears the most impacted by the dietary specialization, showing many unique characters. Among these characters, we found that both coracoids are not only fused to the sternum, they are also fused together. Moreover, coracoids are fused cranially via the acromion to the furcula and more ventrally via the procoracoid process too, enhancing the solidity of the anterior part of the sternum complex. Lateral and medial fenestrae and manubrial foramen are not present on the hoatzin sternum, probably to increase the rigidity of the sternum complex. The craniolateral processes of the sternum are not present; these processes should be the attachment site of the muscle

sternocoracoideus which should inserts on the coracoids (Baumel et al., 1993; Harvey, Kaiser, and Rosenberg, 1969). Thus, this muscle responsible of a backward movement of the coracoid could be missing too, which is congruent with the observed coracoid sternum fusion (Harvey, Kaiser, and Rosenberg, 1969; Owre, 1967). But, this result could lead us to think that the morphological changes on the hoatzin sternum complex could have more muscular implications on the scapular complex than only on the muscles directly link to the flight behavior (Grajal et al., 1989). The muscular anatomy of the hoatzin needs further study and dissection work.

Considering previous results on the unique characters of the hoatzin sternum, we decided to perform comparative analyses of the shape of the bones of the scapular girdle using a comparative sample of collection specimens. We first tested the impact of the preparation on the shape of the scapular girdle bones using both intra and interspecific datasets. It appears that at an intraspecific level these preparation effects could have an impact on the bone shape and further anatomical studies. Whereas, we found that these deformations have little effect at the interspecific level. We also point out that the texture and the color of a considered bone could be a good proxy of the bone deformation such as a very powdery and white bone is more likely to have non-natural deformation than an oily and yellowness one.

Taking into account previous results on non-natural effect on the bone shape, we carefully selected bones of the scapular girdle from osteological collections belonging to fifty-nine species. This comparative dataset encompasses a broad diversity of species across the phylogeny and with different ecologies. We used literature flight type classifications to test if scapular bone shapes could be link to specific locomotor type (Close and Rayfield, 2012; Hui, 2002; Mitchell et al., 2017). Our results showed that the whole 3D shape of the furcula seems not to be as informative as previous studies have shown with 2D measurements (Close and Rayfield, 2012; Hui, 2002; Mitchell et al., 2017). This surprising result can be due to the sample that we used, that is different from others studies performed on the furcula. It important to note that flightless birds in our dataset do not have furcula (such as Ratites species) and some flight group are

underrepresented. Because some locomotor categories are underrepresented, our results can be due to a lack of statistical power. However, we found that the scapula, coracoid, sternum and the mainly the humerus were good proxies of flight type in birds.

As predicted by the literature, flightless birds are differentiated from all the other flying birds by the absence of a carina on their sternum (Cano, 2012; Gussekloo and Cubo, 2013). Nevertheless, the carina shape is more complex than just its presence or absence. We demonstrated that other morphological characters of the carina were also informative concerning the flight type in birds. For example, the position and orientation of the carina on the sternum or its height are different between flight types. Furthermore, the sternum body shape is an important parameter to take into account for hydrodynamic needs in semi aquatic birds (Kaiser, 2007). All aerial birds (flapping, gliding birds, as well as poor flyers) showed robust coracoids with a short shaft and large epiphyses whereas all semi-aquatic and fully aquatic birds displayed an elongated one. This difference in shape can be related to the biomechanical role of this bone as it needs to act as a pulley (Baier, Gatesy, and Dial, 2013; Jenkins, Dial, and Goslow, 1988). Indeed, a robust and shortened shape as in aerial birds could be associated with higher forces needed during the upstroke of the wing. On the contrary, an elongated coracoid such as that observed in semi-aquatic and fully aquatic birds may provide greater leverage for animals moving in a dense medium like water (Kaiser, 2007). Scapula shapes distinguished aquatic birds which have very enlarged blades compared to other birds. As the main functional role of the scapula is to stabilize the shoulder, an enlarged blade may allow a larger surface of attachment of the muscles providing higher resisting forces when moving the wings under water (Baumel et al., 1993; Dial, 1992; Kaiser, 2007). On the opposite, flapping birds, gliding birds and poor flyers have a scapula with a very thin blade and appear not to require a strong stabilization of the shoulder. The humeri of gliding and flapping birds have large proximal epiphysis for flight muscle insertions. The distal epiphysis seems more developed in gliding species than in flapping species, which could be related to the full wing stabilization needed in gliding birds. Both gliding and flapping species have a rounded and curved shaft which has been suggested to reduce the stresses by transferring flight forces towards the joints (Kaiser, 2007). On the contrary, swimming birds have very short and flat humeri which might contribute to decreased drag by presenting a thinner cross-section as the wing passes through the water (Kaiser, 2007). Moreover, a flat bone is designed to cope with large

stresses generated by wing movement through a dense medium like water if the orientation of the forces is predictable (Kaiser, 2007). Moreover, the head of the humerus that articulates with the shoulder is distinctly curved in flapping, gliding and semi aquatic species such that most of the wing stroke can occur below the horizontal (Kaiser, 2007). The physics of flight suggest that the lower part of the wing stroke is the most important because its power is vectored inward and downward against the other wing, instead of dispersing outward (Baier, Gatesy, and Dial, 2013; Dial, 2003; Goslow, Dial, and Jenkins, 1990; Kaiser, 2007).

The morphospaces obtained in our results showed that the hoatzin falls within the morphospace of most other birds suggesting that in terms of shape the bones of the scapular girdle may not be as different as initially suggested. Although the shape of the scapular bones of the hoatzin thus does not seem to be radically different compared to other birds, even if its sternum appears largely modified. Specifically, its keel reduction and its “resting pad”, another functional consequence of the unique dietary specialization, appear to be key traits. Indeed, the sternum keel is the main insertion site of flight muscles: the supracoracoids and the pectorals muscles. In fact, the modifications of the sternum shape reported here are the reasons why previous authors predicted the hoatzin not to be a good flyer (Cherrie, 1909; Chin and Lentink, 2017; Grajal, 1995; Grajal et al., 1989; Grimmer, 1962; Strahl, 1988).

Cherrie (1909) reported that the hoatzin is rarely seen in flight, that its wings are large and ample but the flight weak and labored, as such doubting its capability to fly more than a few hundred yards. Grimmer (1962) described the hoatzin as “one of the world’s most inept flyers” capable of flying less than a hundred yards. He completed the description adding that its take off look like a “clumsy helicopter” and the landing as a “crash land in the trees”. Strahl (1988) described a flapping flight stronger than previously described by Grimmer (1962). He claimed that the hoatzin has been seen flying up to 350m without rest and reported no crash landings during non-disturbed flights. Grajal et al. (1989) described the hoatzin as a poor flyer based on its reduced carina which decreased the area of attachment for flight muscles. However, they specify that its flying abilities allow the hoatzin to have a selective diet and to perform fermentation efficiently. Grajal (1995) described further that the hoatzin prefers to hop

from branch to branch. More recently Chin and Lentink (2017) considered that the hoatzin is capable of foraging flight with no more detail. To sum up, it appears that no quantitative data are available on the locomotion of the hoatzin, whereas its social and territorial behavior has been well documented (Müllner, 2004; Strahl, 1988; VanderWerf and Strahl, 1990).

Given the lack of quantitative *in vivo* data on flight in the hoatzin we decided to use a comparative dataset of bird scapular girdles to explore whether the shape of the sternum and the other scapular bones of the hoatzin may be driving its suggested poor flying ability. Based on the results of our comparative sample all the bone shape of the scapular girdle, except the scapula, suggested that the hoatzin have a similar morphology than those of gliding birds. Following these results, the sternum shape of the hoatzin seems not to be the reason of its poor flying abilities, as other birds with similar morphologies do appear capable of excellent flight. More quantitative analyses on flying abilities in birds are needed in relation to the musculoskeletal system of the scapular girdle in order to better understand the flying abilities of this enigmatic bird. It could be interesting to go further in the analyses of the ontogenetic series to be able to identify how the digestive system is set up and how muscles associated to the scapular girdle develop with this physical constraint. Some morphological characteristics unique to the hoatzin such as the complete fusion of the sternum, furcula and coracoids are not included in this analysis and may influence its flight type (Gadow, 1892; Grajal, 1995; J. Hughes and Baker, 1999; Parker, 1868). Indeed, its fusion likely prevents the furcular spring action and coracoid movement which are important for energy recovery during wing beating and thus this may induce a higher energetic cost (Jenkins et al., 2017). Moreover, some physiological traits could influence its flight type too. Indeed, as the hoatzin is fully folivorous, and as the energy derived from plant matter is rather low this could impact its ability to use energy and may drive its long perching for digestion (Grajal et al., 1989; Müllner, 2004). Many other parameters have to be taken into account, however. The flight itself could maybe be qualified as glide, but the take-off could be heavily energy consuming because of the fusion of the sternum complex, or because of its large body mass as observed in Phasianidae (Tobalske and Dial, 2000). Landing is also not considered here but may impose specific constraints on flight as well.

Finally, our comparative dataset may shed light on the evolution of the unusual morphology of the hoatzin by including fossil bones of extinct species (Mayr, Alvarenga, and Mourer-Chauviré, 2011). This would allow us to possibly infer the flight type of extinct relatives of the hoatzin lineage (Mayr, Alvarenga, and Mourer-Chauviré, 2011; Mayr and De Pietri, 2014; Mourer-Chauviré, 2003). Two extinct species, *Namibiavis* and *Hoazinavis*, have already been scanned and the 3D models of humeral extremity, scapula proximal part and coracoids are available (Figures 42-43-44). These bones being well preserved in 3D show great similarity with the extant hoatzin suggesting that it may be possible to make solid inferences on the evolution of the scapular girdle of this unique bird.

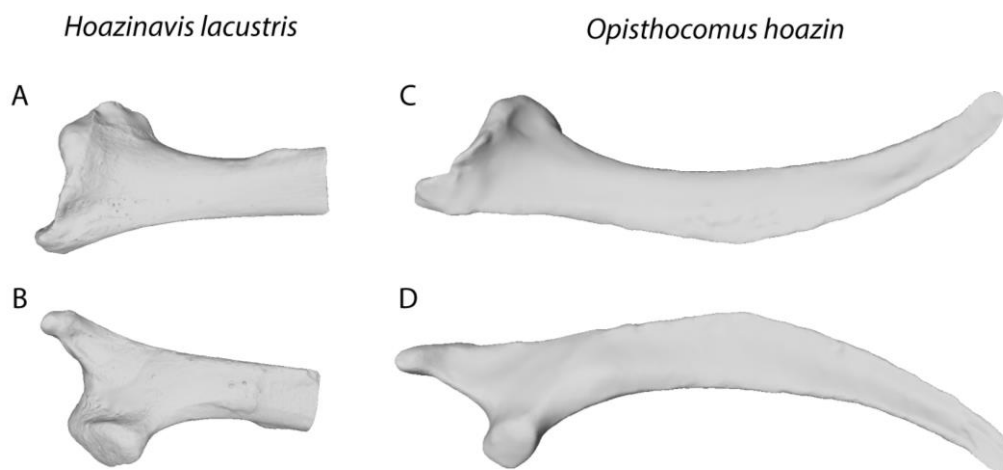


Figure 42 : 3D models of both fossil and extant left scapula bones of the hoatzin lineage. *Hoazinavis lacustris* (A medial view and B lateral view) and extant hoatzin (E medial view and F lateral view).

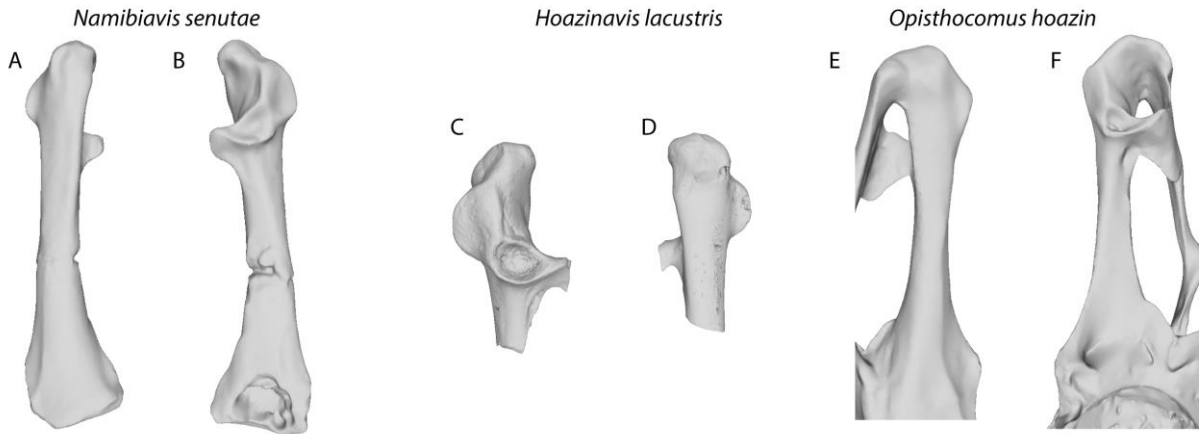


Figure 43 : 3D models of both fossil and extant coracoid bones of the hoatzin lineage. *Namibiavis senutae* (A ventral view and B dorsal view), *Hoazinavis lacustris* (C dorsal view and D ventral view) and extant hoatzin (E ventral view and F dorsal view).

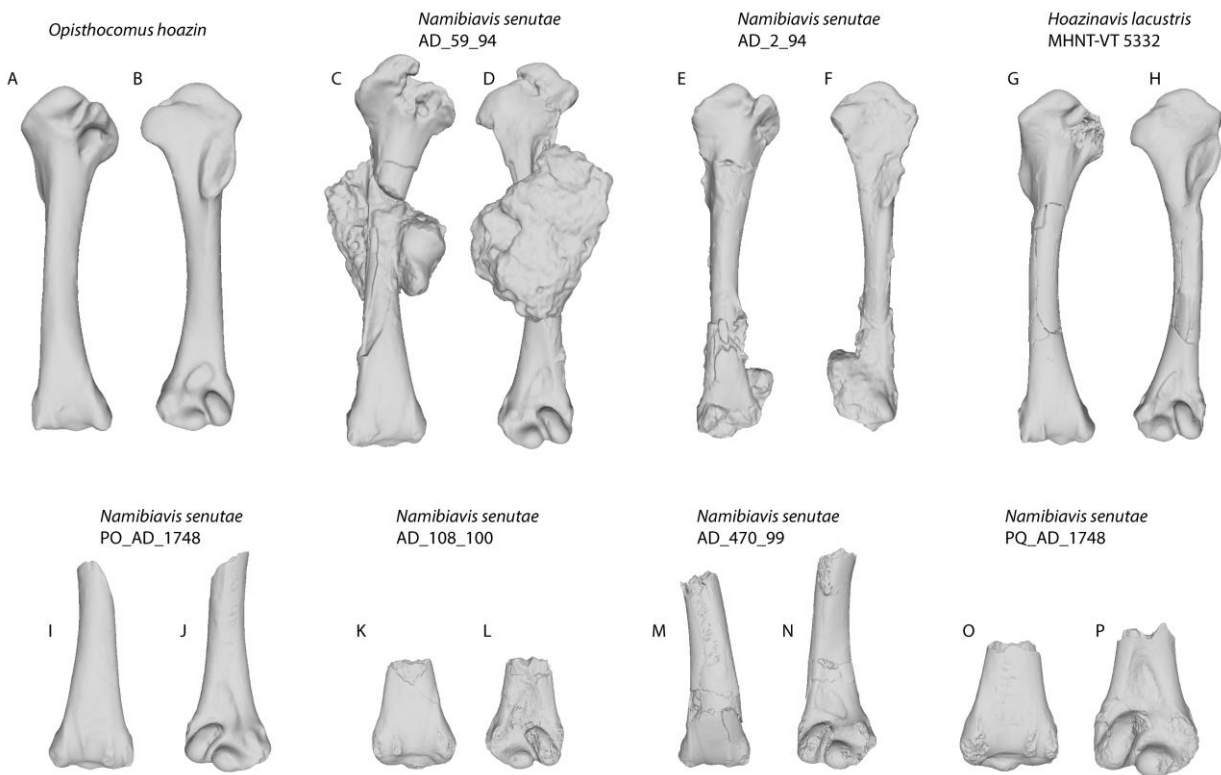


Figure 44 : 3D models of both fossil and extant humerus bones of the hoatzin lineage. Extant hoatzin (A medial view and B lateral view), *Namibiavis senutae* (C-E-I-K-M-O medial view and D-F-J-L-N-P lateral view) and *Hoazinavis lacustris* (G medial view and H lateral view).

Conclusion

This thesis provided new information on the anatomy of the hoatzin, including functional interpretations in relation to its physiological constraints. 3D data on our ontogenetic series allowed us to describe the order of ossification of each part of the skeleton and thus to determine that the sternum shape is setup early in the development. In contrast, the complete fusion of the sternum, furcula, and coracoid complex happens in later juveniles. The use of a comparative dataset and 3D geometric morphometric methods allowed us to generate quantitative data on the morphological specificities of the hoatzin. The flight type of the hoatzin has been much debated in the literature but this work provides a preliminary answer to the role of its sternum shape and reduced carina in its flight abilities. Some muscular, functional, ecological and physiological parameters should be tested in relation to bone shape to be able to better infer flight type of this enigmatic bird. Our comparative bone shape analysis in relation to the locomotor mode will allow us to include data on fossils and infer flight type of extinct species belonging to the hoatzin lineage (Mayr, Alvarenga, and Mourer-Chauviré, 2011). More generally, it will be of great interest to complete our comparative dataset with more representative species of each flight type and try to infer locomotor types of fossil taxa providing insights into the origin of flight and the anatomical modification of the scapular girdle required.

References

References

- Abourachid A, Castro I, Provini P. 2019. How to walk carrying a huge egg? Trade-offs between locomotion and reproduction explain the special pelvis and leg anatomy in kiwi (Aves; Apteryx spp.). *J. Anat.* 1–12. DOI: 10.1111/joa.13072
- Abourachid A, Herrel A, Decamps T, Pagès F, Fabre A, Van Hoorebeke L, Adriaens D, Garcia Amado MA. 2019. Hoatzin nestling locomotion: Acquisition of quadrupedal limb coordination in birds. *Sci. Adv.* 5. DOI: 10.1126/sciadv.aat0787
- Adams DC, Otárola-Castillo E. 2013. Geomorph: An R package for the collection and analysis of geometric morphometric shape data. *Methods Ecol. Evol.* 4: 393–399. DOI: 10.1111/2041-210X.12035
- Ainsworth SJ, Stanley RL, Evans DJR. 2010. Developmental stages of the Japanese quail. *J. Anat.* 216: 3–15. DOI: 10.1111/j.1469-7580.2009.01173.x
- Arnold KE, Owens IPF. 1998. Cooperative breeding in birds: A comparative test of the life history hypothesis. *Proc. R. Soc. B Biol. Sci.* 265: 739–745. DOI: 10.1098/rspb.1998.0355
- Ashley-Ross MA, Gillis GB. 2002. A brief history of vertebrate functional morphology. *Integr. Comp. Biol.* 42: 183–189
- Atalgin SH, Kürtül I. 2009. A morphological study of skeletal development in turkey during the pre-hatching stage. *J. Vet. Med. Ser. C Anat. Histol. Embryol.* 38: 23–30. DOI: 10.1111/j.1439-0264.2008.00887.x
- Baier DB, Gatesy SM, Dial KP. 2013. Three-Dimensional, High-Resolution Skeletal Kinematics of the Avian Wing and Shoulder during Ascending Flapping Flight and Uphill Flap-Running. *PLoS One* 8. DOI: 10.1371/journal.pone.0063982
- Bardua C, Felice RN, Watanabe A, Fabre A-C, Goswami A. 2019. A practical guide to sliding and surface semilandmarks in morphometric analyses. *Integr. Org. Biol.* DOI: 10.1093/iob/obz016
- Baumel JJ, King AS, Breazile JE, Evans HE, Vanden Berge JC. 1993. Handbook of Avian Anatomy: Nomina Anatomica Avium, Second Edition, Publications of the Nuttall Ornithological Club. 779p. DOI: 10.2307/1369201

- Baylac M, Frieß M. 2005. Fourier Descriptors, Procrustes Superimposition, and Data Dimensionality: An Example of Cranial Shape Analysis in Modern Human Populations., in: Slice D.E. (Eds) *Modern Morphometrics in Physical Anthropology. Developments in Primatology: Progress and Prospects*. Springer, Boston, MA
- Beddard FE. 1889. Contributions to the Anatomy of the Hoatzin (*Opisthocomus cristatus*), with particular Reference to the Structure of the Wing in the Young. *Ibis (Lond. 1859)*. 31: 283–293. DOI: 10.1111/j.1474-919X.1889.tb06447.x
- Blanke A, Watson PJ, Holbrey R, Fagan MJ. 2017. Computational biomechanics changes our view on insect head evolution. *Proc. R. Soc. B Biol. Sci.* 284. DOI: 10.1098/rspb.2016.2412
- Bookstein FL. 1997. Landmark methos for forms without landmarks: morphometrics of group difference in outline shape. *Med. Image Anal.* 1: 225–243
- Bosque C, Pacheco MA, Siegel RB. 1999. Maintenance Energy Costs of Two Partially Folivorous Tropical Passerines. *Auk* 116: 246–252. DOI: 10.2307/4089474
- Bribiesca-Contreras F, Sellers WI. 2017. Three-dimensional visualisation of the internal anatomy of the sparrowhawk (*Accipiter nisus*) forelimb using contrast-enhanced micro-computed tomography. *PeerJ* 5. DOI: 10.7717/peerj.3039
- Bright JA, Marugán-Lobón J, Cobb SN, Rayfield EJ. 2016. The shapes of bird beaks are highly controlled by nondietary factors. *Proc. Natl. Acad. Sci. U. S. A.* 113: 5352–5357. DOI: 10.1073/pnas.1602683113
- Brown JW, Rest JS, García-Moreno J, Sorenson MD, Mindell DP. 2008. Strong mitochondrial DNA support for a Cretaceous origin of modern avian lineages. *BMC Biol.* 6: 1–18. DOI: 10.1186/1741-7007-6-6
- Cano FG. 2012. *Interactive Avian Anatomy : Functional and clinical aspects*
- Carril J, Tambussi CP. 2017. Skeletogenesis of *Myiopsitta monachus* (Psittaciformes) and sequence heterochronies in Aves. *Evol. Dev.* 19: 17–28. DOI: 10.1111/ede.12211
- Cherrie GK. 1909. The Hoatzin. *Museum News (Brooklyn Inst. Arts Sci.* 4: 50–53
- Chin DD, Lentink D. 2017. How birds direct impulse to minimize the energetic cost of foraging flight. *Sci. Adv.* 3. DOI: 10.1126/sciadv.1603041
- Clifton GT, Carr JA, Biewener AA. 2018. Comparative hindlimb myology of foot-propelled

- swimming birds. *J. Anat.* 232: 105–123. DOI: 10.1111/joa.12710
- Close RA, Rayfield EJ. 2012. Functional morphometric analysis of the furcula in mesozoic birds. *PLoS One* 7: 1–20. DOI: 10.1371/journal.pone.0036664
- Constantinescu GM. 2018. Comparative anatomy of the mouse and the rat: a color atlas and text. CRC Press INC. DOI: 10.1111/j.1911-3846.1997.tb00533.x
- Cornette R, Tresset A, Houssin C, Pascal M, Herrel A. 2015. Does bite force provide a competitive advantage in shrews? The case of the greater white-toothed shrew. *Biol. J. Linn. Soc.* 114: 795–807. DOI: 10.1111/bij.12423
- Cox PG, Jeffery N. 2008. Geometry of the semicircular canals and extraocular muscles in rodents, lagomorphs, felids and modern humans. *J. Anat.* 213: 583–96. DOI: 10.1111/j.1469-7580.2008.00983.x
- Cracraft J. 1971a. A new family of hoatzin-like birds (order Opisthocomiformes) from the Eocene of South Africa. *Ibis (Lond. 1859)*. 113: 229–233
- Cracraft J. 1971b. The functional morphology of the hind limb of the domestic pigeon, *Columba livia*. *Bull. Am. Museum Nat. Hist.* 144: 173–268
- Davesne D, Friedman M, Barriel V, Lecointre G, Janvier P, Gallut C, Otero O. 2014. Early fossils illuminate character evolution and interrelationships of Lampridiformes (Teleostei, Acanthomorpha). *Zool. J. Linn. Soc.* 172: 475–498. DOI: 10.1111/zoj.12166
- Dawson MM, Metzger KA, Baier DB, Brainerd EL. 2011. Kinematics of the quadrate bone during feeding in mallard ducks. *J. Exp. Biol.* 214: 2036–2046. DOI: 10.1242/jeb.047159
- de Bakker MAGG, Fowler DA, Oude K Den, Dondorp EM, Carmen Garrido Navas M, Horbanczuk JO, Sire J-YY, Szczerbińska D, Richardson MK, den Oude K, Dondorp EM, Navas MCG, Horbanczuk JO, Sire J-YY, Szczerbińska D, Richardson MK. 2013. Digit loss in archosaur evolution and the interplay between selection and constraints. *Nature* 500: 445–449. DOI: 10.1038/nature12336
- De Margerie E, Sanchez S, Cubo J, Castanet J. 2005. Torsional resistance as a principal component of the structural design of long bones: Comparative multivariate evidence in birds. *Anat. Rec. - Part A Discov. Mol. Cell. Evol. Biol.* 282: 49–66. DOI: 10.1002/ar.a.20141

- del Hoyo J, Elliott A, Sargatai J. 1993. Handbook of the Birds of the World, Volume 3 (Hoatzin to Auks)
- del Hoyo J, Elliott A, Sargatai J. 1991. Handbook of the Birds of the World
- DeLaurier A, Burton N, Bennett M, Baldock R, Davidson D, Mohun TJ, Logan MPO. 2008. The Mouse Limb Anatomy Atlas: An interactive 3D tool for studying embryonic limb patterning. *BMC Dev. Biol.* 8: 1–7. DOI: 10.1186/1471-213X-8-83
- Descamps E, Sochacka A, de Kegel B, Loo D Van, Hoorebeke L, Adriaens D. 2014. Soft tissue discrimination with contrast agents using micro-ct scanning. *Belgian J. Zool.* 144: 20–40
- Dial KP. 2003. Evolution of Avian Locomotion : Correlates of Flight. *Auk* 120: 941–952. DOI: 10.1642/0004-8038(2003)120
- Dial KP. 1992. Avian Forelimb Muscles and Nonsteady Flight : Can Birds Fly without Using the Muscles in Their Wings ? *Auk* 109: 874–885
- Dominguez-Bello MG, Lovera M, Saurez P, Michelangeli F. 1993. Microbial digestive symbionts of the crop of the hoatzin (*Opisthocomus hoazin*) - An avian foregut fermenter. *Physiol. Zool.* 66: 374–383
- Domínguez-Bello MG, Michelangeli F, Ruiz MC, García A, Rodríguez E. 1994. Ecology of the Folivorous Hoatzin (*Opisthocomus hoazin*) on the Venezuelan Plains. *Auk* 111: 643–651
- Druzinsky RE, Balhoff JP, Crompton AW, Done J, German RZ, Haendel MA, Herrel A, Herring SW, Lapp H, Mabee PM, Muller HM, Mungall CJ, Sternberg PW, Van Auken K, Vinyard CJ, Williams SH, Wall CE. 2016. Muscle logic: New knowledge resource for anatomy enables comprehensive searches of the literature on the feeding muscles of mammals. *PLoS One* 11: 1–19. DOI: 10.1371/journal.pone.0149102
- Fain MG, Houde P. 2004. Parallel radiations in the primary clades of birds. *Evolution (N. Y.)*. 58: 2558–2573. DOI: 10.1554/04-235
- Feduccia A. 1993. Evidence from Claw Geometry Indicating Arboreal Habits of Archaeopteryx. *Adv. Sci.* 259: 790–793. DOI: 10.1126/science.259.5096.790
- Fisher HI. 1940. The occurrence of vestigial wing claws on the wings of birds. *Am. Midl. Nat.* 23: 234–243

- Gadow H. 1892. Crop and sternum of *Opisthocomus cristatus*. A contribution to the question of the correlation of organs and the inheritance of acquired characters. *Proc. R. Irish Acad. Ser. III* 2: 147–154
- Garrod AH. 1879. Notes on points in the anatomy of the Hoatzin (*Opisthocomus cristatus*). *Prosector to Soc.* 103–114. DOI: 10.1038/154714a0
- Gatesy SM, Dial KP. 1996. Locomotor Modules and the Evolution of Avian Flight. *Evolution (N. Y.)* 50: 331–340. DOI: 10.2307/2410804
- Genbrugge A, Herrel A, Boone M, Van Hoorebeke L, Podos J, Dirckx J, Aerts P, Dominique A. 2011. The head of the finch: The anatomy of the feeding system in two species of finches (*Geospiza fortis* and *Padda oryzivora*). *J. Anat.* 219: 676–695. DOI: 10.1111/j.1469-7580.2011.01437.x
- Gill FB. 2007. Ornithology, 3rd Editio. ed. 766p. DOI: 10.1017/CBO9781107415324.004
- Godoy-Vitorino F, Ley RE, Gao Z, Pei Z, Ortiz-Zuazaga H, Pericchi LR, Garcia-Amado MA, Michelangeli F, Blaser MJ, Gordon JI, Domínguez-Bello MG. 2008. Bacterial community in the crop of the hoatzin, a neotropical folivorous flying bird. *Appl. Environ. Microbiol.* 74: 5905–5912. DOI: 10.1128/AEM.00574-08
- Goslow, GE, Dial KP, Jenkins, FA. 1990. Bird Flight: Insights and Complications. *Bioscience* 40: 108–115. DOI: 10.2307/1311343
- Grajal A. 1995. Structure and function of the digestive tract of the hoatzin (*Opisthocomus hoazin*): a folivorous bird with foregut fermentation. *Auk* 112: 20–28. DOI: 10.2307/4088763
- Grajal A, Strahl SD, Parra R, Dominguez-bello MG, Neher A. 1989. Foregut fermentation in the hoatzin, a neotropical leaf-eating bird. *Science (80-.)*. 245: 1236–1238
- Grimmer JL. 1962. Strange Little World of the Hoatzin. *Natl. Geogr. Mag.* 390–401
- Guillaud E, Cornette R, Béarez P. 2016. Is vertebral form a valid species-specific indicator for salmonids? The discrimination rate of trout and Atlantic salmon from archaeological to modern times. *J. Archaeol. Sci.* 65: 84–92. DOI: 10.1016/j.jas.2015.11.010
- Gunz P, Mitteroecker P. 2013. Semilandmarks: A method for quantifying curves and surfaces. *Hystrix* 24. DOI: 10.4404/hystrix-24.1-6292

- Gunz P, Mitteroecker P, Bookstein FL. 2005. Semilandmarks in Three Dimensions, in: Modern Morphometrics in Physical Anthropology. pp. 73–98. DOI: 10.1007/0-387-27614-9_3
- Gussekkloo SWS, Cubo J. 2013. Flightlessness affects cranial morphology in birds. *Zoology* 116: 75–84. DOI: 10.1016/j.zool.2012.09.001
- Hackett SJ, Kimball RT, Reddy S, Bowie RCK, Braun EL, Braun MJ, Chojnowski JL, Cox WA, Han K, Harshman J, Huddleston CJ, Marks BD, Miglia KJ, Moore WS, Sheldon FH, Steadman DW, Witt CC, Yuri T. 2008. A Phylogenomic Study of Birds Reveals Their Evolutionary History. *Science* (80-.). 320: 1763–1768. DOI: 10.1126/science.1157704
- Harvey EB, Kaiser HE, Rosenberg LE. 1969. An atlas of the domestic turkey (*Meleagris gallopavo*): myology and osteology, Energy. United States, 247p. DOI: 10.2172/4811958
- Hawkins BA, Diniz-Filho JAF, Jaramillo CA, Soeller SA. 2006. Post-Eocene climate change, niche conservatism, and the latitudinal diversity gradient of New World birds. *J. Biogeogr.* 33: 770–780. DOI: 10.1111/j.1365-2699.2006.01452.x
- Hawkins, José Alexandre Felizola Diniz-Filho, Jaramillo, Soeller. 2007. Climate, Niche Conservatism, and the Global Bird Diversity Gradient. *Am. Nat.* 170: S16. DOI: 10.2307/4541088
- Hofmann RR. 1989. Evolutionary Steps of Ecophysiological Adaptation and Diversification of Ruminants: A Comparative View of Their Digestive System. *Oecologia* 78: 443–457
- Hughes J, Baker A. 1999. Phylogenetic relationships of the enigmatic hoatzin (*Opisthocomus hoazin*) resolved using mitochondrial and nuclear gene sequences. *Mol. Biol. Evol.* 16: 1300–7
- Hughes JM, Baker AJ. 1999. Phylogenetic relationships of the enigmatic hoatzin (*Opisthocomus hoazin*) resolved using mitochondrial and nuclear gene sequences. *Mol. Biol. Evol.* 16: 1300–1307
- Hui CA. 2002. Avian furcula morphology may indicate relationships of flight requirements among birds. *J. Morphol.* 251: 284–293. DOI: 10.1002/jmor.1089
- Huxley TH. 1868. On the Classification and Distribution of the Alectoromorphae and

Heteromorphae. *Proc. Zool. Soc. London* 294–319. DOI: 10.1038/154714a0

Jarvis ED, Mirarab S, Aberer AJ, Li B, Houde P, Li C, Ho SYW, Faircloth BC, Nabholz B, Howard JT, Suh A, Weber CC, da Fonseca RR, Alfaro-Núñez A, Narula N, Liu L, Burt D, Ellegren H, Edwards S V, Stamatakis A, Mindell DP, Cracraft J, Braun EL, Warnow T, Jun W, Gilbert MTP, Zhang G. 2015. Phylogenomic analyses data of the avian phylogenomics project. *Gigascience* 4: 1–9. DOI: 10.1186/s13742-014-0038-1

Jarvis ED, Mirarab S, Aberer AJ, Li B, Houde P, Li C, Ho SYW, Faircloth BC, Nabholz B, Howard JT, Suh A, Weber CC, da Fonseca RR, Li J, Zhang F, Li H, Zhou L, Narula N, Liu L, Ganapathy G, Bousseau B, Bayzid MS, Zavidovych V, Subramanian S, Gabaldon T, Capella-Gutierrez S, Huerta-Cepas J, Rekepalli B, Munch K, Schierup M, Lindow B, Warren WC, Ray D, Green RE, Bruford MW, Zhan X, Dixon A, Li S, Li N, Huang Y, Derryberry EP, Bertelsen MF, Sheldon FH, Brumfield RT, Mello C V., Lovell P V., Wirthlin M, Schneider MPC, Prosdocimi F, Samaniego JA, Velazquez AMV, Alfaro-Núñez A, Campos PF, Petersen B, Sicheritz-Ponten T, Pas A, Bailey T, Scofield P, Bunce M, Lambert DM, Zhou Q, Perelman P, Driskell AC, Shapiro B, Xiong Z, Zeng Y, Liu S, Li Z, Liu B, Wu K, Xiao J, Yinqi X, Zheng Q, Zhang Y, Yang H, Wang J, Smeds L, Rheindt FE, Braun M, Fjeldsa J, Orlando L, Barker FK, Jønsson KA, Johnson W, Koepfli K-P, O'Brien S, Haussler D, Ryder OA, Rahbek C, Willerslev E, Graves GR, Glenn TC, McCormack J, Burt D, Ellegren H, Alström P, Edwards S V., Stamatakis A, Mindell DP, Cracraft J, Braun EL, TandyWarnow, Jun W, Gilbert MTP, Zhang G. 2014. Whole-genome analyses resolve early branches in the tree of life of modern birds. *Science (80-.)*. 346: 1311–1320. DOI: 10.1126/science.1251385

Jenkins FA, Dial KP, Goslow, GE. 1988. A Cineradiographic Analysis of Bird Flight : The Wishbone in Starlings is a Spring. *Science (80-.)*. 241: 1495–1498

Jenkins FA, Dial KP, Goslow GE, Goslow, GE. 2017. A Cineradiographic Analysis of Bird Flight : The Wishbone in Starlings is a Spring. *Science (80-.)*. 241: 1495–1498

Jones R., Amado MAG, Dominguez-Bello M. 2000. Comparison of the digestive ability of crop fluid from the folivorous Hoatzin (*Opisthocomus hoazin*) and cow rumen fluid with seven tropical forages. *Anim. Feed Sci. Technol.* 87: 287–296. DOI: 10.1016/S0377-8401(00)00199-1

Kaiser GW. 2007. *The Inner Bird: Anatomy and Evolution*, Journal of Chemical Information and Modeling. UBC Press, 1689–1699p.

- Kardong K V. 2012. Vertebrates: Comparative anatomy, Function, Evolution, Washington State University. 816p. DOI: 10.1007/s13398-014-0173-7.2
- Karp DS, Root TL. 2009. Sound the stressor: how Hoatzins (*Opisthocomus hoazin*) react to ecotourist conversation. *Biodivers. Conserv.* 18: 3733–3742. DOI: 10.1007/s10531-009-9675-6
- Kendall DG. 1977. The Diffusion of Shape. *Adv. Applied Probab.* 9: 428–430
- Keneisenuo K, Choudhary OP, Debroy S, Arya RS, Kalita PC, Doley PJ, Rajkhowa TK, Kalita A. 2019. Comparative gross anatomical studies on the shoulder girdle of crested serpent eagle (*Spilornis cheela*) and brown wood owl (*Strix leptogrammica*). *Indian J. Anim. Res.* DOI: 10.18805/ijar.B-3819
- Korzoun LP, Erard C, Gasc J-P. 2003. Les adaptations de l'hoazin (*Opisthocomus hoazin*) : la folivorie. Caractéristiques morphologiques et particularités fonctionnelles des appareils du bec et hyoïdien. *Comptes Rendus - Biol.* 326: 75–94. DOI: 10.1016/S1631-0691(03)00007-6
- Korzoun LP, Erard C, Gasc J. 2001. Les particularités morphofonctionnelles des appareils du bec et hyoïdien chez les touracos (*Aves*, Musophagidae) : relations avec la frugivorie. *Life Sci.* 324: 965–977. DOI: 10.1016/S0764-4469(01)01363-4
- Lawing AM, Polly PD. 2010. Geometric morphometrics: Recent applications to the study of evolution and development: REVIEW. *J. Zool.* 280: 1–7. DOI: 10.1111/j.1469-7998.2009.00620.x
- Lecointre G, Le Guyader H, Visset D. 2016. Classification phylogénétique du vivant. Tome 1. 583p.
- Livezey BC, Zusi RL. 2007. Higher-order phylogeny of modern birds (Theropoda, Aves: Neornithes) based on comparative anatomy. Analysis and discussion. *Zool. J. Linn. Soc.* 149: 1–95. DOI: 10.1111/j.1096-3642.2006.00293.x
- Livezey BC, Zusi RL. 2006. Phylogeny of neornithes. *Bull. Carnegie Museum Nat. Hist.* 37: 1–544. DOI: 10.2992/0145-9058(2006)37
- MacArthur RH, MacArthur JW. 1961. On Bird Species Diversity. *Ecology* 42: 594–598
- Mallarino R, Campas O, Fritz JA, Burns KJ, Weeks OG, Brenner MP, Abzhanov A. 2012. Closely related bird species demonstrate flexibility between beak morphology and

- underlying developmental programs. *Proc. Natl. Acad. Sci.* 109: 16222–16227. DOI: 10.1073/pnas.1206205109
- Mariani F V., Martin GR. 2003. Deciphering skeletal patterning: Clues from the limb. *Nature* 423: 319–325. DOI: 10.1038/nature01655
- Maxwell EE. 2008a. Evolution of Avian Ossification Sequences. 315p.
- Maxwell EE. 2008b. Ossification sequence of the avian order anseriformes, with comparison to other precocial birds. *J. Morphol.* 269: 1095–1113. DOI: 10.1002/jmor.10644
- Maxwell EE. 2008c. Comparative embryonic development of the skeleton of the domestic turkey (*Meleagris gallopavo*) and other galliform birds. *Zoology* 111: 242–257. DOI: 10.1016/j.zool.2007.08.004
- Maxwell EE, Harrison LB. 2008. Ossification sequence of the common tern (*Sterna hirundo*) and its implications for the interrelationships of the Lari (Aves, Charadriiformes). *J. Morphol.* 269: 1056–1072. DOI: 10.1002/jmor.10633
- Maxwell EE, Harrison LB, Larsson HCE. 2010. Assessing the phylogenetic utility of sequence heterochrony: evolution of avian ossification sequences as a case study. *Zoology* 113: 57–66. DOI: 10.1016/j.zool.2009.06.002
- Maxwell EE, Larsson HCE. 2009. Comparative ossification sequence and skeletal development of the postcranium of palaeognathous birds (Aves: Palaeognathae). *Zool. J. Linn. Soc.* 157: 169–196. DOI: 10.1111/j.1096-3642.2009.00533.x
- Mayr G. 2014. A hoatzin fossil from the middle Miocene of Kenya documents the past occurrence of modern-type Opisthocomiformes in Africa. *Am. Ornithol. Union* 131: 55–60. DOI: 10.1642/AUK-13-134.1
- Mayr G. 2011. Metaves, Mirandornithes, Strisores and other novelties - a critical review of the higher-level phylogeny of neornithine birds. *J. Zool. Syst. Evol. Res.* 49: 58–76. DOI: 10.1111/j.1439-0469.2010.00586.x
- Mayr G, Alvarenga H, Mourer-Chauviré C. 2011. Out of Africa: Fossils shed light on the origin of the hoatzin, an iconic Neotropical bird. *Naturwissenschaften* 98: 961–966. DOI: 10.1007/s00114-011-0849-1
- Mayr G, Clarke J. 2003. The deep divergences of neornithine birds: A phylogenetic

- analysis of morphological characters. *Cladistics* 19: 527–553. DOI: 10.1111/j.1096-0031.2003.tb00387.x
- Mayr G, De Pietri VL. 2014. Earliest and first Northern Hemispheric hoatzin fossils substantiate Old World origin of a “neotropic endemic.” *Naturwissenschaften* 101: 143–148. DOI: 10.1007/s00114-014-1144-8
- Miller AH. 1953. A Fossil Hoatzin from the Miocene of Colombia. *Auk* 70: 484–489. DOI: 10.2307/4081360
- Mitchell J, Legendre LJ, Lefèvre C, Cubo J. 2017. Bone histological correlates of soaring and high-frequency flapping flight in the furculae of birds. *Zoology* 122: 90–99. DOI: 10.1016/j.zool.2017.03.004
- Mitchell PC. 1896. A contribution to the anatomy of the Hoatzin (*Opisthocomus cristatus*). *Proc. Zool. Soc. London* 64: 618–628
- Mitgutsch C, Wimmer C, Sánchez-Villagra MR, Hahnloser R, Schneider RA. 2011. Timing of Ossification in Duck, Quail, and Zebra Finch: Intraspecific Variation, Heterochronies, and Life History Evolution. *Zoolog. Sci.* 28: 491–500. DOI: 10.2108/zsj.28.491
- Mourer-Chauviré C. 2003. Birds (Aves) from the Middle Miocene of Arrisdrift (Namibia). Preliminary study with description of two new genera: *Amanuensis* (Accipitriformes, Sagittariidae) and *Namibiavis* (Guriformes, Idiornithidae), in: Pickford, M., Senu, B. (Eds.), *Geology and Palaeobiology of the Central and Southern Namib*. Vol. 2: Paleontology of the Orange River Valley. pp. 103–113
- Müllner A. 2004. Breeding ecology and related life-history traits of the Hoatzin, *Opisthocomus hoazin*, in a primary rainforest habitat. Bayerischen Julius-Maximilians-Universität Würzburg, 159p.
- Olson SL. 1992. A New Family of Primitive Landbirds From the Lower Eocene Green River Formation of Wyoming. *Pap. avian Paleontol. Honor. Pierce Brodtkorb*
- Owre OT. 1967. Adaptations for Locomotion and Feeding in the Anhinga and the Double-Crested Cormorant. *Am. Ornithol. Soc.* 119: 1–138. DOI: 10.1525/auk.2011.10248
- Parker WK. 1891. On the Morphology of a Reptilian Bird, *Opisthocomus cristatus*. *Trans. Zool. Soc. London* 13: 43–85. DOI: 10.1111/j.1096-3642.1891.tb00045.x

- Parker WK. 1868. A monograph of the structure and development of the shoulder-girdle and sternum in the Vertebrata, Ray Society, London. 237p. DOI: 10.5962/bhl.title.31928
- Perin JB. 1875. On the myology of *Opisthocomus cristatus*. *Trans. Zool. Soc. London* 9: 353–370
- Porro LB, Richards CT. 2017. Digital dissection of the model organism *Xenopus laevis* using contrast-enhanced computed tomography. *J. Anat.* 231: 169–191. DOI: 10.1111/joa.12625
- Pradel A, Didier D, Casane D, Tafforeau P, Maisey JG. 2013. Holocephalan Embryo Provides New Information on the Evolution of the Glossopharyngeal Nerve, Metotic Fissure and Parachordal Plate in Gnathostomes. *PLoS One* 8: 4–9. DOI: 10.1371/journal.pone.0066988
- Prum RO, Berv JS, Dornburg A, Field DJ, Townsend JP, Moriarty Lemmon E, Lemmon AR, Lemmon EM, Lemmon AR, Moriarty Lemmon E, Lemmon AR. 2015. A comprehensive phylogeny of birds (Aves) using targeted next-generation DNA sequencing. *Nature* 526: 569–573. DOI: 10.1038/nature15697
- Queiroz KDE, Good DA. 1988. The scleral ossicles of *Opisthocomus* and their phylogenetic significance. *Auk* 105: 29–35
- Ripley BD. 1996. Pattern Recognition via Neural Networks. *Cambridge Univ. Press. Cambridge*
- Rohlf FJ, Slice D. 1990. Extensions of the Procrustes Method for the Optimal Superimposition of Landmarks. *Syst. Zool.* 39: 40. DOI: 10.2307/2992207
- Russell DA. 1982. Plutarch and the Antique Hero. *Yearb. English Stud.* 12: 24. DOI: 10.2307/3507396
- Schlager S. 2017. Morpho and Rvcg - Shape Analysis in R: R-Packages for Geometric Morphometrics, Shape Analysis and Surface Manipulations, Statistical Shape and Deformation Analysis: Methods, Implementation and Applications. 217–256p. DOI: 10.1016/B978-0-12-810493-4.00011-0
- Serrano FJ, Chiappe LM, Palmqvist P, Figueirido B, Marugán-Lobón J, Sanz JL. 2018. Flight reconstruction of two European enantiornithines (Aves, Pygostylia) and the achievement of bounding flight in Early Cretaceous birds. *Palaeontology* 61: 359–

368. DOI: 10.1111/pala.12351

- Shufeldt RW. 1918. Notes on the Osteology of the Young of the Hoatzin (*Opisthocomus cristatus*) and Other Points on Its Morphology. 18p.
- Sorenson MD, Oneal E, García-Moreno J, Mindell DP. 2003. More taxa, more characters: The hoatzin problem is still unresolved. *Mol. Biol. Evol.* 20: 1484–1498. DOI: 10.1093/molbev/msg157
- Souter T, Cornette R, Pedraza J, Hutchinson J, Baylac M. 2010. Deux applications de morphométrie par semi-landmarks 3D impliquant une conception différente du template: le pelvis des théropodes et le crâne des musaraignes. *Comptes Rendus - Palevol* 9: 411–422. DOI: 10.1016/j.crpv.2010.09.002
- Stegmann BC. 1978. Opisthocomiformes, in: Relationships of the Superorders Alectoromorphae and Charadriomorphae. Nuttall Ornithological Club, p. 120
- Strahl SD. 1988. The social organization and behaviour of the Hoatzin *Opisthocomus hoazin* in central Venezuela. *Ibis (Lond. 1859)*. 130: 483–502. DOI: 10.1111/j.1474-919X.1988.tb02714.x
- Tobalske BW, Dial KP. 2000. Effects of body size on take-off flight performance in the phasianidae (AVES). *J. Exp. Biol.* 203: 3319–3332
- Torres BC. 1987. The Ecology of the Hoatzin (*Opisthocomus hoazin*) in Peru. 71p.
- VanderWerf EA, Strahl SD. 1990. Effects of Unit Size and Territory Defense on Communal Nest Care in the Hoatzin (*Opisthocomus hoazin*). *Auk* 107: 626–628
- Venables WN, Ripley BD. 2002. Modern Applied Statistics with S. Springer
- Viscor G, Fuster JF. 1987. Relationships between morphological parameters in birds with different flying habits. *Comp. Biochem. Physiol. -- Part A Physiol.* 87: 231–249. DOI: 10.1016/0300-9629(87)90118-6
- Vlassenbroeck J, Dierick M, Masschaele B, Cnudde V, Van Hoorebeke L, Jacobs P. 2007. Software tools for quantification of X-ray microtomography at the UGCT. *Nucl. Instruments Methods Phys. Res. Sect. A Accel. Spectrometers, Detect. Assoc. Equip.* 580: 442–445. DOI: 10.1016/j.nima.2007.05.073
- Voeten DFAE, Cubo J, De Margerie E, Röper M, Beyrand V, Bureš S, Tafforeau P, Sanchez S. 2018. Wing bone geometry reveals active flight in *Archaeopteryx*. *Nat. Commun.*

9. DOI: 10.1038/s41467-018-03296-8

Watson PJ, Fitton LC, Meloro C, Fagan MJ, Gröning F. 2018. Mechanical adaptation of trabecular bone morphology in the mammalian mandible. *Sci. Rep.* 8: 1–12. DOI: 10.1038/s41598-018-25597-0

Watson PJ, Gröning F, Curtis N, Fitton LC, Herrel A, McCormack SW, Fagan MJ. 2014. Masticatory biomechanics in the rabbit: A multi-body dynamics analysis. *J. R. Soc. Interface* 11. DOI: 10.1098/rsif.2014.0564

Annexes

Annex A

Annex A : Summary of the dataset used in the chapter 3. NC is for not present in collection. NA is for not assigned. Present is for bones present in collection and added to the dataset. Both is when both paired bones were present and added to the dataset. Right/Left is for the side of the paired bone sampled. Absent is for bones absent in living specimens. We obtained 44 furculae, 52 sternums, 94 coracoids, 75 scapulae and 90 humeri.

Species	Order	Family	Furcula	Sternum	Coracoid	Scapula	Humerus	Flight type
<i>Accipiter_gentilis</i>	Accipitriformes	Accipitridae	Present	Present	Both	Both	Right	Gliding
<i>Anseranas_semipalmata</i>	Anseriformes	Anseranatidae	Present	Present	Both	Both	Both	Flapping
<i>Aptenodytes_patagonicus</i>	Sphenisciformes	Spheniscidae	Present	Present	Both	Right	Both	Swimming
<i>Apteryx_australis</i>	Apterygiformes	Apterygidae	Absent	Present	NC	NC	NC	Flightless
<i>Aquila_chrysaetos</i>	Accipitriformes	Accipitridae	Present	Present	Both	Both	Both	Gliding
<i>Ara_ararauna</i>	Psittaciformes	Psittacidae	Present	Present	Both	Both	Both	Flapping
<i>Asio_flammeus</i>	Strigiformes	Strigidae	NC	Present	Both	Both	NC	Flapping
<i>Balearica_pavonina</i>	Gruiformes	Gruidae	Present	Present	NC	Left	Both	Flapping
<i>Buceros_bicornis</i>	Bucerotiformes	Bucerotidae	NC	NC	Both	Both	Both	Flapping
<i>Burhinus_oedicnemus</i>	Charadriiformes	Burhinidae	Present	Present	Both	Left	NC	Flapping
<i>Cariama_cristata</i>	Cariamiformes	Cariamidae	Present	NC	Both	Right	Both	Poor fliers
<i>Casuarius_casuarius</i>	Casuariiformes	Casuarius	Absent	Present	NC	NC	NC	Flightless
<i>Cathartes_aura</i>	Accipitriformes	Cathartidae	Present	Present	Both	Both	Both	Gliding
<i>Chauna_torquata</i>	Anseriformes	Anhimidae	Present	Present	Both	Both	Left	Gliding
<i>Coracias_benghalensis</i>	Coraciiformes	Coraciidae	Present	Present	Both	Both	Both	Flapping
<i>Corvus_cornix</i>	Passeriformes	Corvidae	NC	Present	NC	NC	NC	Gliding
<i>Coturnix_coturnix</i>	Galliformes	Phasianidae	Present	Present	Both	Both	Both	Poor fliers
<i>Coua_cristata</i>	Cuculiformes	Cuculidae	Present	Present	Both	Both	Both	Poor fliers
<i>Cryptorellus_tataupa</i>	Tinamiformes	Tinamidae	NC	Present	NC	NC	NC	Poor fliers
<i>Cuculus_canorus</i>	Cuculiformes	Cuculidae	NC	Present	NC	NC	Both	Flapping
<i>Cygnus_olor</i>	Anseriformes	Anatidae	Present	Present	Both	Both	Both	Flapping
<i>Dacelo_novaeguineae</i>	Coraciiformes	Alcedinidae	Present	Present	Both	Left	Right	Flapping
<i>Diomedea_exulans</i>	Procellariiformes	Diomedeidae	Present	Present	Both	Both	Both	Gliding
<i>Dromaius_novaehollandiae</i>	Casuariiformes	Dromaiidae	Absent	Present	NC	NC	Left	Flightless
<i>Dryocopus_martius</i>	Piciformes	Picidae	Present	Present	Both	Both	Both	Flapping
<i>Ducula_aenea</i>	Columbiformes	Columbidae	Present	Present	Right	Left	Both	Flapping

<i>Eudytes_chrysocome</i>	Sphenisciformes	Spheniscidae	Present	Present	Both	Both	Both	Swimming
<i>Eurypyga_helias</i>	Eurypygiformes	Eurypygidae	NC	NC	Both	Both	Both	Poor fliers
<i>Eurystomus_glaucurus</i>	Coraciiformes	Coraciidae	Present	Present	Both	Both	Right	Flapping
<i>Falco_concolor</i>	Falconiformes	Falconidae	Present	Present	Both	NC	Both	Flapping
<i>Fratercula_arctica</i>	Charadriiformes	Alcidae	Present	Present	Both	Left	Both	Semi-aquatic
<i>Gavia_arctica</i>	Gaviiformes	Gaviidae	Present	Present	Both	Both	Both	Semi-aquatic
<i>Glareola_pratincola</i>	Charadriiformes	Glareolidae	Present	NC	Both	Left	Both	Flapping
<i>Grus_grus</i>	Gruiformes	Gruidae	NC	NC	Both	Both	Both	Gliding
<i>Larus_hyperboreus</i>	Charadriiformes	Laridae	Present	Present	Both	Both	Both	Gliding
<i>Leptoptilos_javanicus</i>	Ciconiiformes	Ciconiidae	Present	Present	Both	Left	Both	Gliding
<i>Meleagris_gallopavo</i>	Galliformes	Phasianidae	Present	Present	Both	Both	Both	Gliding
<i>Merops_superciliosus</i>	Coraciiformes	Meropidae	Present	NC	Both	NC	Both	Gliding
<i>Mycteria_americana</i>	Ciconiiformes	Ciconiidae	Present	Present	Both	NC	NC	Gliding
<i>Opisthocomus_hoazin</i>	Opisthocomiformes	Opisthocomidae	Present	Present	Right	Both	Both	NA
<i>Pandion_haliaetus</i>	Accipitriformes	Pandionidae	Present	Present	Both	Both	Both	Flapping
<i>Pelecanus_onocrotalus</i>	Pelecaniformes	Pelecanidae	NC	Present	Both	NC	Both	Gliding
<i>Phaethon_aethereus</i>	Phaethontiformes	Phaethontidae	Present	Present	Both	Right	Both	Flapping
<i>Phalacrocorax_carbo</i>	Suliformes	Phalacrocoracidae	Present	Present	Both	Both	Both	Flapping
<i>Phoenicopterus_ruber</i>	Phoenicopteriformes	Phoenicopteridae	Present	Present	Both	Both	Both	Flapping
<i>Pica_pica</i>	Passeriformes	Corvidae	Present	Present	Both	Both	Both	Flapping
<i>Psophia_crepitans</i>	Gruiformes	Psophiidae	NC	Present	NC	Right	Right	Poor fliers
<i>Recurvirostra_avosetta</i>	Charadriiformes	Recurvirostridae	Present	Present	Both	Both	Both	Flapping
<i>Rhea_americana</i>	Rheiformes	Rheidae	Absent	Present	NC	NC	NC	Flightless
<i>Rhynochetos_jubatus</i>	Eurypygiformes	Rhynochetidae	Present	Present	Left	Right	Both	Flightless
<i>Sagittarius_serpentarius</i>	Accipitriformes	Sagittariidae	Present	Present	Both	Right	Left	Gliding
<i>Steatornis_caripensis</i>	Caprimulgiformes	Steatornithidae	Present	Present	Both	Both	Both	Flapping
<i>Struthio_camelus</i>	Struthioniformes	Struthionidae	Absent	Present	NC	NC	NC	Flightless
<i>Sula_bassana</i>	Suliformes	Sulidae	Present	Present	Both	Left	Left	Gliding
<i>Tauraco_persa</i>	Cuculiformes	Musophagidae	NC	Present	Both	Both	Right	Poor fliers
<i>Tringa_totanus</i>	Charadriiformes	Scolopacidae	Present	NC	Both	Both	Both	Flapping
<i>Tyto_alba</i>	Strigiformes	Tytonidae	Present	Present	Both	NC	Right	Flapping
<i>Uria_aalge</i>	Charadriiformes	Alcidae	Present	Present	Both	NC	Both	Semi-aquatic
<i>Vultur_gryphus</i>	Accipitriformes	Cathartidae	Present	Present	Left	Both	Both	Gliding

Annex B

Annex B : Summary of the comparative dataset of the ossification sequences used in the chapter 4. Numbers refer to days of development.

Element	<i>Meleagris gallopavo</i>	<i>Gallus gallus</i>	<i>Coturnix coturnix</i>	<i>Anas platyrhynchos</i>	<i>Eudromia elegans</i>	<i>Sterna hirundo</i>	<i>Stercorarius skua</i>	<i>Larus argentatus</i>	<i>Larus ridibundus</i>	<i>Larus canus</i>	<i>Dromaius novaehollandiae</i>	<i>Rhea americana</i>	<i>Struthio camelus</i>	<i>Opisthocomus hoazin</i>	<i>Myiopsittacus monachus</i>	<i>Cairina moschata</i>	<i>Somateria mollissima</i>
Basioccipital	17	17		12	5	10	9		16	14	14-21	8	14-15	4	22	12	6
Exoccipital	12	13	10	10	7	13	8	7	13	11	14	8	16	2	21	12	5
Supraoccipital	13 to 16	17		10	7	14	11		18	14	18	6	14	3	31	12	5
Parasphenoid rostrum	6	8	5	8	4	6		4	9	6	6	3	5	2	11	3 to 6	2
Parasphenoid ala	16		10	10	7	8					12	6	16	2	14	3 to 6	6
Parasphenoid lamina	15		10	10	4	7	8		17	12	14	4	16	2		3 to 6	6
Basisphenoid	9 to 11	17	10	10	4 to 6	7	5	7	10	10	10 to 12	6	8 to 10	2	14	8	2
Laterosphenoid	18 to 21	22 to 24		20	7	20-23			21	16	13-18	8	16	5	32	17	7
Prootic	19	19		15	7	18			17	14	25	8	17	x	12	13	8
Opisthotic	20	22 to 24		15	7	19					22	8	18	x	12	14	9
Epiotic	22	22 to 24		21	8						21	8	18	x	12	19	12
Squamosal	4	2	1	1	3	3	3	3	5	4	3	2	4	1	7	3	2
Parietal	9	13	8	5	4	8	12	7	18	14	12	6	7	2	25	6	2
Frontal	8	9	6	6	4	6	6	7	11	8	11	6	8	1	18	5	2
Lacrimal	7	7 to 9	5	2	4	5	6	6	7	8	6	2	6	1	12	3	2
Mesethmoid	22	29		20	7	22			22	18	18	8	14	6	34	21	11 to 17
Trabeculae				x									23	x		x	11 to 17
Nasal	7	5	5	2	3	5	5	4	6	7	8	4	6	1	8	3	2
Premaxilla	6	9	5	3	2	5	5	4	6	6	4	2	5	1	8	4	2
Maxilla	6	4	5	2	3	4	5	3	4	3	7	2	4	2	7	3	2
Palatine	5	4	5	2	3	4	5	3	4	4	3	2	5	1	7	3 to 4	2
Pterygoid	5	4	5	2	3 to 4	4	5	3	4	3	3	2	3 to 5	1	6	3 to 4	2
Vomer		<20		7	3	?	6	4	9	6	5	2	6	2		3 to 6	2

Jugal	6	4	2	3	3	5	6	4	6	6	3 to 5	2	5	1	6	4	2
Quadratojugal	1	1	1	1	2	4	3	4	4	3	2	2	4	1	6	3	2
Quadrate	6 to 8	10	7	5	4	12	10	7	17	14	11	5	11	3	16	8	2
Dentary	6	4	5	3	3						2	4	3	1	3	4	2
Supra-angular	2 to 6	4	5	1	3	5	6	4	5	5	2	2	4	2	3	4	2
Angular	2	2	1 to 4	1	3	5	5	3	4	3	1	2	4	1	3	2	2
Splénial	6	9		8	3	5	6	2	4	3	7	4	5	1	3	4 to 5	2
Prearticular	24	11		11	4 to 6	6	6	4	5	4	9	4	10	1	4	12	7
Articular				19		<13		7			23	9	19	6	34	15	8
Mandibular							16							x			
Entoglossal				x					5	5				x	20	x	x
Basihyal				x										x	34	x	x
Urohyal														x	34		
Ceratobranchial	6	8 to 9	3	3	4	5	8	4	5	6	13	5	9 to 11	1	10	4	2
Epibranchial				x										x	34	x	x
Cervical centra	14	15 to 17	10	9	7	13	8		11	15	15	5	13	4	26	12	5
Thoracic centra	19	19		12	4 to 6	13	8		11	14	15	4	11	3	28	12	5
Synsacral centra	20	21		12	4 to 6	13	9				16	7	11	3	30	12	5
Caudal centra	24 to 25	28		18		19	14				19-24		16-18	6	30	16	8
Pygostyle	24			21							27-29		20	6	37	20	15
Cervical arch	19	24		14	7	18	12		13		17	8	14	4	26	17	7
Thoracic transverse processes	19	24		16	8	17-19					20	9	14	4	30	18	7
Synsacral transverse processes	24	28		22		21					27	10	19	6	30	23	10 to 12
Caudal neural arches	24	31		24		20-22							20-22	9	33	21	12
Synsacral arch		30		23		23						11	21	9	32	22	11
Cervical ribs	19 to 24	20		11	8	18	14				17	77	14	5	13	14	6
Dorsal ribs	8	9	7	4	4	8-10	5		8	8	3 to 7	5	7	4		7	2
Sternal ribs	18	16		x							15	9	22-23	x	34	x	16
Uncinate processes		28 to 31		x								11		x	34	x	x
Sternum				x							25	10		8	39	x	16

(body)																	
Laterocranial processes	25	31		x								6 to 11		6		x	x
Laterocaudal processes	23	27		x										6		x	x
Scapula	6	9	5	3	2	9	5	4	4	3	5 to 7	5	10	1	9	4	2
Coracoid	9 to 11	9	7	6	5	10	8	5 to 7	11	11	15-18	5	14	2	9	8	2 to 4
Furcula	1 to 6	3	1	1	3 to 4	2	3	1	3	2	5 to 7			1	9	2	2
Humerus	1	3	1 to 4	1	1	1	1	1	1	1	1	2	2	1	1	1	1
Radius	2	3	1 to 3	1	1	1	1	1	1	1	7	2	2	1	1	1	1
Ulna	2	4	1 to 3	1	1	1	1	1	1	1	7	2	2	1	1	1	1
Radiale				x										x	38	x	x
Ulnare				x										x	38	x	x
Metacarpal II				24									19	6	35	x	12 to 15
Phalanx 1	9 to 11	11	7	6	4	8	11	7	12	13		5 to 9	12	2	24	8	2
Phalanx 2		11 to 31	9 to 11	10 to 25		20						10	16-23	5		7 to 12	2 to 11
Metacarpal III	6	7	1 to 3	2	2	3	6	2	4	3	4 to 7	4	5 to 8	1	4	3	2
Phalanx 1	7	14	7	8	4	6 to 8	8	7	13	8	21-29	10	9 to 14	3	17	8	3
Phalanx 2	11	11	7	8	4	9	9	7	13	11		11	9 to 14	3	19	8	4
Phalanx 3				24 to 25							20-25		20-23	5	5	7 to 19	10
Metacarpal IV	6	8	1 to 3	2	3	4	6	2	4	3	25-30	4	5 to 8	1	35	4	2
Phalanx 1	23			x			11		21			10	14	5		x	11 to 15
Phalanx 2													21-23	x			
Ilium	9 to 11	11	7	6	4	10	6	7	8	8	9	4	12	2	15	10	3 to 5
Ischium	12	17	8	6	5	10	6	7	7	5	7 to 9	4	5 to 7	2	15	5	2
Pubis	8	9	6	7	5	8	5	4	15	13	8	4	5 to 7	2	15	6	2
Femur	1	4	1	1	1	2 to 4	2	1	2	2	1	1	2	1	1	1	1
Tibia	2	4	1	1	1	1	1	1	1	1	1	1	1	1	1	1	1
Fibula	3	4	1 to 3	1	1	1	1	1	1	1	1	1	2	1	1	1	1
Patella				x										x		x	x
Ascending process of the astragalus	17 to 24	26		17	6	20					14	8	13	x		12 to 14	8
Tarsals				x							28	10		x		x	13
Metatarsal I	16	18		13 to 17		12 to 15			20					3	27	17 to 18	8

Phalanx 1	11	12	5 to 9	10		12 to 16			12	17			2	29	9	5	
Phalanx 2	9 to 17	11	5 to 9	10		12 to 15	13		19	14			2	29	9 to 11	2	
Claws													4				
Metatarsal II	3	6	1 to 4	1	2	4	6	2	4	3	1	1	2	1	2	1	1
Phalanx 1	9	12	5 to 7	5	2	5	7	4	12	9	7	4		2	29	7	2
Phalanx 2	10	15	7	6	2	9	8	7	12	11		10		3	29	7	3
Phalanx 3	9 to 17	11	7 to 10	7	4	12	13	7	17	11	7	4		4	29	8 to 11	4
Metatarsal III	3	6	1 to 4	1	2	4	3	1	4	3	1	1	2	1	2	1	1
Phalanx 1	9	11	5 to 7	4	2	5	7	4	12	8	7	4	5	2	28	7	2
Phalanx 2	9	15	5 to 7	8	2	5	8	7	12	11	8 to 13	5	7	3	29	10	4
Phalanx 3	10	15	7	10	3	12	9	7	13	13	25	9	14	3	30	8	4
Phalanx 4	9	11	7 to 10	7	4	9 to 11	13	7	14	11	7	4	11	4	29	8 to 11	2
Metatarsal IV	3	6	1 to 4	1	2	4	4	1	4	3	1	1	2	1	2	1	1
Phalanx 1	9	11	5 to 7	4	2	5	7	4	13	9	7	5	6	2	23	7	2
Phalanx 2	11 to 21	23	7 to 10	10	4	6 to 9	11	7	16	11	26-29	9	16	3	35	11	5
Phalanx 3	21	25	7 to 10	14	4	10 to 12	13	7	18	13		10	19	3	35	19	6
Phalanx 4	19 to 21	18	7 to 10	10	4	14	13	7	18	13		11	21	3	30	7 to 8	5
Phalanx 5	9 to 11	11	7 to 10	8	4	12	13	7	16	11	7	4	16-23	4	29	8 to 11	2

Annex C

EVOLUTIONARY BIOLOGY

Hoatzin nestling locomotion: Acquisition of quadrupedal limb coordination in birds

Anick Abourachid^{1*}, Anthony Herrel^{1,2}, Thierry Decamps¹, Fanny Pages¹, Anne-Claire Fabre¹, Luc Van Hoorebeke³, Dominique Adriaens², Maria Alexandra Garcia Amado⁴

The evolution of flight in birds involves (i) decoupling of the primitive mode of quadrupedal locomotor coordination, with a new synchronized flapping motion of the wings while conserving alternating leg movements, and (ii) reduction of wing digits and loss of functional claws. Our observations show that hoatzin nestlings move with alternated walking coordination of the four limbs using the mobile claws on their wings to anchor themselves to the substrate. When swimming, hoatzin nestlings use a coordinated motion of the four limbs involving synchronous or alternated movements of the wings, indicating a versatile motor pattern. Last, the proportions of claws and phalanges in juvenile hoatzin are radically divergent from those in adults, yet strikingly similar to those of *Archaeopteryx*. The locomotor plasticity observed in the hoatzin suggests that transitional forms that retained claws on the wings could have also used them for locomotion.

INTRODUCTION

Birds are flying theropods that power their flight by flapping both wings simultaneously. Developmental data indicate that the reduction of wing digits and the loss of claws are concomitant during bird evolution (1) such that the wings lose their grasping function. Although some birds such as chukars, ducks, rails, and owls retain claws on the wing (2), they do not use them for locomotion. Hoatzin (*Opisthocomus hoazin*) nestlings, however, retain functional claws on the wing and have been suggested to use them to climb in the vegetation. This is possibly one of the most remarkable but also the least documented traits in this unusual bird. The first description of this behavior was provided by C. G. Young in 1888: “As soon as the young escape from the egg, they creep about with the assistance of these hands, stretching out their wings and digging these claws into hooking on whatever they meet.” He further added that a “specimen, by means of these claws walked out of a calabash” (3). Another unusual trait in hoatzin nestlings is to escape by jumping into the water below the nest and to swim back to the vegetation. Although hoatzins are not rare, quantitative data on locomotion in nestlings during either climbing or swimming have never been collected and references to locomotion in these animals all refer back to the original publication on their behavior (3).

Juvenile extant birds may provide key insights into our understanding of the evolutionary and functional transformations that took place toward the evolution of modern birds (2). Before they are capable of active flight, most juveniles flap their wings in the context of wing-assisted incline running (WAIR) to move up steep slopes. During WAIR, the wings generate aerodynamic forces that help the animal ascend obstacles (4, 5). As the synchronous wing coordination observed during flying and WAIR is shared by many birds across the majority of clades, it is likely basal for the group (6). The neuronal networks, functionally organized early during develop-

ment, drive the in-phase movements of the wings during bird locomotion. This determinism is so robust that the experimental substitution of a brachial spinal cord segment by a lumbosacral segment and vice versa during the early stages of development in chickens leads to synchronized movements of the limbs connected to the brachial segment of the spinal cord and alternated movements of the wings connected to the lumbosacral segment (7). In that context, the hoatzin is remarkable. Do hoatzin nestlings move using an alternating quadrupedal walk, as suggested by Young’s description (3), or do they use the wings and claws in an opportunistic reflex-like way to grasp branches when possible, as when a newborn child grasps a finger (8), or do they use a kind of WAIR behavior during climbing, as do all other birds? Here, we provide the first quantitative data on the locomotion of nestling hoatzins that inform on the use of the claws and the coordination pattern of the limbs. We filmed four nestlings, caught in nests along the Cojedes River in Venezuela, while moving on an inclined substrate and while swimming. Whereas movements were spontaneous in water, nestlings needed to be encouraged to move on the inclined surface by touching their tail or hind feet. The inclined substrate was covered with a towel, providing grip for the claws on the wings.

RESULTS

The limbs moved in an alternating fashion, with the movement of a leg being followed by the movement of the contralateral wing, then the other leg, and the other wing (Fig. 1). The claws were hooked onto the substrate and the wing flexed, pulling the body upward. Locomotor cycles were most often irregular, as the lack of an immediate attachment of the claws to the substrate destabilized the nestling bird. When the claw did not hook into the substrate, the motion of the wing continued further laterally until the claw attached. If it did not, the wing was reversed and a new movement cycle of the same wing was initiated. The quadrupedal locomotion observed was rather irregular with birds stopping typically after two or three cycles. However, the movements of the four limbs were coordinated. The swing phase duration of the forelimbs was longer than the swing phase duration of the hindlimbs (i.e., the wing duty factor was smaller than the foot duty factor). The time lag between

Copyright © 2019
The Authors, some
rights reserved;
exclusive licensee
American Association
for the Advancement
of Science. No claim to
original U.S. Government
Works. Distributed
under a Creative
Commons Attribution
NonCommercial
License 4.0 (CC BY-NC).

¹Département Adaptations du Vivant, UMR 7179 CNRS/MNHN, 57 rue Cuvier, Case postale 55, 75231, Paris Cedex 5, France. ²Evolutionary Morphology of Vertebrates, Ghent University, Campus Ledeganck, K.L. Ledeganckstraat 35, B-9000 Gent, Belgium. ³UGCT—Department of Physics and Astronomy, Ghent University, Proeftuinstraat 86, 9000 Ghent, Belgium. ⁴Centro de Biofísica y Bioquímica, Instituto de Investigaciones Científicas (IVIC), Caracas, Venezuela.

*Corresponding author. Email: abourach@mnhn.fr

the movements was more irregular for the wings than for the legs. However, the tendency is clearly to move the limbs in an alternating way (Table 1) (9), with a coordination typical of a quadrupedal walking pattern [fore lag (FL), hind lag (HL), and pair lag (PL) close to 0.5]. This suggests that the use of the wings is not limited to an opportunistic grasping reflex.

The alternating coordination pattern of the wings also does not correspond to WAIR, where the wings flap in phase to create aerodynamic forces. At hatching, chukars (*Alectoris chukar*) can ascend slopes by crawling on all four limbs (6), but the wings, without claws, cannot anchor to the substrate. No alternated wing coordination has been reported. The hoatzin coordination pattern of the four limbs is typical of a quadrupedal walking gait, a trait lost in all other modern birds. This symmetrical gait (9) secures at least three points of contact with the substrate and is the most stable of the quadrupedal coordination patterns.

When placed in the pool, the nestlings swam vigorously and with great ease, either under water or with the head kept outside of

the water. Irrespective of the coordination, the swimming cycles were rather regular, even if a bit more variable for the wings compared to the legs. The wing power phases were shorter than the recovery phases, whereas they were longer for the legs. The coordination between the leg and the wing (PL) was variable (high SDs). The movements of the legs were alternated (HL close to 0.5), while the wings typically moved in phase (FL close to 0; Table 1) (Fig. 2). Out of the 50 locomotor cycles observed, only 4 of them showed an out-of-phase coordination pattern. The coordination during most swimming cycles was thus generally similar to that observed during WAIR (in other birds, but in a different mechanical context).

In a more complex environment with branches, hoatzin nestlings used a quadrupedal walking coordination, but due to the irregularity of the substrate, the coordination was far less regular than on our experimental substrate. The head was also used as a hook: It was flexed so that the base of the beak was positioned on the branch, the neck appearing to pull the body upward and helping the

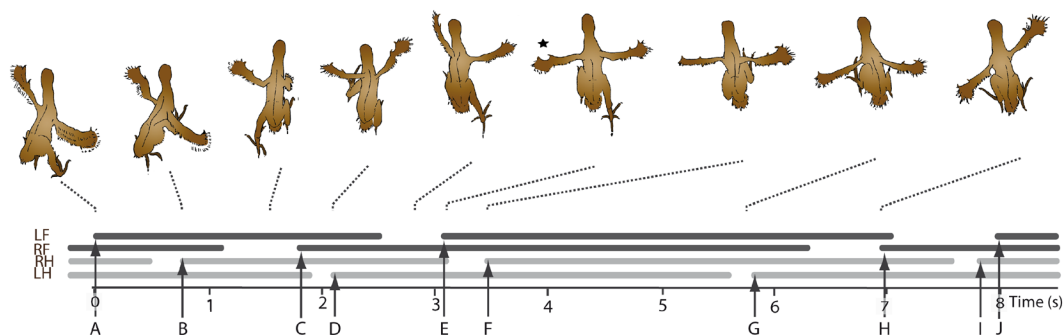


Fig. 1. Schematic illustration of a hoatzin nestling climbing on a 45° inclined surface. The x axis represents time. Each line represents the time when a leg is in contact with the substrate. The movements of the four legs are alternating: The left wing moves and grips the substrate (A). Next, the right foot moves up and touches down (B), followed by the right wing that moves forward (C). The left foot then moves forward and touches down (D), and the left wing moves again (E) followed by the right foot (F). However, the left claw was unable to grip the substrate at its most forward position (star), resulting in it moving backward until gripping the substrate (E). The lateral position of the wing perturbs the progression and changes the coordination pattern. The pattern is still alternated but with the left foot (G) moving before the right foot (I) and the right wing (H) before the left wing (J). LF, left fore (wing); RF, right fore (wing); RH, right hind (foot); LH, left hind (foot).

Table 1. Gait characteristics and limb coupling during climbing and swimming. n, number of cycles analyzed.

Climbing											
	Cycle duration (s)				Duty factor				FL	HL	PL
	RF	LF	RH	LH	RF	LF	RH	LH			
Mean	4.20	3.10	5.58	6.31	0.86	0.83	0.94	0.96	0.36	0.48	0.56
SD	1.61	2.27	2.25	2.97	0.10	0.05	0.04	0.01	0.33	0.10	0.22
n	11	10	12	11	10	7	10	11	8	9	9
Swimming											
In-phase coordination											
Mean	0.77	0.82	0.75	0.74	0.43	0.41	0.54	0.53	0.05	0.42	0.32
SD	0.18	0.18	0.06	0.07	0.08	0.11	0.08	0.04	0.07	0.09	0.18
n	12	12	15	13	12	12	15	13	9	9	10
Out-of-phase coordination											
Mean	0.72	0.72	0.71	0.7	0.34	0.31	0.62	0.53	0.52	0.52	0.18
SD	0.16	0.06	0.07	0.08	0.05	0.07	0.07	0.06	0.13	0.12	0.16
n	4	4	4	4	4	4	4	4	4	4	4

wings. The claws on the fingers were actively moved independent of the movements of the rest of the hand skeleton. Contrast-enhanced microcomputed tomography (μ CT) images of a late-stage embryo show that the hoatzin has multiple muscles and tendons attaching onto the finger bones, as observed in most other birds (10–13). However, an additional tendon of one of the digital flexor muscles attaches onto the distal phalanx of the alula (Fig. 3). This likely allows the active gripping of the branches by the claws. A comparison of the proportions of the phalanges of the hoatzin nestlings with those of *Archaeopteryx* (14) shows a remarkable similarity in pro-

portions between the two (Fig. 4). The proportions in adult hoatzin are, however, quite different from those observed in nestlings.

DISCUSSION

Quadrupedal locomotion requires a coupling of the forelimbs, a coupling of the hindlimbs, and a coupling between the limb pairs at the level of the spinal neuronal network (9, 15). In vertebrates, locomotion is initiated at the level of the brainstem and generated by a central spinal network (16). In mammals, which are able to use in-phase and out-of-phase movements for each limb pair, two sets of commissural interneurons are involved in the right-left coordination. An inhibitory pool of neurons is activated for alternating, out-of-phase coordination, and an excitatory pool is activated for synchronous, in-phase coordination (17). Their interplay depends on the behavioral context and the associated locomotor speed. In birds, the neural network is organized early during development (7) and triggers in-phase movement of the wings. The in-phase flapping of the wings could thus have arisen from either the loss of the inhibitor commissural neuron pool or its silencing. The hoatzin nestlings exhibit both in-phase movements during swimming and out-of-phase movements during climbing. This suggests that they have both excitatory and inhibitory connections between the interneuronal networks of the limbs. The plasticity exhibited in the coupling between the excitatory and inhibitory connections in the hoatzin nestling could then arise either from descending drive or from the effects of proprioceptive feedback, or both. The quadrupedal coordination goes hand in hand with the presence of functional claws on the wing (1), since without claws the wings cannot anchor the body to the substrate and would thus be unable to generate the locomotor forces. During slow movements, the locomotor mechanics

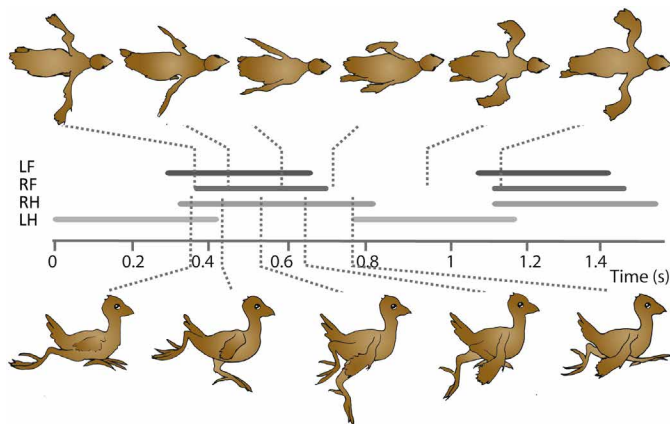


Fig. 2. Schematic illustration of a hoatzin nestling swimming. The x axis represents time. Each line represents the propulsive phase when the limb is moving backward. The dorsal view shows a synchronized motions of the wings; the lateral view shows the alternated motion of the limbs. LF, left fore (wing); RF, right fore (wing); RH, right hind (foot); LH, left hind (foot).

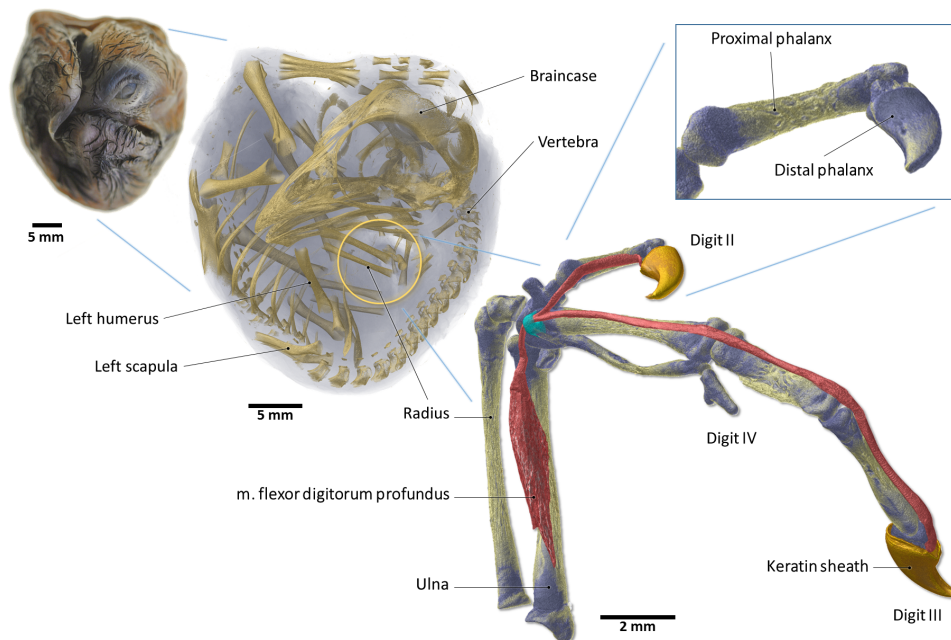


Fig. 3. Musculoskeletal anatomy of a hoatzin shortly before hatching. Left: Fetus as positioned in the egg. Middle: Reconstructed mineralized parts of the skeleton of the bird, showing the position of the wing skeleton (yellow circle). Right: Detailed reconstruction of the contrast-enhanced μ CT data of the wing (ventral view), with the position of the additional tendon of the flexor digitorum profundus attaching to the alula digit illustrated. Inset: Detail of the alula digit, with the keratin sheet removed, showing the claw-like distal phalanx. Blue, cartilage; yellow, bone; red, muscle; cyan, connective tissue sling of the muscle tendon; orange, keratin.

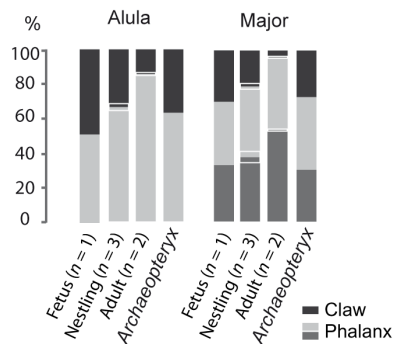


Fig. 4. Proportions of the digit phalanx in the *Archaeopteryx* compared to three hoatzin developmental stages. Values are in percent of the digit length. Variability is shown with white line.

require at least three anchoring points for stability, preventing the coordination of wings into an in-phase motion. Proprioceptive feedback may participate in the reactivation of a silent inhibitory motoneuron pool during quadrupedal locomotion.

Birds originate from theropods, bipedal animals that did not use the forelimbs for walking. Although the exact position of the hoatzin in the bird tree of life remains controversial (18–22), its divergence seems to have occurred after the origin of Paleognaths, Galloanseres, and other neoavian radiations (22). None of the species of these clades are known to use the wings for climbing. Furthermore, the forelimb in-phase coordination is determined early in the development in the chicken (*Gallus gallus*) (7), a Galloanseres species from a clade more basal than the Opisthocomiformes (22). The quadrupedal walking coordination of the hoatzin nestling thus represents the reappearance of a trait lost during bipedal saurischian dinosaur evolution (23), without the loss of a trait that has arisen later in the evolution of birds (wing flapping during flight retained in adult hoatzin). The quadrupedal coordination may be the expression of the conservative nature of the central nervous system, with a basic interneural network reactivation in response to proprioceptive feedback, driven by the contact of the claws to the substrate. It is possible that the interneuronal networks show greater plasticity and diversity among birds than has been previously recognized due to a sparse sampling of “model animal” species in neurophysiological studies. As *Archaeopteryx* shows large claws on the wing similar in proportion to those observed in the hoatzin nestlings, the latter might be used as a functional analog to infer the locomotor repertoire in transitional forms like *Archaeopteryx*. Our results thus suggest the existence of a larger locomotor repertoire in transitional forms likely including both WAIR wing flapping and quadrupedal limb coordination during climbing allowed by the presence of claws on wings (24).

MATERIALS AND METHODS

Animals and filming

Animals were caught in October 2014 along the Cojedes River near the town of El Baul under permit number 950 issued by the Venezuelan government. Animals were transported back to the field laboratory and filmed with three HDR-CX740VE Sony cameras at 50 Hz. Animals were induced to climb up an inclined surface covered with a cloth to provide grip and then climb on branches. Subsequently, animals were induced to swim in an aquarium (100 cm × 50 cm × 50 cm)

with a water depth of 15 cm. All the procedures were approved by the ethics committees of the Muséum National d’Histoire Naturelle (MNHN) (Comité Cuvier) and Instituto Venezolano de Investigaciones Científicas (IVIC) (COBIANIM).

μCT scanning

A late-stage hoatzin embryo (egg length, 4.1 mm), four juveniles, and two adults were μCT-scanned at the Centre for X-ray Tomography at Ghent University (UGCT). A first in toto scan of each specimen was performed to get a complete overview of the mineralized skeletal anatomy using the in-house developed HECTOR scanner (25). A total of 2400 x-ray projections over 360° were taken at 120-kV tube voltage and 20-W target power with a PerkinElmer detector (pixel pitch, 0.2 mm; exposure time, 1000 ms per image), yielding an isotropic voxel pitch of 20 μm. Subsequently, the left wing was cut off of the late-stage embryo and transferred to 50% ethanol and phosphate-buffered saline (1 hour), after which it was treated with 2.5% phosphomolybdic acid for 1 week, to visualize soft tissues with μCT. The wing was then gradually transferred back to 70% ethanol and scanned at HECTOR under similar settings (but at 100 kV and 10 W) at an isotropic voxel pitch of 10 μm. Virtual cross sections were reconstructed using the in-house developed software Octopus [version 8.8.2.1; (26)]. Bone and soft tissues were segmented and visualized using Amira (version 6.0, FEI). Proportions of the phalanges and claws in *Archaeopteryx* were measured on the basis of the illustrations of Griffiths (14).

Gait analysis

Climbing

On the videos, we noted the time when the limbs gripped the cloth and stopped moving as well as the time when the claws were released from the cloth. Even if the delays between the movements may be long and the coordination may be perturbed by additional grips, the coordination remained similar across the more than 20 locomotor cycles analyzed: The movement of a wing was followed by the movement of the opposite foot, then the other wing moved followed by the other foot. Last, the first wing moved again (Fig. 1). The movements were, however, very slow and irregular. For our quantitative analysis, we kept only the cycles with stance phases lasting less than 10 s and swing phases less than 2 s. As the birds often stopped, we did not always have two successive complete cycles so that we calculate the gait parameters for each limb even if it was not possible to quantify all the parameters for all of them in a given cycle. The swing phase was defined as the time when the limb is off the substrate; the stance phase was defined as the time during which the claw gripped the cloth. Cycle duration was quantified as the sum of the swing phase duration plus the stance phase duration. The duty factor was defined as the participation of the stance to the total cycle duration (i.e., the stance duration divided by the cycle duration). We also calculated coordination parameters (27): The FL was defined as the time lag between the beginning of the two wing stance phases. The HL was defined as the time lag between the beginning of the two foot stance phases. Last, the PL was defined as the time lag between the stance phase of a wing and the stance phase of the ipsilateral foot.

Swimming

Fifty swimming cycles were observed. In four of them, the wings moved in phase. In all the other cases, the wings and the feet moved out of phase. We observed different coupling (Fig. 2) between the

forelimbs and the hindlimbs. Because of the constraints of the field experiments, we were not able to quantify all the cycles observed. We selected the sequences when the birds moved parallel to the camera in lateral view, allowing us to see the motion of both the hindlimbs. The motion of the wings was visible but not accurate enough to be measured on the lateral view. The two wings were clearly visible on the dorsal views, but the hindlimbs were often hidden by the wings or by reflections on the water. We selected sequences where it was possible to synchronize the motion of the wings and the legs for our quantitative analysis. We considered the power phase of a limb to be the phase when it moved backward and the recovery phase when it moved forward (hindlimbs) or laterally (wings).

SUPPLEMENTARY MATERIALS

Supplementary material for this article is available at <http://advances.sciencemag.org/cgi/content/full/5/5/eaat0787/DC1>

Movie S1. Videos of the experimental conditions, climbing, and swimming in hoatzin nestlings.

REFERENCES AND NOTES

- M. A. G. de Bakker, D. A. Fowler, K. den Ouden, E. M. Dondorp, M. C. Garrido Navas, J. O. Horbanczuk, J.-Y. Sire, D. Szczerbińska, M. K. Richardson, Digit loss in archosaur evolution and the interplay between selection and constraints. *Nature* **500**, 445–448 (2013).
- A. M. Heers, K. P. Dial, From extant to extinct: Locomotor ontogeny and the evolution of avian flight. *Trends. Ecol. Evol.* **27**, 296–305 (2012).
- C. G. Young, On the habits and anatomy of *Opisthocomus crissatus*, Illig. *Notes Leyden Mus.* **10**, 169–174 (1888).
- K. P. Dial, Wing-assisted incline running and the evolution of flight. *Science* **299**, 402–404 (2003).
- B. W. Tobalske, K. P. Dial, Aerodynamics of wing-assisted incline running in birds. *J. Exp. Biol.* **210**, 1742–1751 (2007).
- K. P. Dial, B. E. Jackson, P. Segre, A fundamental avian wing-stroke provides a new perspective on the evolution of flight. *Nature* **451**, 985–989 (2008).
- C. H. Narayanan, V. Hamburger, Motility in chick embryos with substitution of lumbosacral by brachial by lumbosacral spinal cord segments. *J. Exp. Zool.* **178**, 415–431 (1971).
- J. M. Schott, M. N. Rossor, The grasp and other primitive reflexes. *J. Neurol. Neurosurg. Psychiatry* **74**, 558–560 (2003).
- L. Maes, A. Abourachid, Gait transitions and modular organization of mammal locomotion. *J. Exp. Biol.* **216**, 2257–2265 (2013).
- J. C. Vanden Berge, G. Zweers, Myologia, in *Handbook of Avian Anatomy: Nomina Anatomica Avium*, J. J. Baumel, A. S. King, J. E. Breazile, H. E. Evans, J. C. Vanden Berge, Eds. (Nuttall Ornithological Club, 1993), pp. 189–247.
- A. J. Berger, On the anatomy and relationships of *Fregilupus varius*, an extinct starling from the Mascarene islands. *Bull. Am. Mus. Nat. Hist.* **113**, 225–272 (1957).
- E. L. Corvidae, R. O. Bierregaard, S. E. Peters, Comparison of wing morphology in three birds of prey: Correlations with differences in flight behavior. *J. Morphol.* **267**, 612–622 (2006).
- Z. H. Zhang, Y. Yang, Forelimb myology of the golden pheasant (*Chrysolophus pictus*). *Int. J. Morphol.* **31**, 1482–1490 (2013).
- P. J. Griffiths, The claws and digits of *Archaeopteryx lithographica*. *Geobios* **16**, 101–106 (1993).
- M. Falgairelle, J. R. Cazalets, Metachronal coupling between spinal neuronal networks during locomotor activity in newborn rat. *J. Physiol.* **580**, 87–102 (2007).
- S. Grillner, T. M. Jessell, Measured motion: Searching for simplicity in spinal locomotor networks. *Curr. Opin. Neurobiol.* **19**, 572–586 (2009).
- A. E. Talpalar, J. Bouvier, L. Borgius, G. Fortin, A. Pierani, O. Kiehn, Dual-mode operation of neuronal networks involved in left-right alternation. *Nature* **500**, 85–88 (2013).
- S. B. Hedges, M. D. Simmons, M. A. Van Dijk, G. J. Caspers, W. W. de Jong, C. G. Sibley, Phylogenetic relationships of the hoatzin, an enigmatic South American bird. *Proc. Natl. Acad. Sci. U.S.A.* **92**, 11662–11665 (1995).
- J. M. Hughes, A. J. Baker, Phylogenetic relationships of the enigmatic hoatzin (*Opisthocomus hoazin*) resolved using mitochondrial and nuclear gene sequences. *Mol. Biol. Evol.* **16**, 1300–1307 (1999).
- J. E. McCormack, M. G. Harvey, B. C. Faircloth, N. G. Crawford, T. C. Glenn, R. T. Brumfield, A phylogeny of birds based on over 1,500 loci collected by target enrichment and high-throughput sequencing. *PLOS ONE* **8**, e54848 (2013).
- E. D. Jarvis, S. Mirarab, A. J. Aberer, B. Li, P. Houde, C. Li, S. Y. Ho, B. C. Faircloth, B. Nabholz, J. T. Howard, A. Suh, C. C. Weber, R. R. da Fonseca, J. Li, F. Zhang, H. Li, L. Zhou, N. Narula, L. Liu, G. Ganapathy, B. Boussau, M. S. Bayzid, V. Zavidovych, S. Subramanian, T. Gabaldón, S. Capella-Gutiérrez, J. Huerta-Cepas, B. Rekepalli, K. Munch, M. Schierup, B. Lindow, W. C. Warren, D. Ray, R. E. Green, M. W. Bruford, X. Zhan, A. Dixon, S. Li, N. Li, Y. Huang, E. P. Derryberry, M. F. Bertelsen, F. H. Sheldon, R. T. Brumfield, C. V. Mello, P. V. Lovell, M. Wirthlin, M. P. Schneider, F. Prosdocimi, J. A. Samaniego, A. M. Vargas Velazquez, A. Alfaro-Núñez, P. F. Campos, B. Petersen, T. Sicheritz-Ponten, A. Pas, T. Bailey, P. Scofield, M. Bunce, D. M. Lambert, Q. Zhou, P. Perelman, A. C. Driskell, B. Shapiro, Z. Xiong, Y. Zeng, S. Liu, Z. Li, B. Liu, K. Wu, J. Xiao, X. Yinqi, Q. Zheng, Y. Zhang, H. Yang, J. Wang, L. Smeds, F. E. Rheindt, M. Braun, J. Fjeldsa, L. Orlando, F. K. Barker, K. A. Jönsson, W. Johnson, K. P. Koepfli, S. O'Brien, D. Haussler, O. A. Ryder, C. Rahbek, E. Willerslev, G. R. Graves, T. C. Glenn, J. McCormack, D. Burt, H. Ellegren, P. Alström, S. V. Edwards, A. Stamatakis, D. P. Mindell, J. Cracraft, E. L. Braun, T. Warnow, W. Jun, M. T. Gilbert, G. Zhang, Whole-genome analyses resolve early branches in the tree of life of modern birds. *Science* **346**, 1320–1331 (2014).
- R. O. Prum, J. S. Berv, A. Dornburg, D. J. Field, J. P. Townsend, E. M. Lemmon, A. R. Lemmon, A comprehensive phylogeny of birds (Aves) using targeted next-generation DNA sequencing. *Nature* **526**, 569–573 (2015).
- S. M. Gatesy, K. P. Dial, Locomotor modules and the evolution of avian flight. *Evolution* **50**, 331–340 (1996).
- A. Feduccia, Evidence from claw geometry indicating Arboreal habits of *Archaeopteryx*. *Science* **259**, 790–793 (1993).
- B. Masschaele, M. Dierick, D. Van Loo, M. N. Boone, L. Braant, E. Pauwels, V. Cnudde, L. Van Hoorebeke, HECTOR: A 240kV micro-CT setup optimized for research. *J. Phys. Conf. Ser.* **463**, 012012 (2013).
- J. Vlassenbroeck, M. Dierick, B. Masschaele, V. Cnudde, L. Van Hoorebeke, P. Jacobs, Software tools for quantification of X-ray microtomography at the UGCT. *Nucl. Instrum. Meth. A* **580**, 442–445 (2007).
- A. Abourachid, A new way of analysing symmetrical and asymmetrical gaits in quadrupeds. *C. R. Biol.* **326**, 625–630 (2003).

Acknowledgments: We would like to thank J. González-Fernández from Hato Mataclara and the Hato Pinero staff for their support in the field, J. R. Cazalets and Ph. Janvier for their remarks on the manuscript, and D. Geffard-Kuri for help with the illustrations. We also thank the Ministerio Del Poder Popular para la Ecosocialismo, Habitat y Vivienda for the capture and exportation permits. **Funding:** This work was supported by ATM MNHN, PEPS ExoMod CNRS (A.A.), and IVIC grant no. 67 (M.A.G.A.). **Author contributions:** A.A. conceived the project; M.A.G.A. organized the field work; A.A., A.H., T.D., A.-C.F., and M.A.G.A. participated in the field work and the capturing and filming of the animals; A.A., A.H., T.D., D.A., and F.P. analyzed the data; L.V.H. was responsible for the μ CT scanning of the specimens; D.A. and F.P. segmented the μ CT data; A.A. and A.H. wrote the paper; all authors revised the paper. **Competing interests:** The authors declare that they have no competing interests. **Data and materials availability:** All data needed to evaluate the conclusions in the paper are present in the paper. Additional data related to this paper may be requested from the authors. Hoatzin specimens can be obtained from the Venezuelan Institute for Scientific Research pending scientific review and a completed material transfer agreement. The CT scans for the specimens used in this study are available upon request from the corresponding author.

Submitted 22 January 2018

Accepted 12 April 2019

Published 22 May 2019

10.1126/sciadv.aat0787

Citation: A. Abourachid, A. Herrel, T. Decamps, F. Pages, A.-C. Fabre, L. Van Hoorebeke, D. Adriaens, M. A. García Amado, Hoatzin nestling locomotion: Acquisition of quadrupedal limb coordination in birds. *Sci. Adv.* **5**, eaat0787 (2019).